NASA TECHNICAL NOTE

NASA TN D-3542

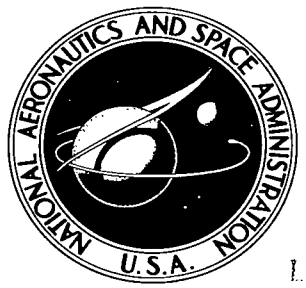

LOW-SPEED WIND-TUNNEL STUDIES RELATING TO PITCH-UP ON A SUPERSONIC TRANSPORT MODEL WITH A HIGH-ASPECT-RATIO VARIABLE-SWEEP WING

by Vernard E. Lockwood

Langley Research Center
Langley Station, Hampton, Va.

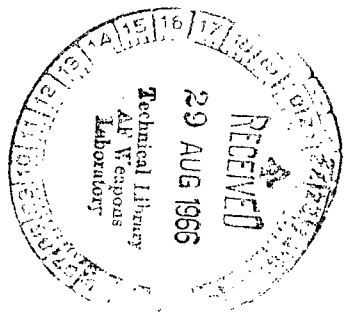

NATIONAL AERONAUTICS AND SPACE ADMINISTRATION • WASHINGTON, D. C. • AUGUST 1966

NASA TN D-3542

LOW-SPEED WIND-TUNNEL STUDIES RELATING TO PITCH-UP ON A SUPERSONIC TRANSPORT MODEL WITH A HIGH-ASPECT-RATIO VARIABLE-SWEEP WING

By Vernard E. Lockwood

Langley Research Center
Langley Station, Hampton, Va.

NATIONAL AERONAUTICS AND SPACE ADMINISTRATION

For sale by the Clearinghouse for Federal Scientific and Technical Information
Springfield, Virginia 22151 – Price $3.00

LOW-SPEED WIND-TUNNEL STUDIES RELATING TO PITCH-UP ON A SUPERSONIC TRANSPORT MODEL WITH A HIGH-ASPECT-RATIO VARIABLE-SWEEP WING

By Vernard E. Lockwood
Langley Research Center

SUMMARY

A low-speed investigation has been made to determine methods of reducing the pitch-up tendency of a high-aspect-ratio variable-sweep wing model. The model represented a three-engine arrangement of a supersonic transport configuration where two of the nacelles were mounted below the wing on pylons supported from the fuselage and a third nacelle was mounted in the vertical tail just above the fuselage. The model had a variable-sweep cambered and twisted wing and an outboard pivot location. Among the variables studied were movable wing sweep and incidence; sweep, size, and deflection of the forewing; canard size and deflection; and horizontal-tail size and deflection. Also included are the effects of fuselage nose cross-sectional shape on the lateral directional stability characteristics.

The investigation showed the basic model to have a pitch-up tendency which increased as the movable wing leading-edge sweep was increased from 0° to 25°. At the wing-sweep angle of 16°, for which most of the investigation was made, the pitch-up started at an angle of attack as low as 8°. The results of the study showed the pitch-up tendency of the model could be reduced materially either by deflection of a forewing flap or by reduction in sweep and size of the forewing. Addition of deflected canards also reduced the pitch-up tendencies. Improvement in the lift-drag ratios was noted for the model with deflected forewings or forewings with reduced sweep and for the canards with small deflections. Positive incidence changes in the movable wing also increased lift-drag ratios. The modifications which improved the stability and lift-drag ratios generally resulted in improved horizontal-tail effectiveness.

A change from the basic cross section of the fuselage nose to a circular section reduced the directional stability at an angle of attack above 10° by reducing the favorable side-force variation with angle of attack.

The investigation was made in the Langley high-speed 7- by 10-foot tunnel at a Mach number of 0.20, which corresponds to a Reynolds number of 10.7×10^6 based on the fuselage length.

INTRODUCTION

Recent wind-tunnel investigations of variable-sweep supersonic transport configurations have indicated pitch-up problems in the intermediate to high angle-of-attack range. One investigation (ref. 1) which employed high-aspect-ratio wing panels with outboard pivots indicated that the pitch-up began at an angle of attack as low as 5^o for the 16^o movable-wing-sweep position. It was thought that the pitch-up was caused by a combination of nonlinear pitching moments of the forewing-fuselage combination reinforced by flow separation on the outer movable wing. The possibility of reducing this pitch-up by raising the horizontal tail from its position in the wing-chord plane was investigated and the results (ref. 1) indicated that the tail gave greater stability at low angles of attack, but contributed destabilizing moments at the high angles of attack because it became immersed in the wing wake. Lower horizontal-tail positions were considered, but were assumed to be impractical because of the proximity of the tail to the engine exhaust. Since it was believed that the forewing-fuselage combination was responsible, to a large degree, for the pitch-up of the configuration, the possibility of variations in forewing geometry was considered as a means of reducing the pitch-up problem.

The present paper is an extension of the investigation of reference 1 to include studies of variables associated with the forewing geometry. The variables included changes in sweep, size, shape, and deflection of a forewing flap. Canards also were studied as a means of reducing the pitch-up of the basic model; in this respect, it was thought that the stalling of the canard might tend to compensate for the nonlinear lift on the forewing.

Most of the investigation was made with the movable-wing leading-edge sweep angle at 16^o and the movable-wing incidence at 0^o. A limited amount of data, however, was also obtained at other sweep angles and incidence angles. The basic horizontal tail of the model (ref. 1) which had 20^o anhedral was used for most of the study, but data also were obtained with the anhedral eliminated and with a flat-plate tail having an area about 51 percent greater than the basic configuration. The investigation included experiments to determine the effect on directional stability of changing the basic fuselage nose cross-sectional shape to one having a circular shape.

The investigation was made in the Langley high-speed 7- by 10-foot tunnel at a Mach number of 0.2 and a Reynolds number of 10.7×10^6 based on the fuselage length.

SYMBOLS

The force and moment data contained herein are referred to the axis system shown in figure 1. The reference dimensions used in reducing the data are given in figure 2 and table I and are the same as those used in reference 1.

Measurements for this investigation were taken in the U.S. Customary System of Units. Equivalent values are indicated herein parenthetically in the International System (SI) in the interest of promoting use of this system in future NASA reports. Details concerning the use of SI, together with physical constants and conversion factors, are given in reference 2.

The moment reference for most of the configurations investigated is at the wing pivot station or 5.715 reference chords behind fuselage station 0. For model configurations with the canards installed or with forewing-sweep angles other than 76°, a moment reference was chosen which would give the same degree of stability as that of the basic model with a movable-wing-sweep angle of 16°.

b reference wing span, 85.84 inches (2.180 meters)

b_c span of canard, inches (meters)

C_D drag coefficient, $\frac{\text{Drag}}{qS}$

C_L lift coefficient, $\frac{\text{Lift}}{qS}$

ΔC_L increment in lift coefficient

C_{L_α} lift-curve slope at $C_L = 0$

C_l rolling-moment coefficient, $\frac{\text{Rolling moment}}{qSb}$

$$C_{l_\beta} = \frac{\left(C_{l,\beta=5^{\circ}} - C_{l,\beta=-5^{\circ}}\right)}{\Delta\beta}$$

C_m pitching-moment coefficient, $\frac{\text{Pitching moment}}{qSc}$

ΔC_m increment in pitching-moment coefficient

$\partial C_m/\partial C_L$ pitching-moment-curve slope at $C_L = 0$

C_n yawing-moment coefficient, $\frac{\text{Yawing moment}}{qSb}$

$C_{n_\beta} = \frac{(C_{n,\beta=5^o} - C_{n,\beta=-5^o})}{\Delta\beta}$

C_Y side-force coefficient, $\frac{\text{Side force}}{qS}$

$C_{Y_\beta} = \frac{(C_{Y,\beta=5^o} - C_{Y,\beta=-5^o})}{\Delta\beta}$

c reference wing chord, 9.93 inches (0.2522 meter)

c_r root chord of canard, inches (meters)

c_t tip chord of canard, inches (meters)

L/D lift-drag ratio

$(L/D)_{max}$ maximum lift-drag ratio

q dynamic pressure, pounds/feet^2 (newtons/meter^2)

S reference wing area, 3.94 feet^2 (0.3660 meter^2)

S_c canard area, feet^2 (meter^2)

x/c moment reference location from nose of model, reference wing chords

α angle of attack of fuselage reference line, degrees

β angle of sideslip, degrees

$\Delta\beta$ increment in sideslip between $\beta = \pm 5^o$, corrected for balance and strut deflection, degrees

δ_h horizontal-tail deflection (positive when trailing edge is down), degrees

δ_f forewing flap deflection (positive when leading edge is down), degrees

i_w movable-wing incidence (positive when leading edge is up), degrees

Λ wing leading-edge sweep angle, degrees

δ_c canard incidence (positive when leading edge is up), degrees

Configuration designations:

B fuselage

B_1, B_2 specific fuselage (see fig. 5)

C canard

C_1, C_2, C_3 specific canard (see fig. 7(b))

$F_1 \ldots F_7$ forewing or forewing flaps (see fig. 6)

H horizontal tail

H_1, H_2, H_3 specific horizontal tail (see fig. 7(a))

N fuselage-mounted engine nacelles

V_N vertical tail with engine nacelle

W movable wing

MODEL

The basic model investigated features a high-aspect-ratio variable-sweep wing with an outboard pivot and a three-engine nacelle arrangement as shown in figure 2. A photograph of the model in the Langley high-speed 7- by 10-foot tunnel with the movable wing at 16^o leading-edge sweep is shown as figure 3. This model is essentially the same model as that investigated and reported in reference 1 except that the airfoil sections are different. The airfoil sections of the present wing are presented to scale in figure 4. Other dimensions of the basic model are given in table I.

During the investigation the basic fuselage nose cross-sectional shape B_1 was altered to a circular section B_2 as shown in figure 5. The cross-sectional-area distribution was identical for the B_1 and B_2 nose sections. The B_2 nose blended into the main body at fuselage station 29.59 in. (0.7516 m).

Several modifications were made to the forewing area between the fuselage and movable wing and also between fuselage stations 29.50 in. (0.7493 m) and 54.13 in. (1.3749 m). The modifications referred to as forewing flaps are portions of the forewing capable of being deflected as shown in figure 6. Forewing flaps F_1, F_2, and F_3 had 76^o leading-edge sweep and hinge lines perpendicular to the plane of symmetry as shown in figure 6(a). Forewing flaps F_4, F_5, and F_6 had leading-edge sweeps of 76^o, 73^o, and 72^o, respectively, as shown in figure 6(b). Forewing flap F_4 had a hinge-line sweep of 70^o whereas forewing flaps F_5 and F_6 had hinge-line sweeps of 66^o. Forewing flap F_7 had a leading-edge sweep of 70^o and was not deflected.

Three horizontal-tail configurations were tested on the model. Tail H_1 corresponds to the basic horizontal tail tested in reference 1 which had 20^o of anhedral as shown in figure 7(a). Configuration H_2 was the same surface as H_1 but with the dihedral angle removed. A larger horizontal tail H_3 made of 0.25 in. (0.0064 m) aluminum plate and having no dihedral was utilized for some tests. Other details concerning the horizontal tails are given in figure 7(a) and tables II and III.

Canards C_1, C_2, and C_3 used in the investigation are illustrated in figure 7(b). They were made of 0.125-in.-thick brass with rounded leading edges and blunt trailing edges. They had an aspect ratio of 3.0 and were mounted with 50 percent of their root chord at fuselage station 10.40 in. (0.2642 m). Other details of the canards are given in figure 7(b) and table IV.

TEST AND CONDITIONS

The investigation was made in the Langley high-speed 7- by 10-foot tunnel. The model was sting mounted, as shown in figure 3. Forces and moments were measured by an internally mounted six-component strain-gage balance. To insure a turbulent boundary layer, transition strips of No. 100 carborundum grit approximately 1/8 inch wide were affixed to the model at 7 percent of the length of the body and at 7 percent of the chord of the wing and all appendages.

The tests were made at a dynamic pressure of 56.9 lb/ft^2 (2723 N/m^2), a Mach number of 0.2, and an average Reynolds number of 10.7×10^6 based on the fuselage length. In addition to the normal angle-of-attack runs at 0^o sideslip, some selected configurations also were tested at $\pm 5^o$ sideslip.

The drag data were corrected to correspond to a pressure at the base of the engine nacelles and the base of the fuselage equal to free-stream static pressure. The nacelles had constant-diameter internal passages, for which an axial-force coefficient of 0.00254 for all three nacelles was calculated as being the internal skin friction due to flow through the nacelles. This value was subtracted from the drag coefficient obtained experimentally.

The jet-boundary corrections calculated for the drag and angle of attack by the method of reference 3 for the reference sweep condition are as follows:

$$C_D = (C_D)_{measured} + (0.006225)C_L^2$$

$$\alpha = \alpha_{measured} + (0.394000)C_L$$

The jet-boundary corrections to the pitching-moment data were found to be negligible. The data were also corrected for wind-tunnel blockage by the method presented in reference 4. The angles of attack and sideslip were corrected for deflection of the sting-support system under load.

PRESENTATION OF DATA

The results of the investigation are presented in the following figures:

DISCUSSION

Longitudinal Stability

Movable-wing sweep.- The movable-wing-sweep effects on the aerodynamic characteristics of the basic configuration $B_1WH_1V_NNF_1$, $\delta_f = 0^o$, and $i_w = 0^o$, are shown in figure 8. It will be noted that pitch-up tendencies exist in the data for all sweep angles and become more pronounced as the wing-sweep angle is increased from 0^o to 25^o. For the wing-sweep angle of 16^o, for which most of the tests were made, the pitch-up started as low as an angle of attack of 8^o. The trend of C_m with α or C_L is similar to that experienced with the model of reference 1 which had the same fuselage and tail configuration but, as previously mentioned, different wing airfoil sections. In the earlier investigation as in the present one, the pitch-up was attributed to airflow separation over the wing combined with increasing lift on the forewing. Wings experienced early separation as indicated by tuft studies beginning at 5^o in the case of reference 1 and at 8^o in the present study.

A plot of the low-lift aerodynamic parameters against sweep angle (fig. 9) shows that the aerodynamic center varies linearly with sweep over the range of sweep angles tested. The overall variation amounts to about 48 percent of the reference chord for movable-wing-sweep angles from 0^o to 25^o.

Movable-wing incidence.- The effects of positive changes in movable-wing incidence are shown in figure 10. The data at high angles of attack show the pitch-up tendency was essentially unchanged for all incidence angles tested. At low angles of attack, the increased incidence gave negative trim changes of sizable magnitude and a small forward shift in the aerodynamic center as indicated in figure 11. The change in trim is equivalent to about 4^o of up elevator (fig. 25). The most noteworthy effect of incidence change, however, was the increase in $(L/D)_{max}$ which amounted to about 2.3 units. The increase in $(L/D)_{max}$ probably results from a more favorable matching of the loading on the outboard panel with that on the highly swept forewing.

Forewing sweep.- One of the modifications tested which improved the low-speed high-angle-of-attack characteristics but which would compromise the high Mach number cruise configuration is lower sweep on the forewing, as indicated in figure 12. Reduction of the sweep angle from 76^o with F_1 to 70^o with F_7 reduced the pitch-up tendency considerably; a sizable reduction was also indicated for the configuration F_5 with 73^o sweep. The improved characteristics probably result from a more linear lift variation with angle of attack over the forewing, decrease of forewing area, smaller induced effects on the adjoining movable wing, and improved flow conditions at the horizontal tail. The improved flow conditions at the tail are in evidence in figure 13 where the horizontal-tail

contribution to stability ΔC_m is shown to be greater at an angle of attack above 12^o for the forewings having 70^o and 73^o of sweep than for the forewing having 76^o sweep.

In addition to the improvements in pitch characteristics, there was also an increase in $(L/D)_{max}$. Reduction of the forewing sweep from 76^o to 70^o resulted in an increase of 1.8 in $(L/D)_{max}$ as shown in figure 12.

Forewing flap deflection.- The deflection of the forewing flaps with 76^o sweep and axes perpendicular to the plane of symmetry F_1, F_2, and F_3 gave considerable reductions in pitch-up tendencies. The reductions in pitch-up which increased as the area of the forewing flap increased appeared to result mainly from losses in lift on the fixed apex as indicated in figure 14. Some of the reduction in pitch-up may also be due to improved flow conditions for the outboard movable panel as well as the horizontal tail. Evidence of the improved flow conditions at the tail is shown in figure 15 in the plot of ΔC_m against α. The tail contribution to stability ΔC_m at high angles of attack is greater with the forewing flap deflected 10^o than with the flap undeflected.

The pitching-moment improvements shown by the deflected flaps were not without compromise to the other characteristics. There were losses in $(L/D)_{max}$ for the large deflections of the flaps which were required for material improvements in the high-angle-of-attack stability. Additional losses in $(L/D)_{max}$ would occur in trimming out the negative pitching moment resulting from flap deflection.

Figure 16 shows the effect of deflecting forewing flaps F_4 and F_6 about hinge lines which have sweep angles of 70^o and 66^o, respectively. These flap configurations as in the case of F_1 and F_2 gave considerable reduction in the pitch-up tendency but unlike F_1 and F_2 gave only minor changes in the variation of C_m or C_L with α in the low-lift range.

Neither flap eliminated the pitch-up, but with 30^o deflection the variation of C_m with C_L or α was closer to being linear with F_6 than with F_4 (which had the larger leading-edge sweep). Both flaps show increases in $(L/D)_{max}$ over the basic configuration (F_4 undeflected) for a wide angle-of-attack range. This characteristic indicates the possibility of improving the low-speed lift-drag ratios of airplanes designed principally from supersonic considerations.

Canards.- A comparison of the aerodynamic characteristics of the basic model with those of the canard (undeflected) configuration is given in figure 17. These data indicate a destabilizing action on the model at high angles of attack with the horizontal tail off, but with the horizontal tail on, the pitch characteristics are similar to those of the basic model. The stabilizing effect of the canards on the horizontal-tail characteristics is shown in figure 18 and is similar to that achieved with deflected forewing flaps or reduced sweep on the forewing. When the canards are deflected positively (fig. 19), a stabilizing tendency is

noted as the result of the canard stall. For example, a 10° deflection of the largest canard C_3 resulted in a loss of lift and an increase in C_L for pitch-up from 0.9 to 1.3. (See fig. 19(c).) A corresponding increase of α also was noted. The stalling of the canards, however, produces a slight loss of lift and an increase of drag that materially reduce the L/D of the configuration.

In contrast to the losses of lift from the deflected canards, the presence of the undeflected canards materially increased the L/D of the basic configuration. (See fig. 17.) In the case of C_2, the untrimmed increment in $(L/D)_{max}$ was about 3.0. These increases in L/D along with those obtained from other modifications indicate that methods are available for increasing the low-speed L/D of configurations designed principally for supersonic cruise.

Fuselage.- Because of the reduced area in the pitch plane, it would be expected that the fuselage with the circular sections B_2 would give less positive pitching moments than the basic fuselage B_1. This configuration, which was tested with forewing flap F_6 deflected 22.5°, is shown in figure 20 and it will be noted that the circular fuselage provided a slight reduction in pitch-up.

Horizontal tail.- A comparison of the aerodynamic characteristics of three horizontal-tail configurations is given in figure 21 and of the three configurations the basic tail with -20° dihedral H_1 is the most effective in reducing pitch-up. The effectiveness of H_2 is reduced at high angles of attack. Although H_3 has a greater degree of initial stability, it tends to diminish in effectiveness as the angle of attack increases above 8°. (See fig. 22.) The -20° dihedral of H_1 probably places it in a more favorable field of downwash than H_2 or H_3.

Longitudinal Control

The longitudinal control parameter $\partial C_m/\partial \delta_h$ determined from the data of figures 23 and 24 for 5° deflection of the horizontal tail is presented in figure 25. The horizontal-tail control is positive everywhere $\left(\text{negative values of } \partial C_m/\partial \delta_h\right)$ within the angle-of-attack range investigated. The values of $\partial C_m/\partial \delta_h$ became more negative (this condition is indicative of an increase of control) at an angle of attack above 3° because of the emergence of this horizontal control from the wing wake. The increased effectiveness of H_3 over H_1 is approximately proportional to the increase in horizontal-tail area.

Lateral Directional Stability

The data of figure 26 show the effect on the lateral directional stability parameters of changing from the basic nose B_1 to the circular nose B_2. This change in cross-sectional shape resulted in C_{n_β} and C_{Y_β} decreasing with $\alpha > 10^{\circ}$. The unusual

variations of C_{n_β} and C_{Y_β}, that is, the positive increase of the parameters in the upper angle-of-attack range, were noted in reference 1 for B_1. It was suggested that a force opposed to the normal cross-flow components was being developed on the nose of the fuselage as a result of the particular cross-sectional shape. Previous experience with two-dimensional noncircular cross sections (ref. 5) had shown that cross-wind forces opposite to those generally expected can develop on cylinders at certain Reynolds numbers and section orientation. It was presumed that this property was responsible for the increase in C_{n_β} and C_{Y_β} exhibited in figure 26 for configurations with vertical tail off and on. This supposition was confirmed when it was shown (fig. 26) that the values of C_{n_β} and C_{Y_β} were considerably less positive at high angles of attack for the circular nose model than for the basic nose model. In fact, the circular nose model with vertical tail became directionally unstable above $\alpha = 21^\circ$.

Although these data suggest the possibility of improving the directional stability characteristics of an airplane configuration employing a long nose by proper selection of a cross-sectional shape, care must be used in applying these data because of Reynolds number effects. Very large differences exist in the cross-section Reynolds number range represented by these tests and those that would exist on a full-scale airplane in the landing or take-off attitude. In addition to Reynolds number and cross-sectional forebody shape nose pointedness appears to be an important factor in the development of favorable side forces, as indicated in reference 6. These data, which are for some isolated bodies having varying cross-sectional ellipticity and which may be employed as fuselage forebodies, show that the side force can be dependent on forebody fineness ratio.

SUMMARY OF RESULTS

An investigation has been made in the Langley high-speed 7- by 10-foot tunnel to determine methods of reducing the pitch-up tendency of a variable-sweep wing configuration employing a highly swept forewing and an outboard pivot. The results of the low-speed investigation are summarized as follows:

1. The basic model exhibited an increasing pitch-up tendency as the movable-wing leading-edge sweep angle was increased from 0° to 25°. For the wing position of 16°, for which most of the investigation was made, the pitch-up tendency started as low as an angle of attack of 8°.

2. The pitch-up tendency of the model could be reduced materially by use of deflected forewing flaps, by substitution of a lower sweep angle of the leading edge of the forewing or addition of deflected canards.

3. Improvements in the maximum lift-drag ratio over the basic model were obtained with several deflected forewing flaps, reduced sweep angle of the forewing, addition of

canards with little or no deflection, or positive change in incidence of the movable wing.

4. The modifications which improved the pitch-up characteristics and lift-drag ratios generally resulted in improved horizontal-tail effectiveness.

5. Changing the cross-sectional shape of the fuselage nose from the basic shape to circular reduced the directional stability at angles of attack above 10° by reducing the favorable side-force variation with angle of attack.

Langley Research Center,
National Aeronautics and Space Administration,
Langley Station, Hampton, Va., March 28, 1966.

REFERENCES

1. Lockwood, Vernard E.; McKinney, Linwood W.; and Lamar, John E.: Low-Speed Aerodynamic Characteristics of a Supersonic Transport Model With a High-Aspect-Ratio Variable-Sweep Warped Wing. NASA TM X-979, 1964.

2. Mechtly, E. A.: The International System of Units – Physical Constants and Conversion Factors. NASA SP-7012, 1964.

3. Gillis, Clarence L.; Polhamus, Edward C.; and Gray, Joseph L., Jr.: Charts for Determining Jet-Boundary Corrections for Complete Models in 7- by 10-Foot Closed Rectangular Wind Tunnels. NACA WR L-123, 1945. (Formerly NACA ARR L5G31.)

4. Herriot, John G.: Blockage Corrections for Three-Dimensional-Flow Closed-Throat Wind Tunnels, With Consideration of the Effect of Compressibility. NACA Rept. 995, 1950. (Supersedes NACA RM A7B28.)

5. Polhamus, Edward C.; Geller, Edward W.; and Grunwald, Kalman J.: Pressure and Force Characteristics of Noncircular Cylinders as Affected by Reynolds Number With a Method Included for Determining the Potential Flow About Arbitrary Shapes. NASA TR R-46, 1959.

6. Spencer, Bernard, Jr.; and Phillips, W. Pelham: Transonic Aerodynamic Characteristics Of a Series of Bodies Having Variations in Fineness Ratio and Cross-Sectional Ellipticity. NASA TN D-2622, 1965.

TABLE I.- BASIC MODEL DIMENSIONS

Fuselage:	
Length	91.00 in. (2.3114 m)
Base area	0.080 sq ft (0.0074 sq m)
Chamber area	0.034 sq ft (0.0032 sq m)
Wing (reference):	
Leading-edge sweep	16.0 deg
Root chord	9.93 in. (0.2522 m)
Tip chord	3.29 in. (0.0836 m)
Span	85.84 in. (2.1803 m)
Area	3.94 sq ft (0.3660 sq m)
Aspect ratio	12.99
Taper ratio	0.33
Wing (actual):	
Leading-edge sweep	16.0 deg
Root chord	10.03 in. (0.2548 m)
Tip chord	3.26 in. (0.0828 m)
Span	85.40 in. (2.1692 m)
Area	3.94 sq ft (0.3660 sq m)
Aspect ratio	12.85
Taper ratio	0.325
Horizontal tail H_1:	
Leading-edge sweep angle	65.4 deg
Root chord	14.40 in. (0.3658 m)
Tip chord	3.86 in. (0.0980 m)
Span, total	18.96 in. (0.4816 m)
Exposed area	0.889 sq ft (0.0826 sq m)
Dihedral angle	-20.0 deg
Vertical tail:	
Leading-edge sweep angle	37.3 deg
Root chord	14.00 in. (0.3556 m)
Tip chord	2.80 in. (0.0711 m)
Span, exposed	10.38 in. (0.2637 m)
Area, exposed	0.606 sq ft (0.0563 sq m)
Aspect ratio	1.24

TABLE II.- HORIZONTAL-TAIL PROJECTED DIMENSIONS

Horizontal tail H_1:		
Root chord	14.40 in.	(0.3658 m)
Tip chord	3.86 in.	(0.0980 m)
Semispan, exposed	7.26 in.	(0.1844 m)
Area, exposed	0.889 sq ft	(0.0826 sq m)
Dihedral angle	-20.0 deg	
Horizontal tail H_2:		
Root chord	14.40 in.	(0.3658 m)
Tip chord	3.86 in.	(0.0980 m)
Semispan, exposed	7.72 in.	(0.1961 m)
Area, exposed	0.889 sq ft	(0.0826 sq m)
Dihedral angle	0.0 deg	
Horizontal tail H_3:		
Root chord	17.34 in.	(0.4404 m)
Tip chord	3.86 in.	(0.0980 m)
Semispan, exposed	9.86 in.	(0.2504 m)
Area, exposed	1.343 sq ft	(0.1248 sq m)
Dihedral angle	0.0 deg	

TABLE III.- H_1 AND H_2 AIRFOIL ORDINATES

Distance from leading edge, percent chord	Surface ordinate,* percent chord
0.0	0.0
10.0	.542
20.0	.959
30.0	1.265
40.0	1.445
50.0	1.500
60.0	1.445
70.0	1.265
80.0	.959
90.0	.542
100.0	.0

*Distance from reference chord.

TABLE IV.- CANARD DIMENSIONS

Canard C_1:

Root chord, c_r	4.62 in.	(0.1173 m)
Tip chord, c_t	0.71 in.	(0.0180 m)
Span, b_c	7.96 in.	(0.2022 m)
Area, S_c	0.147 sq ft	(0.0137 sq m)

Canard C_2:

Root chord, c_r	7.08 in.	(0.1798 m)
Tip chord, c_t	1.08 in.	(0.0274 m)
Span, b_c	12.24 in.	(0.3109 m)
Area, S_c	0.346 sq ft	(0.0322 sq m)

Canard C_3:

Root chord, c_r	8.88 in.	(0.2255 m)
Tip chord, c_t	1.36 in.	(0.0345 m)
Span, b_c	15.36 in.	(0.3901 m)
Area, S_c	0.546 sq ft	(0.0507 sq m)

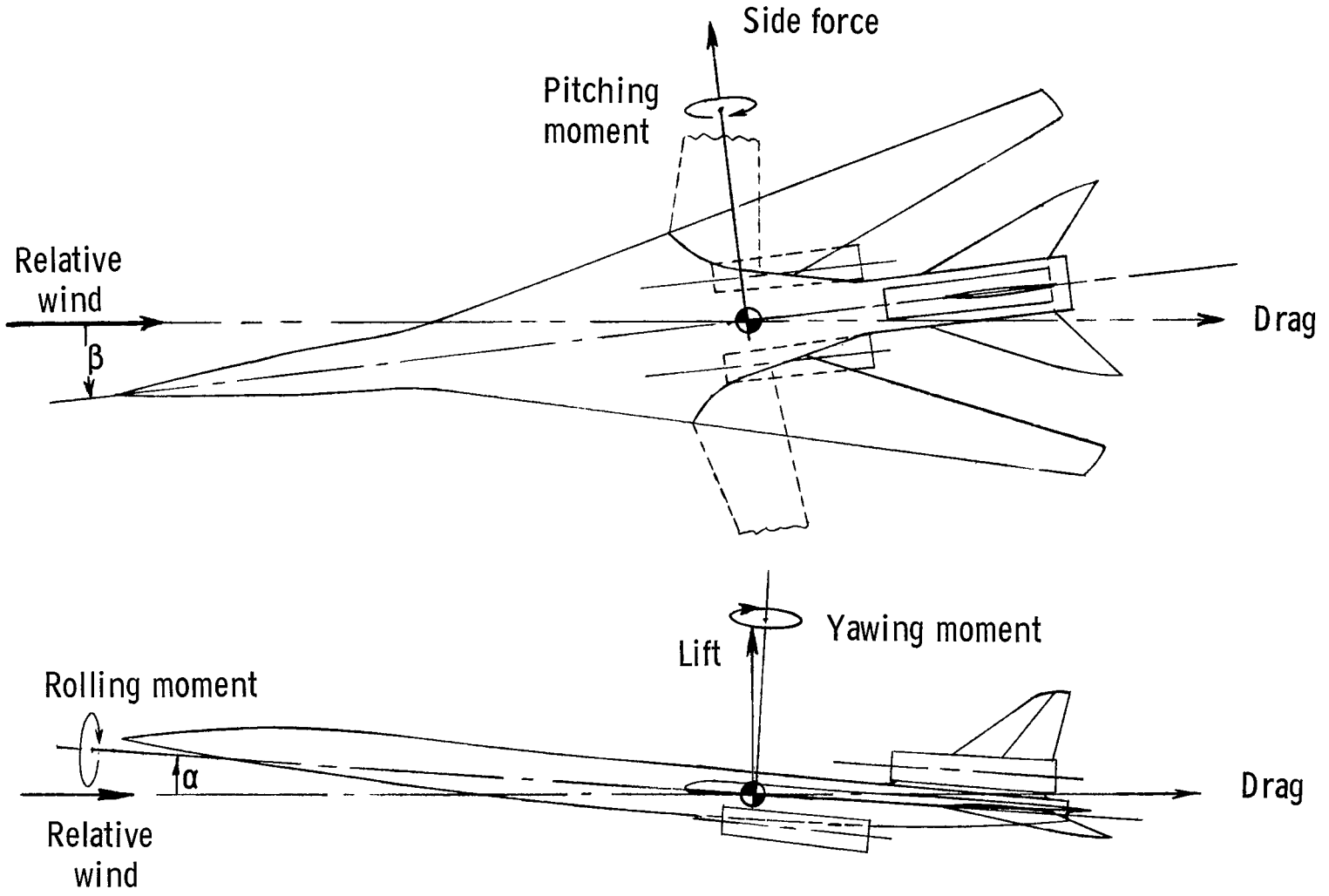

Figure 1.- System of axes used in presentation of data.

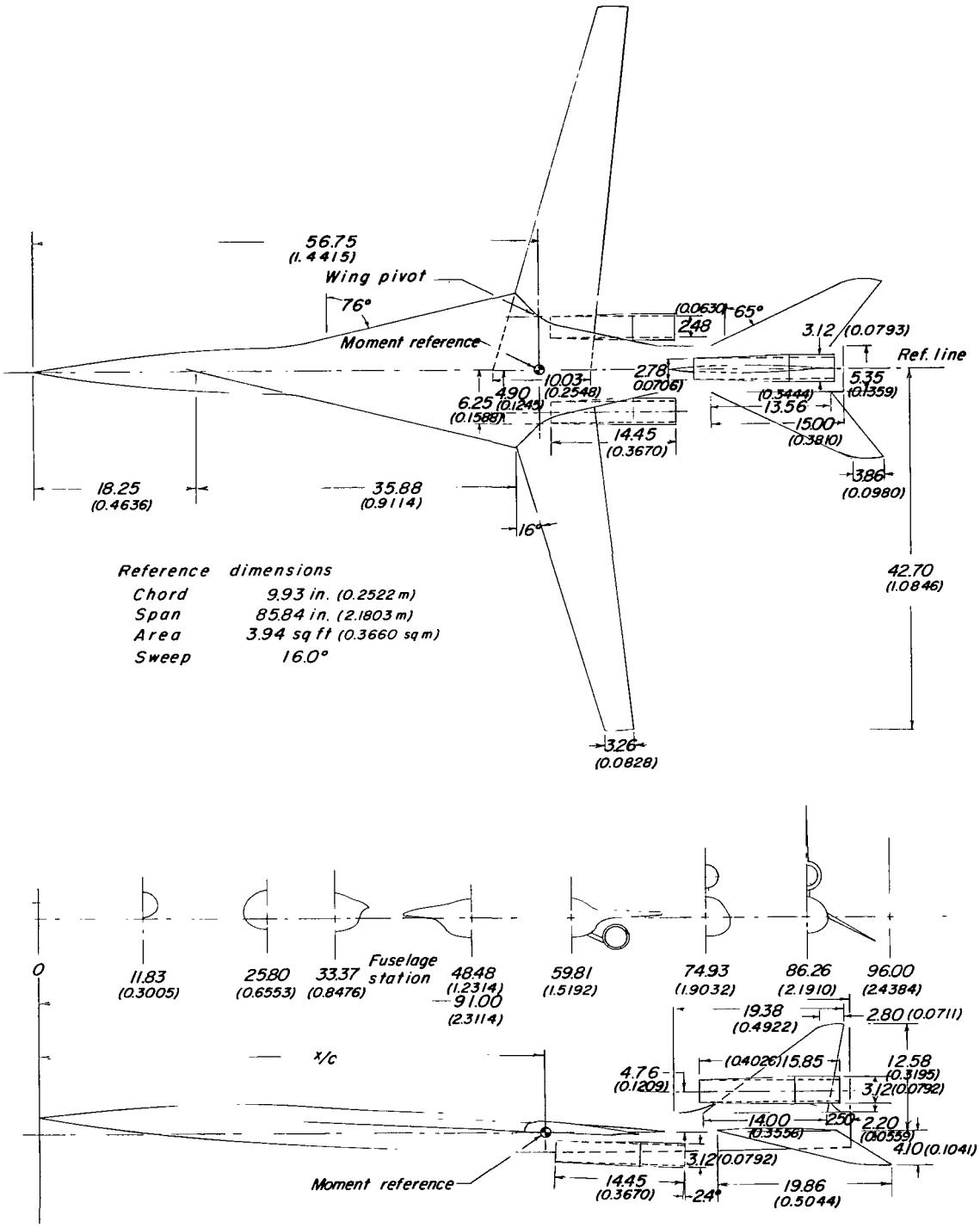

Figure 2.- Three-view drawing of model. All linear dimensions are in inches (meters).

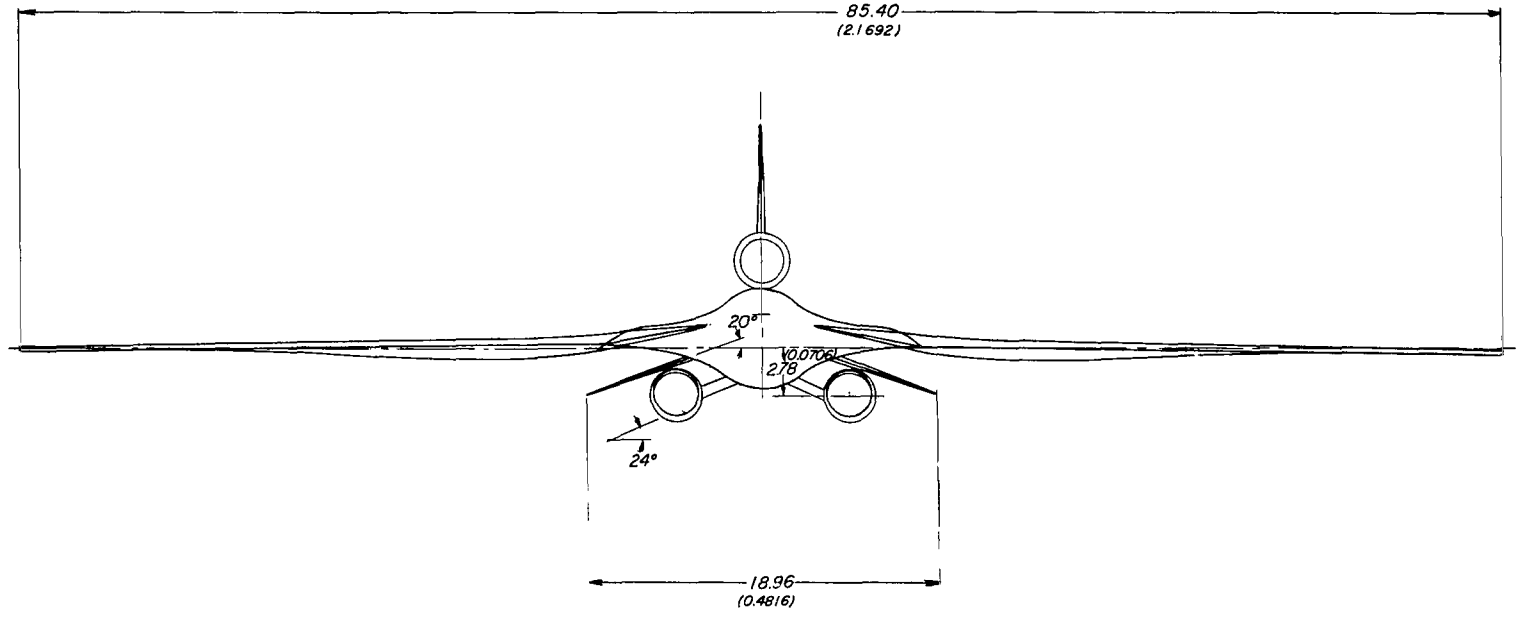

Figure 2.- Concluded.

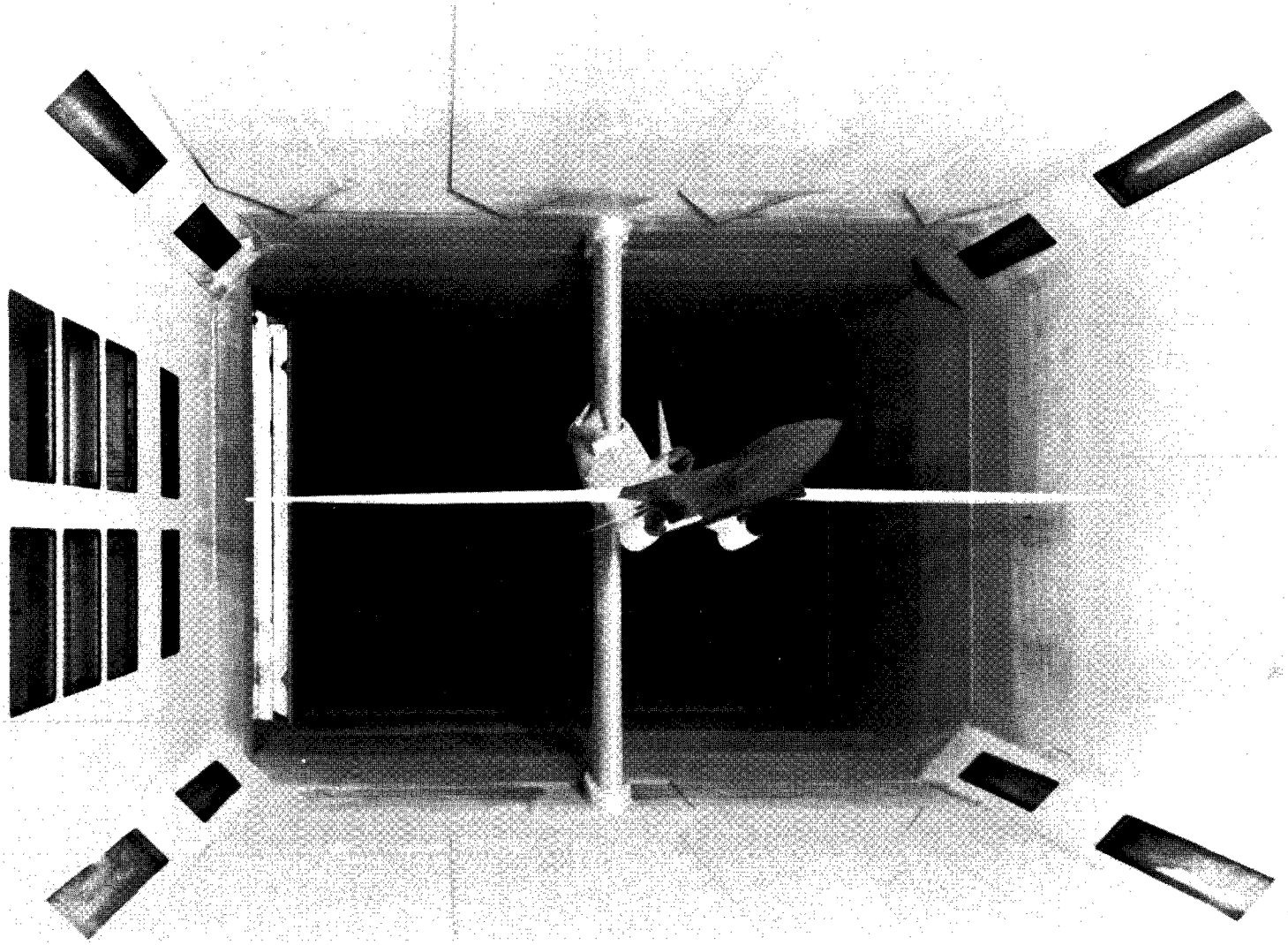

Figure 3.- Photograph of model in Langley high-speed 7- by 10-foot tunnel. L-62-8932

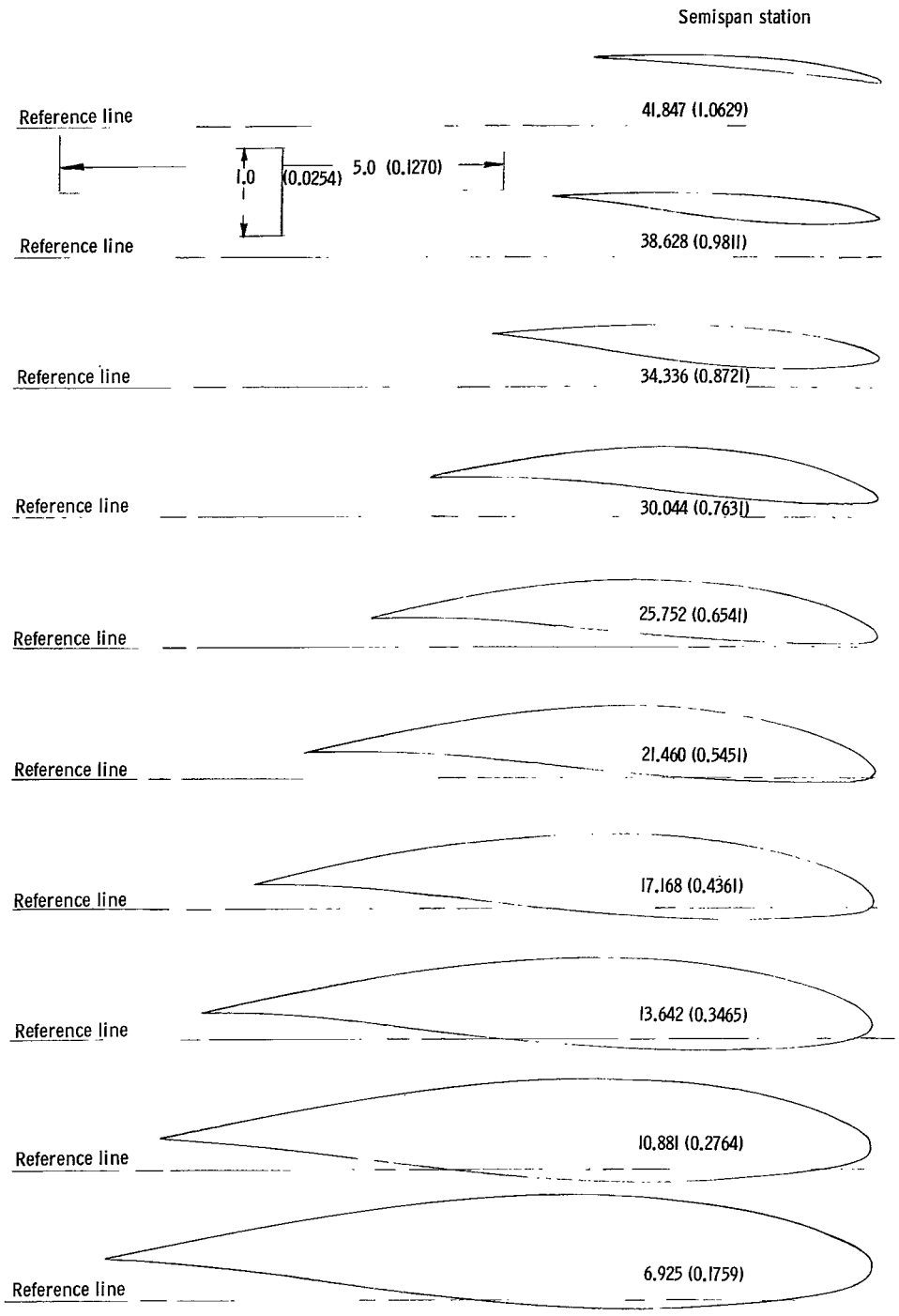

Figure 4.- Airfoil sections of wing. Dimensions are given in inches and parenthetically in meters.

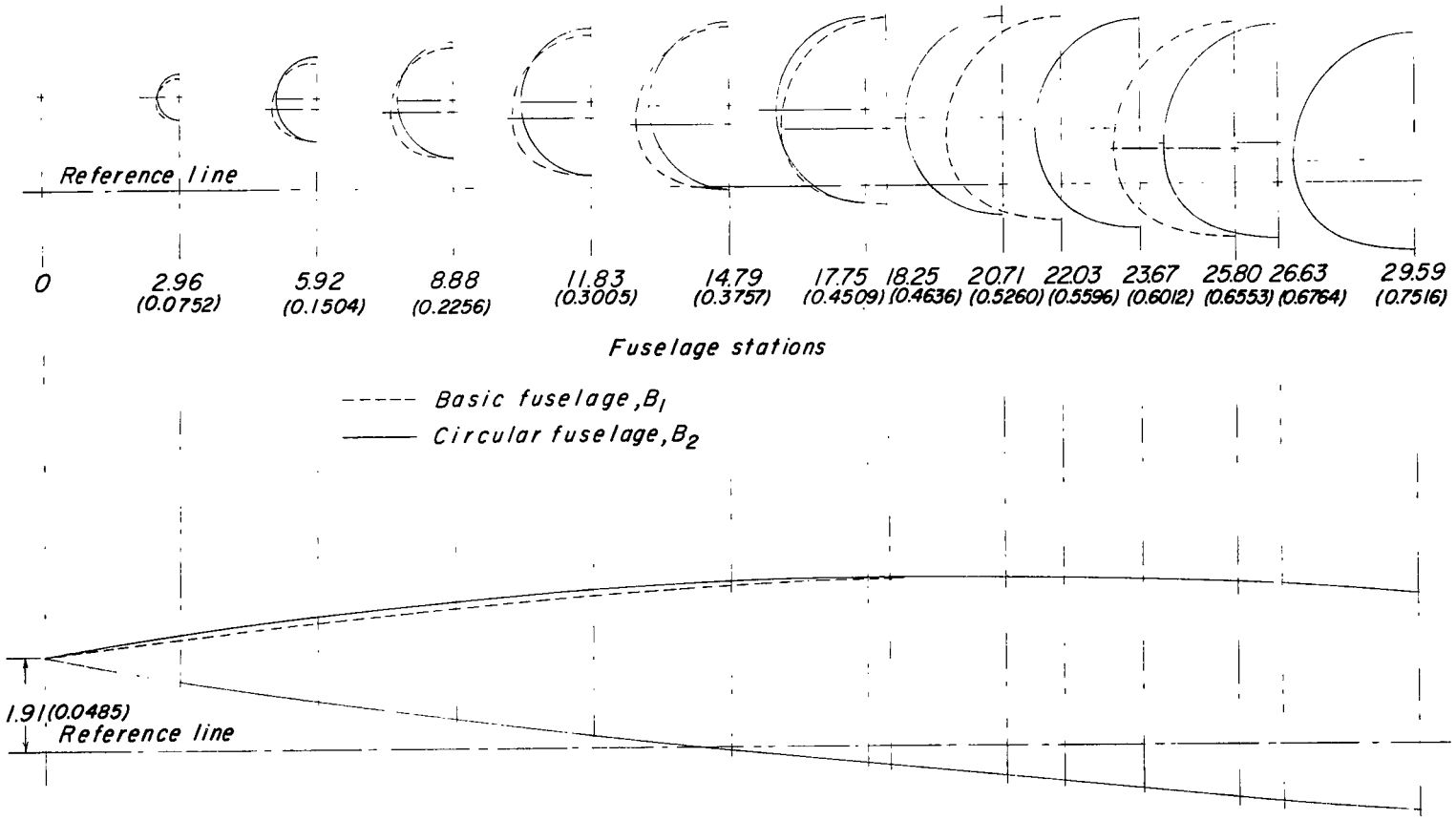

Figure 5:- Comparison of fuselage-nose shapes B_1 and B_2. Dimensions of stations are given in inches and parenthetically in meters.

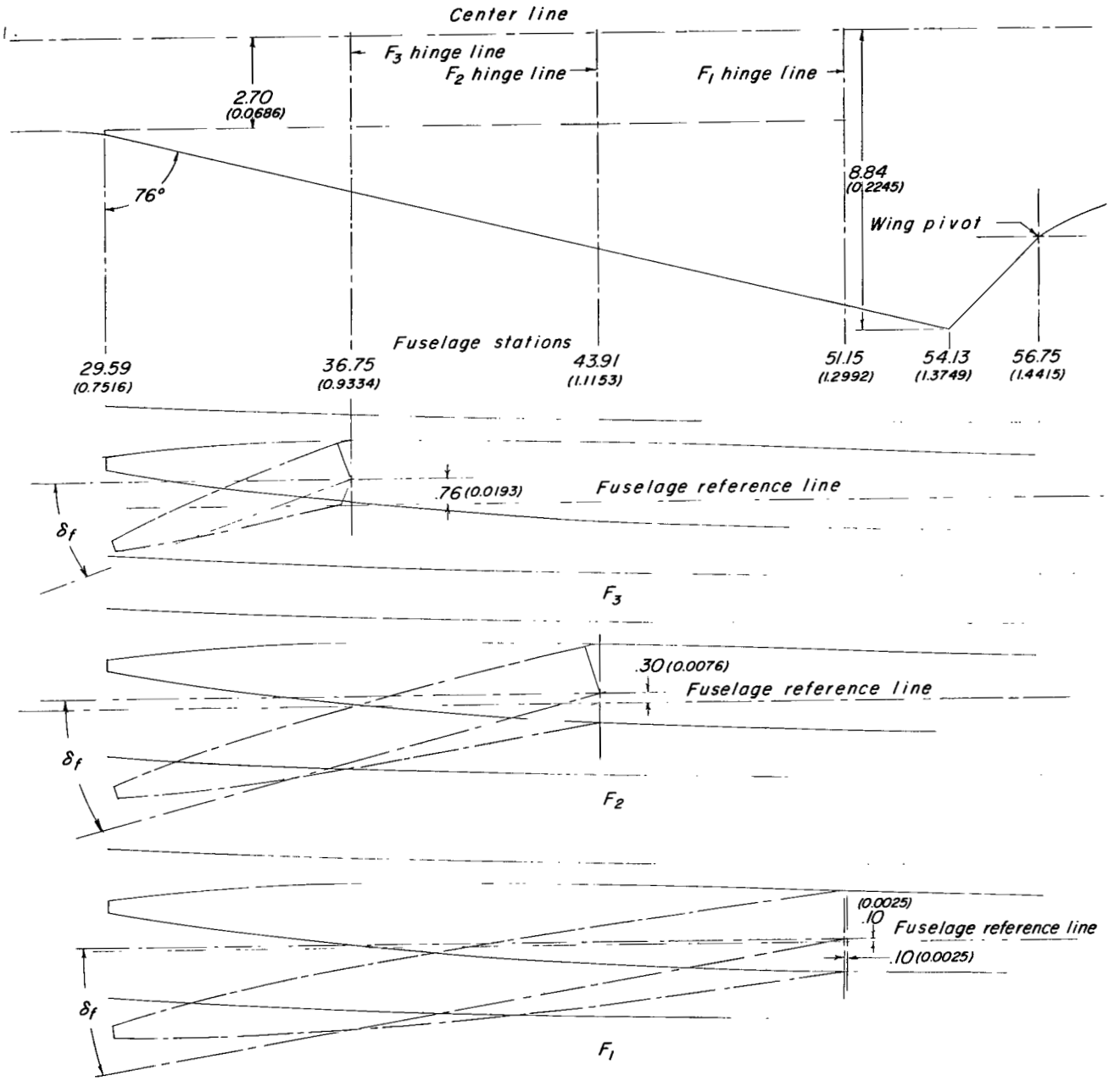

(a) F_1, F_2, and F_3.

Figure 6.- Geometry of forewing flaps. All linear dimensions are given in inches and parenthetically in meters.

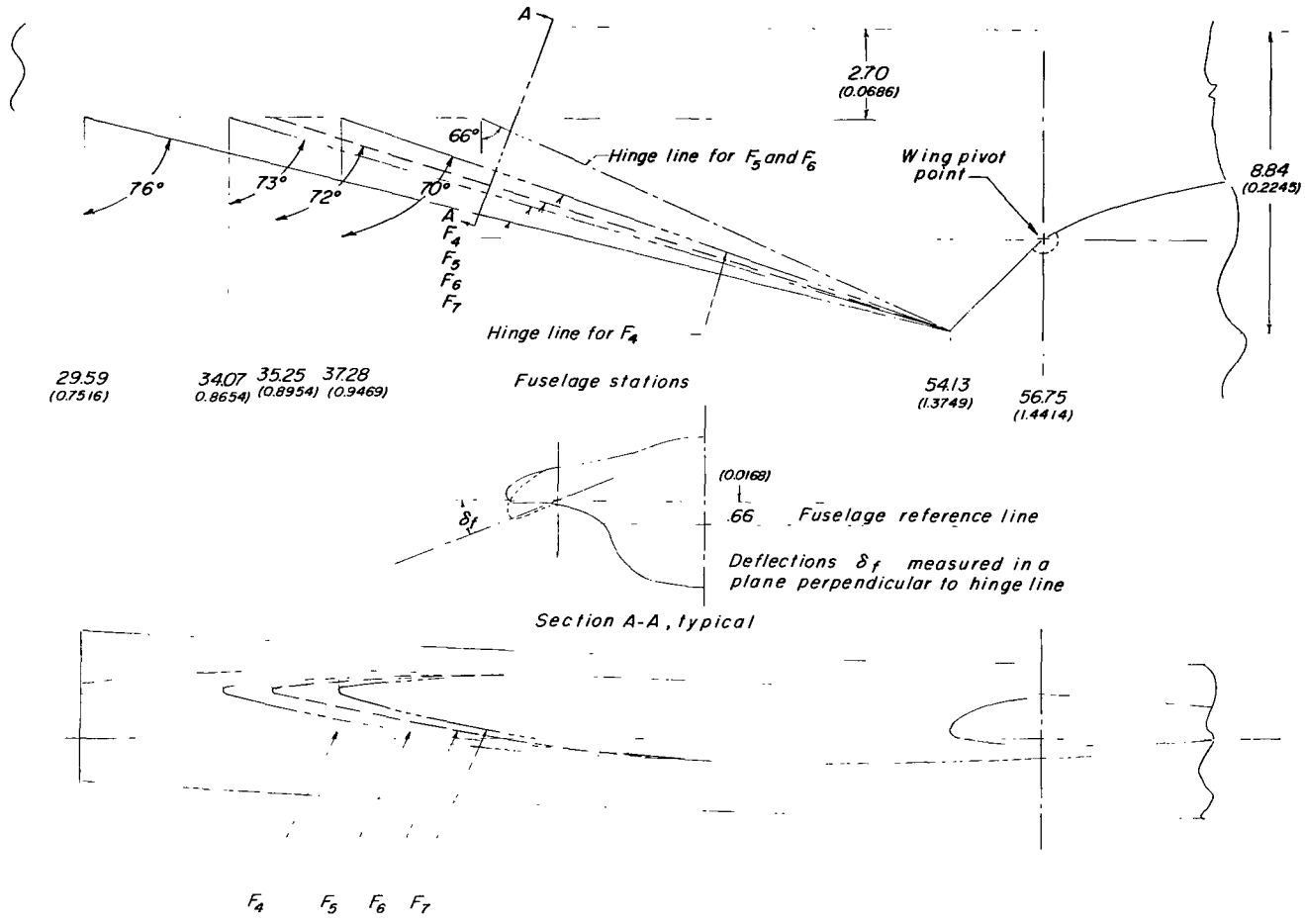

(b) F_4, F_5, F_6, and F_7.

Figure 6.- Concluded.

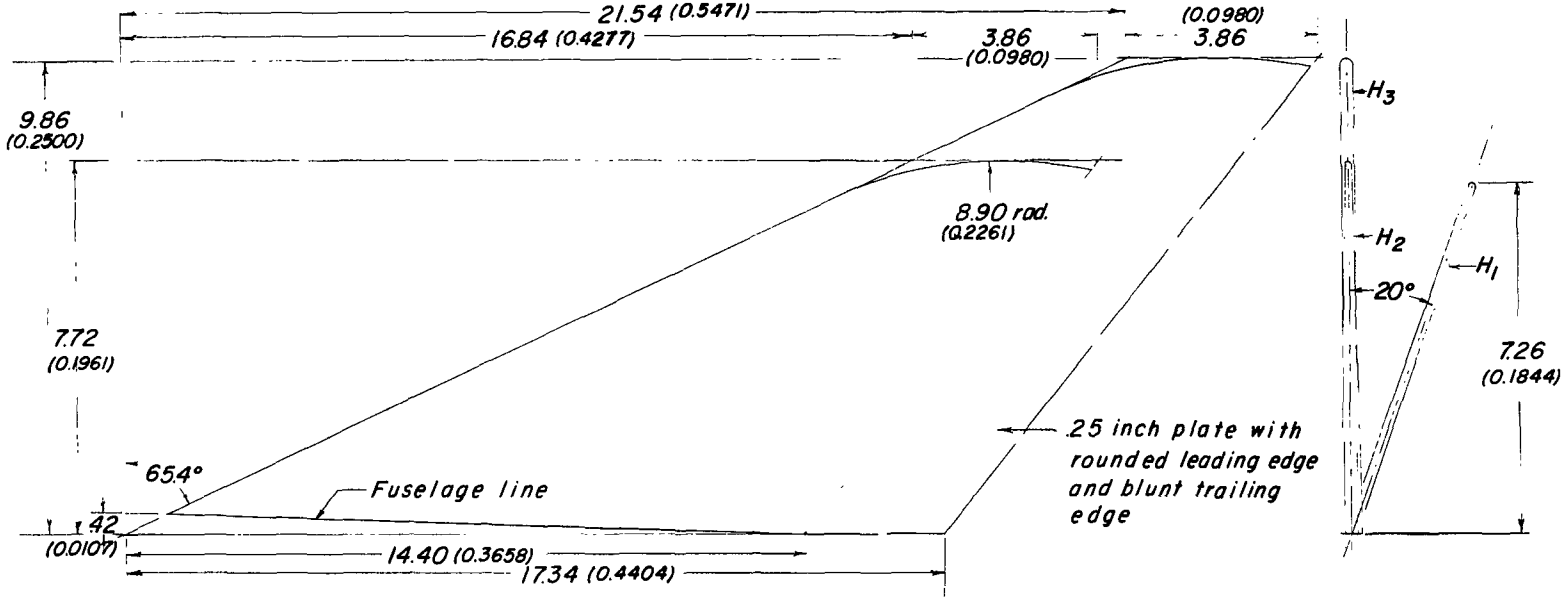

(a) Horizontal tail.

Figure 7.- Geometry of horizontal tails. All linear dimensions are given in inches and parenthetically in meters.

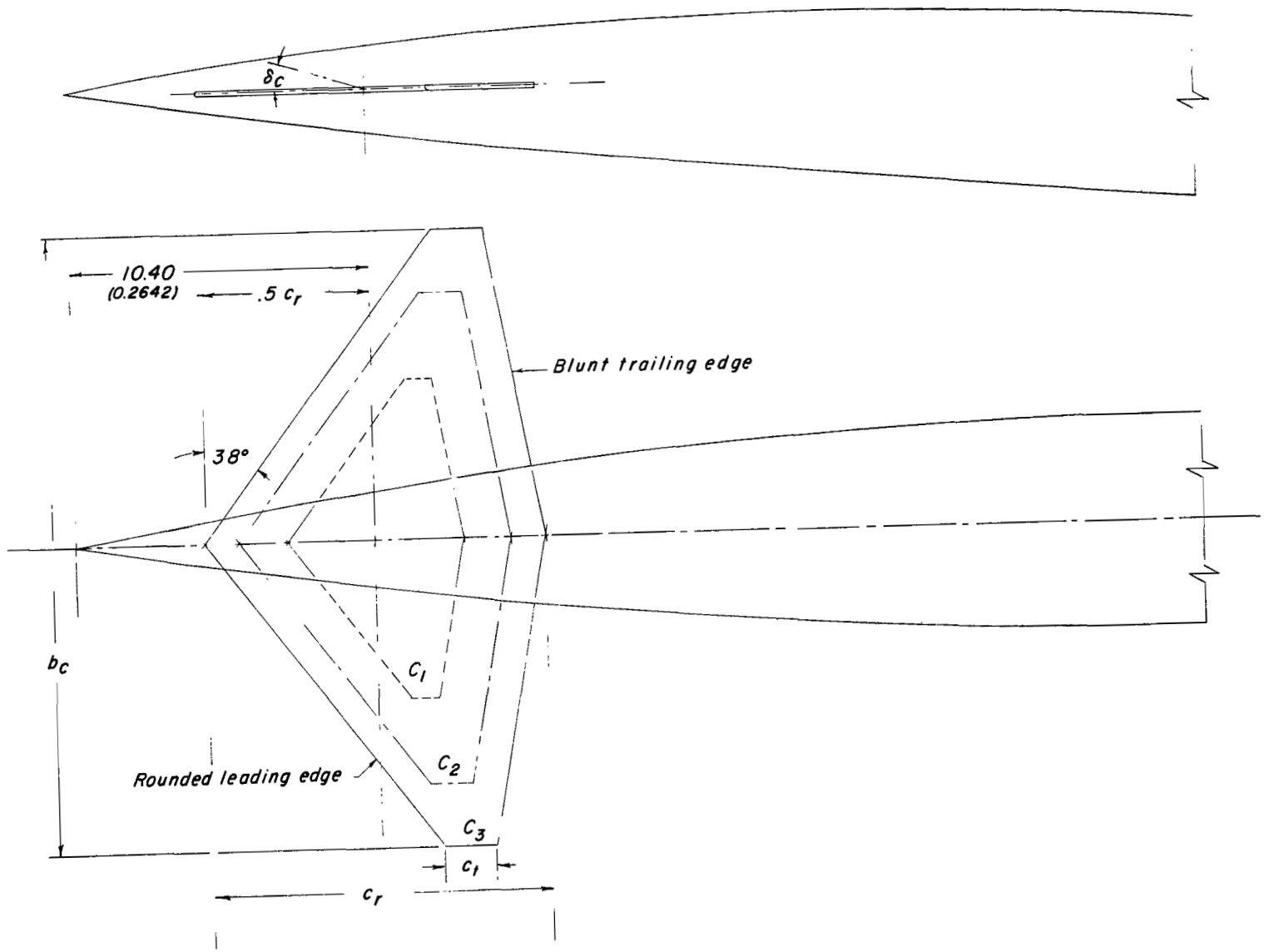

(b) Canards.

Figure 7.- Concluded.

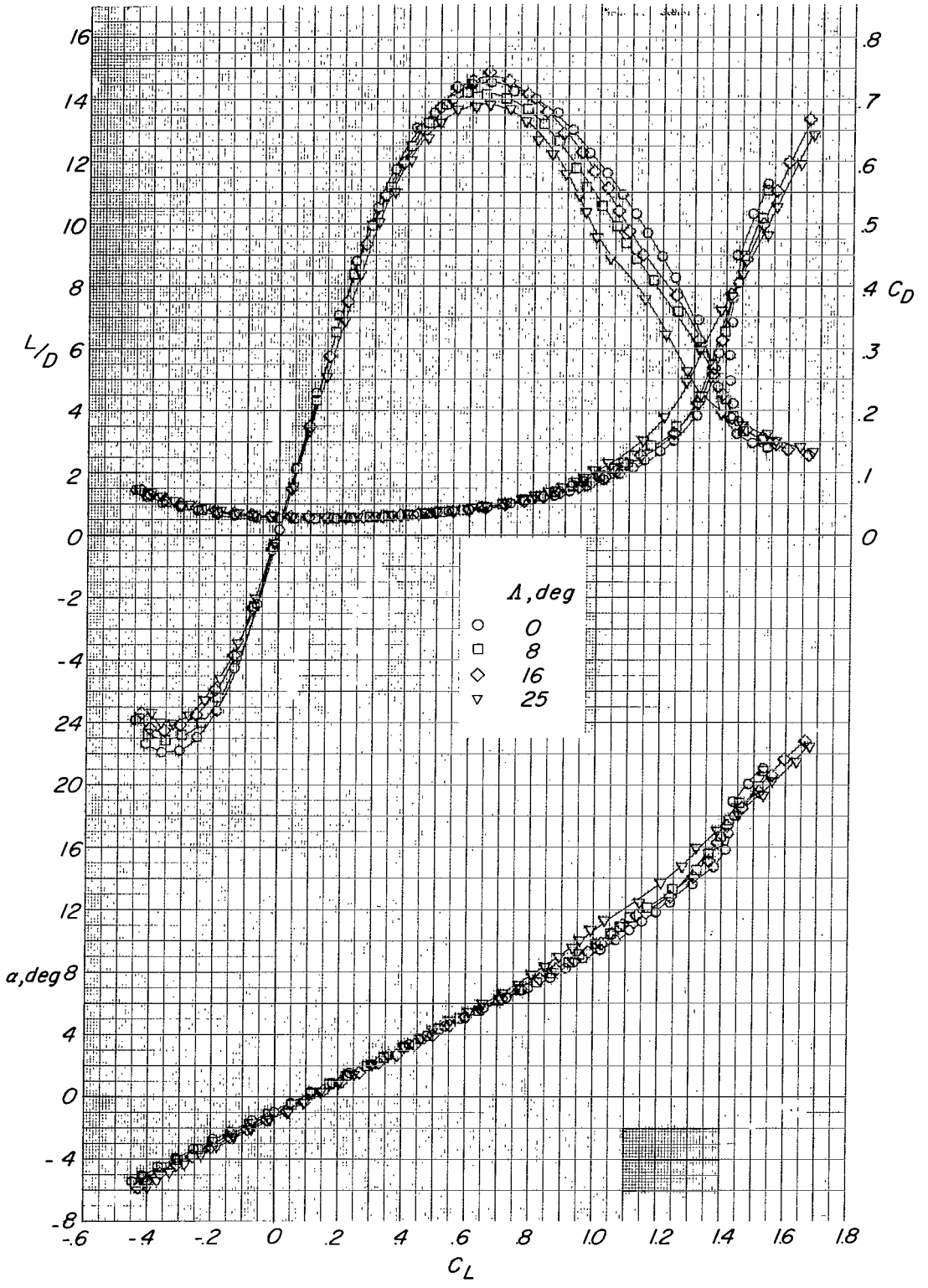

Figure 8.- Effect of wing-sweep angle on aerodynamic characteristics. $B_1WH_1V_NNF_1$. $\Lambda = 16^0$; $\delta_h = 0^0$; $x/c = 5.715$; $\delta_f = 0^0$; $i_w = 0^0$.

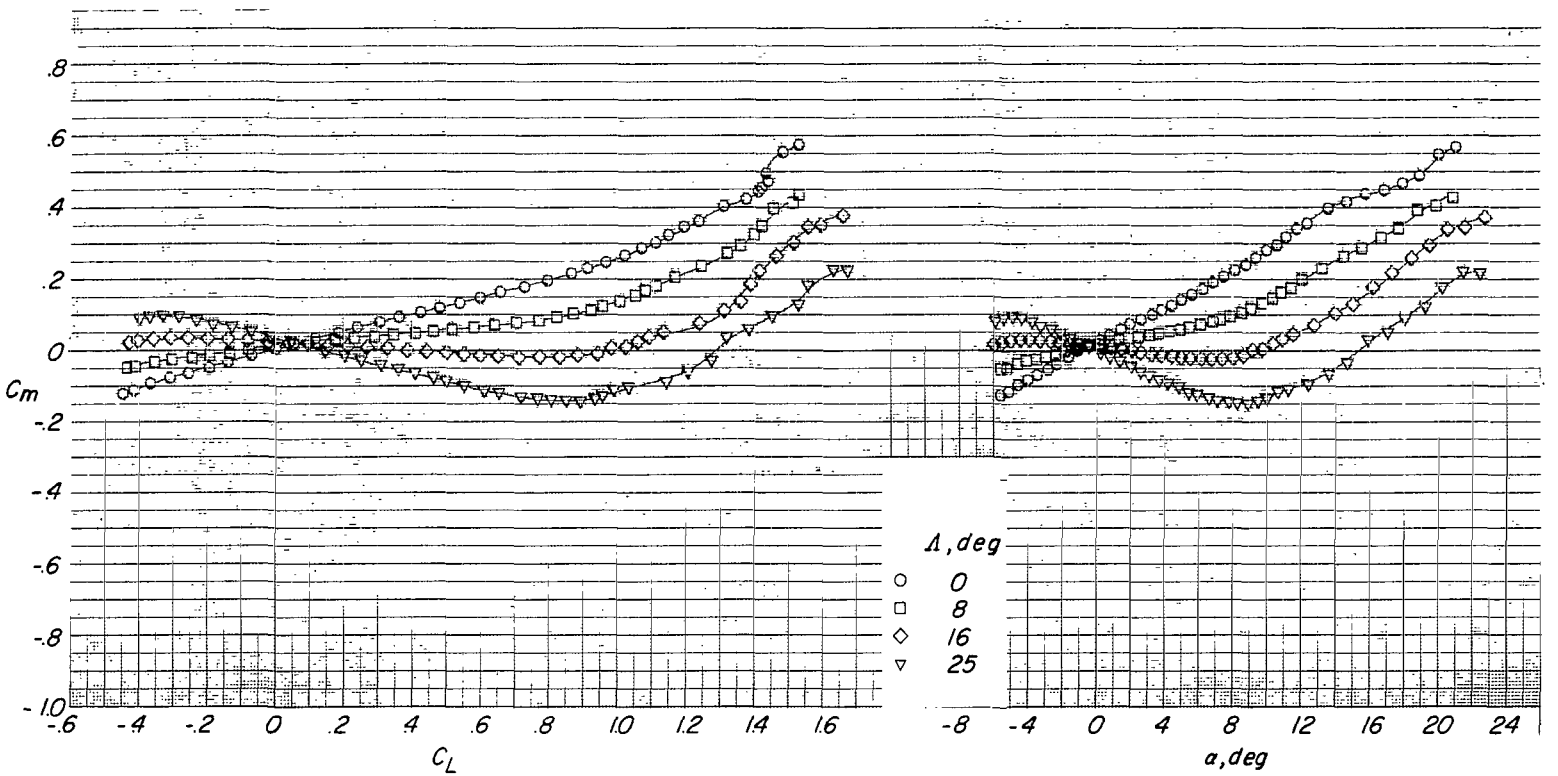

Figure 8.- Concluded.

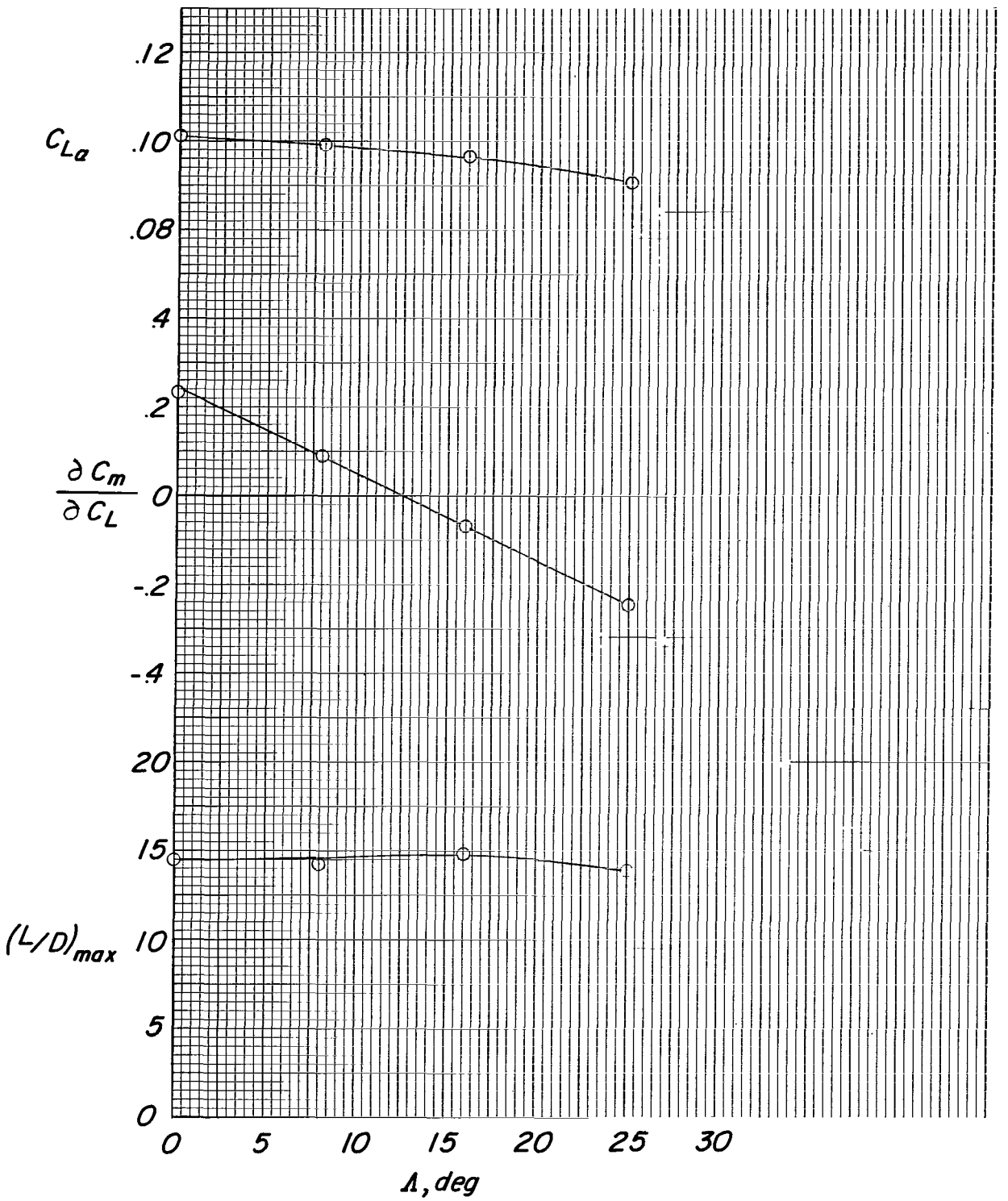

Figure 9.- Variation of aerodynamic parameters C_{L_α}, $\partial C_m/\partial C_L$, and $(L/D)_{max}$ with wing-sweep angle. $B_1WH_1V_NNF_1$; $\delta_h = 0^0$; $\delta_f = 0^0$; $i_w = 0^0$.

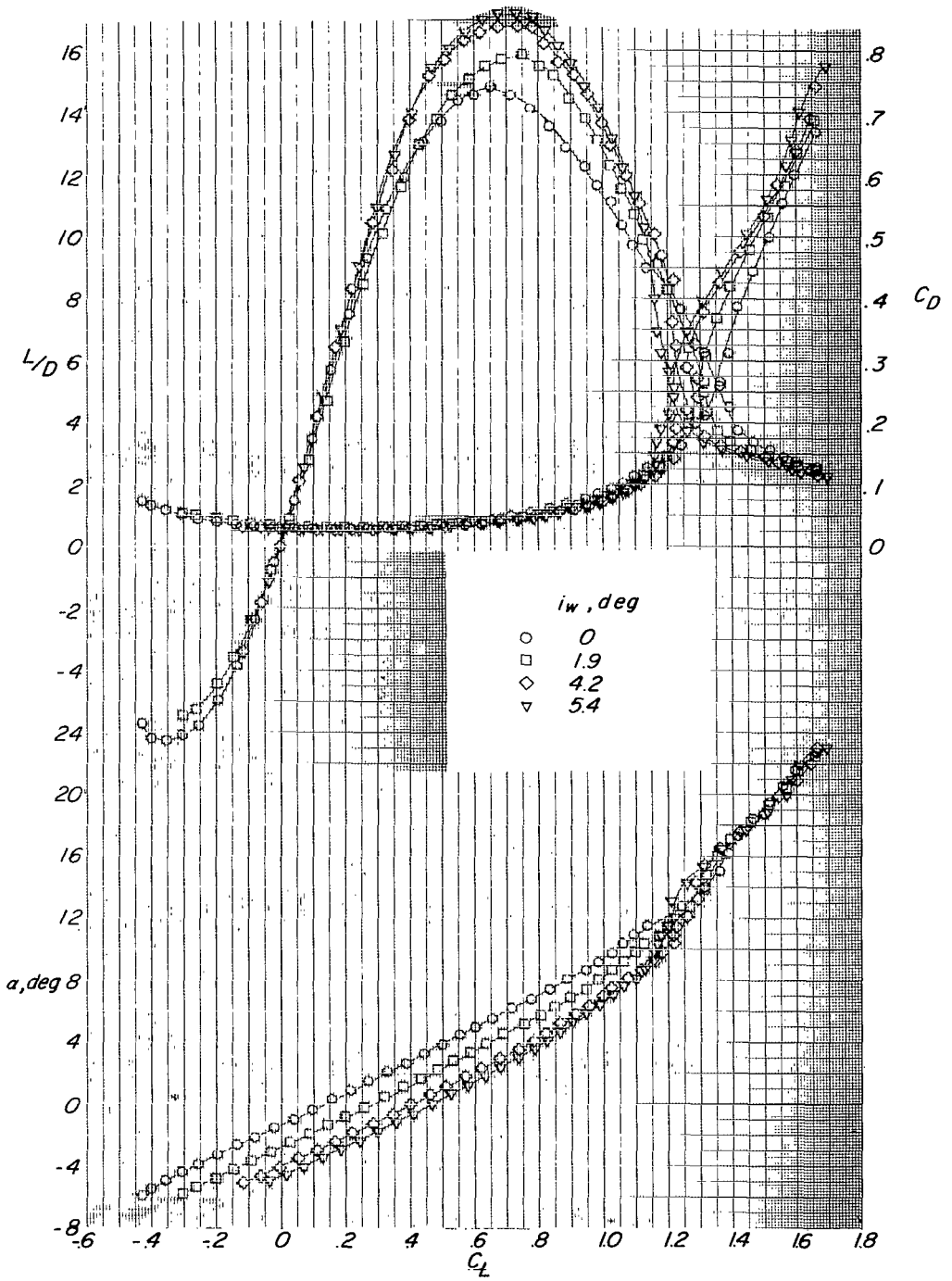

Figure 10.- Effect of movable-wing incidence on aerodynamic characteristics. $B_1WH_1V_NNF_1$; $\Lambda = 16^0$; $\delta_h = 0^0$; $x/c = 5.715$; $\delta_f = 0^0$.

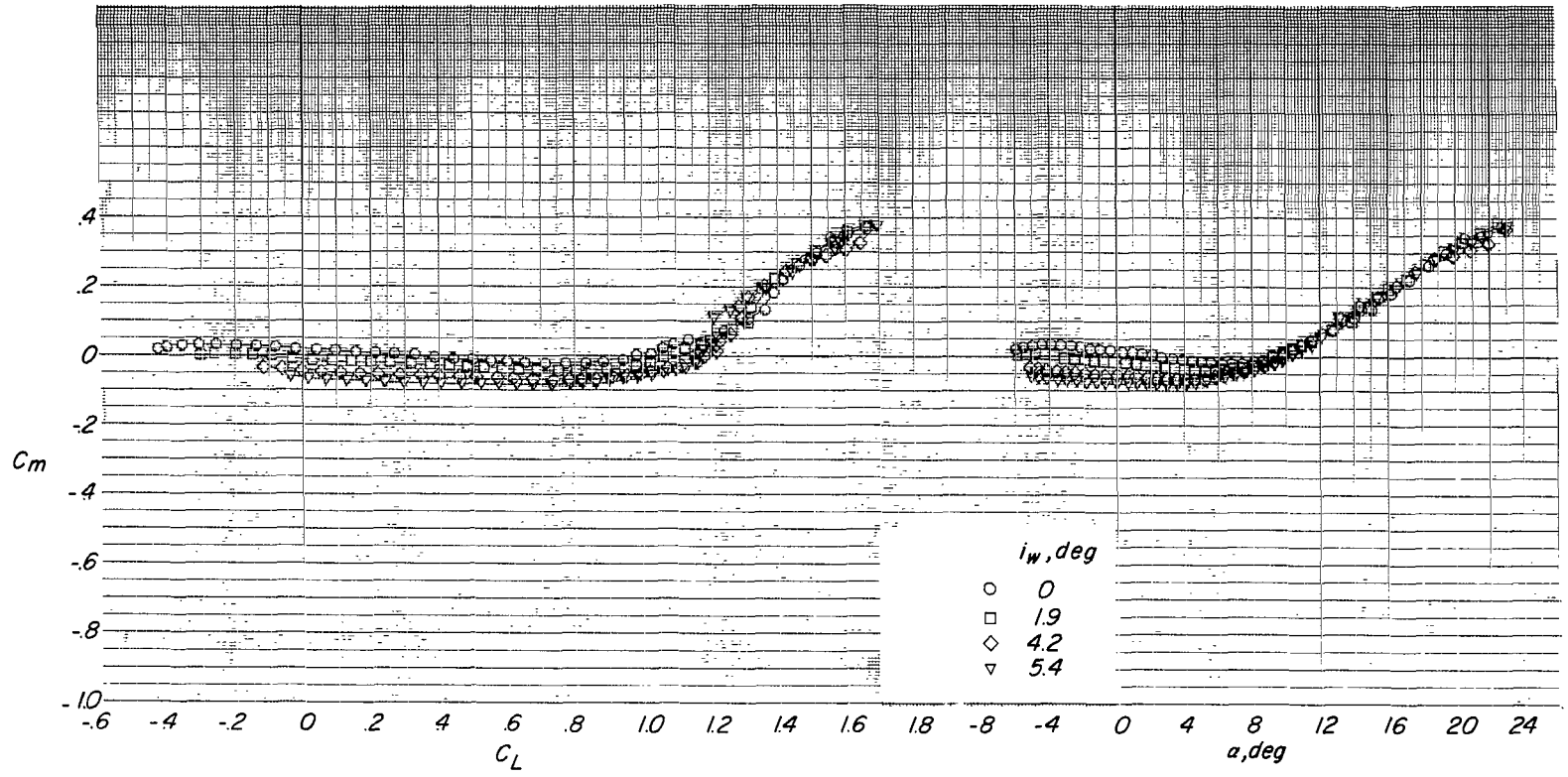

Figure 10.- Concluded.

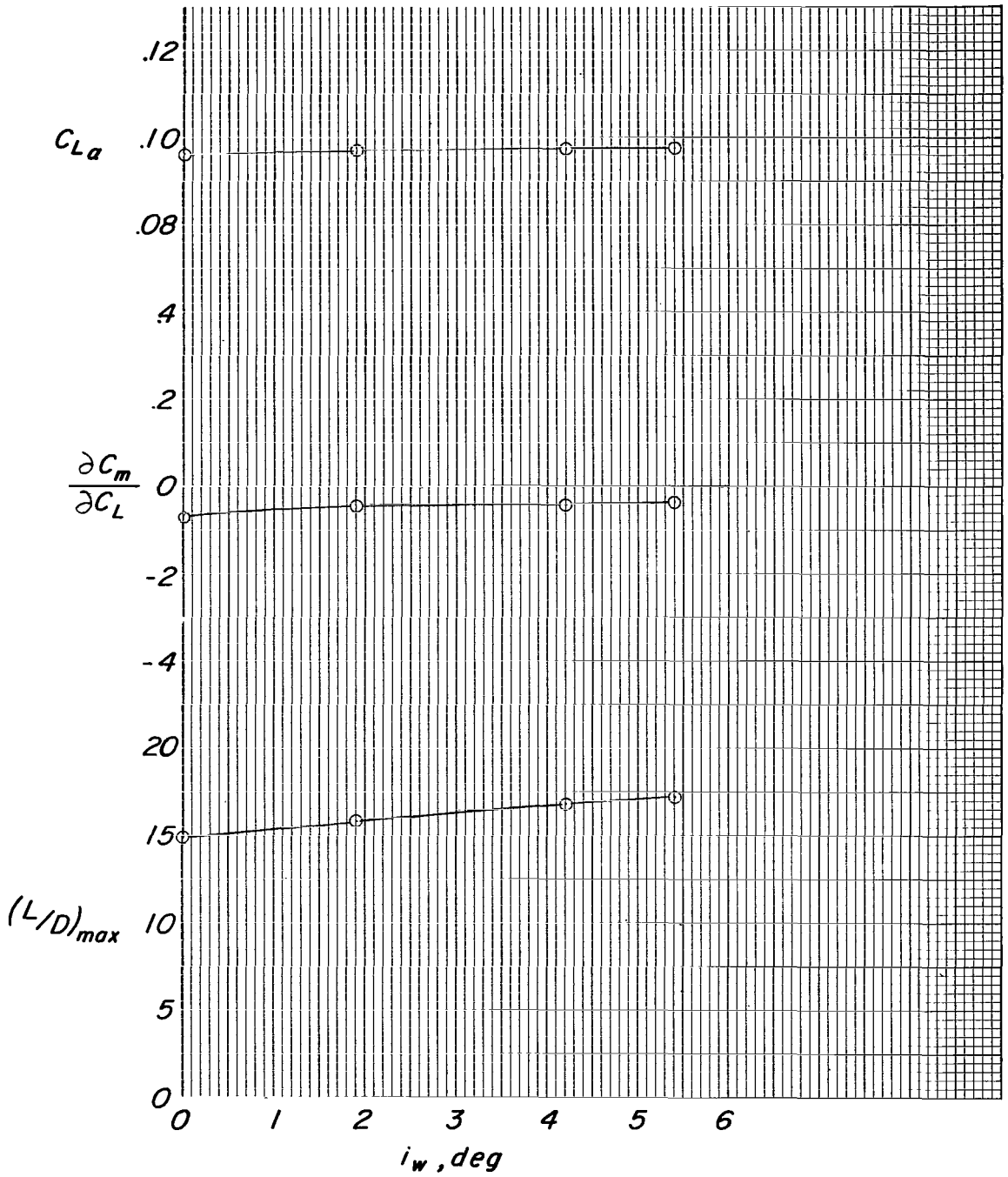

Figure 11.- Variation of the aerodynamic parameter C_{L_α}, $\partial C_m/\partial C_L$, and $(L/D)_{max}$ with wing-incidence angle. $B_1WH_1V_NNF_1$; $\Lambda = 16^0$; $\delta_h = 0^0$; $\delta_f = 0^0$.

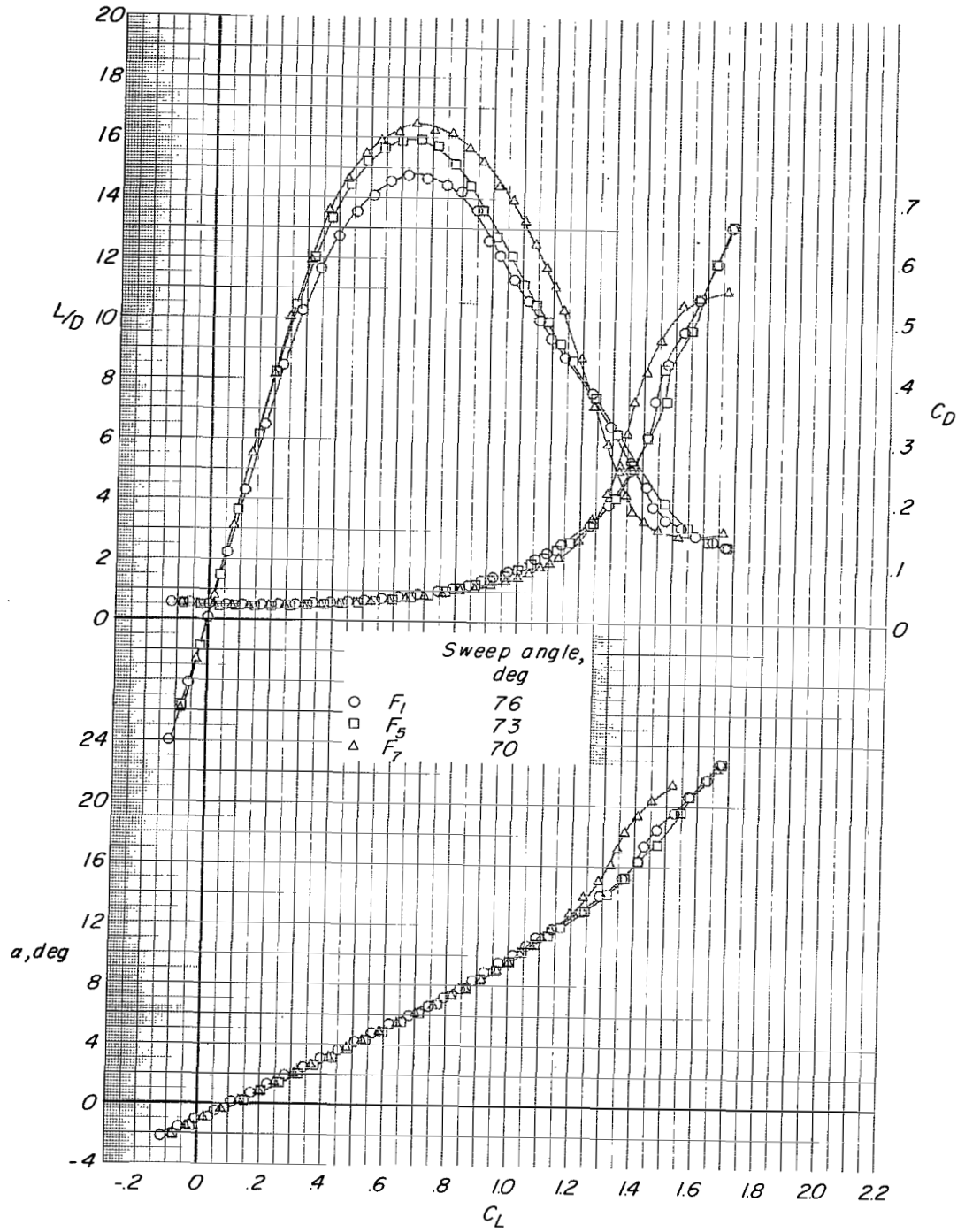

(a) H_1.

Figure 12.- Effect of forewing-flap sweep angle on the aerodynamic characteristics. B_1WHV_NN; $\Lambda = 16^0$; $\delta_h = 0^0$; $\delta_f = 0^0$; $i_w = 0^0$.

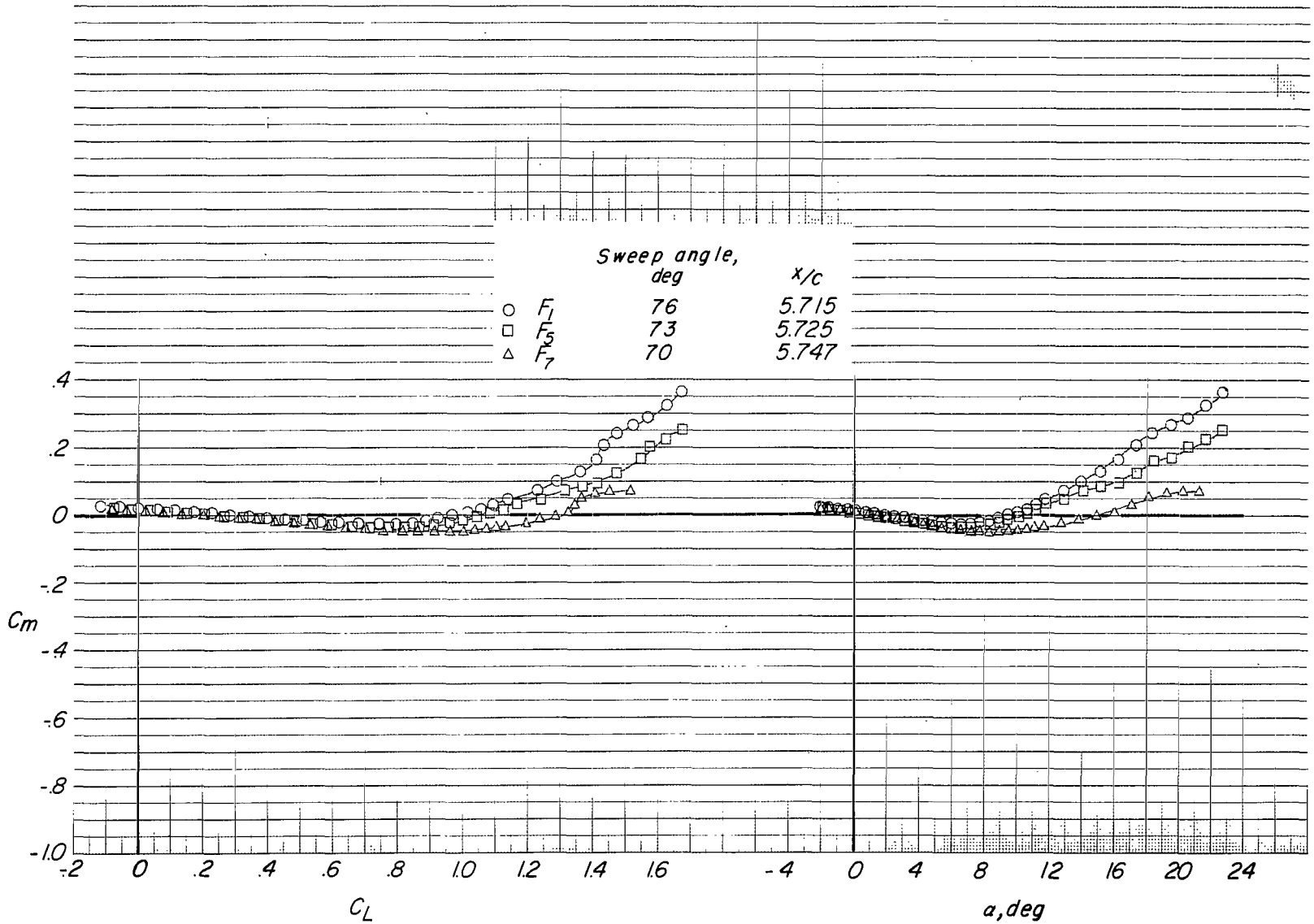

(a) Concluded.

Figure 12.- Continued.

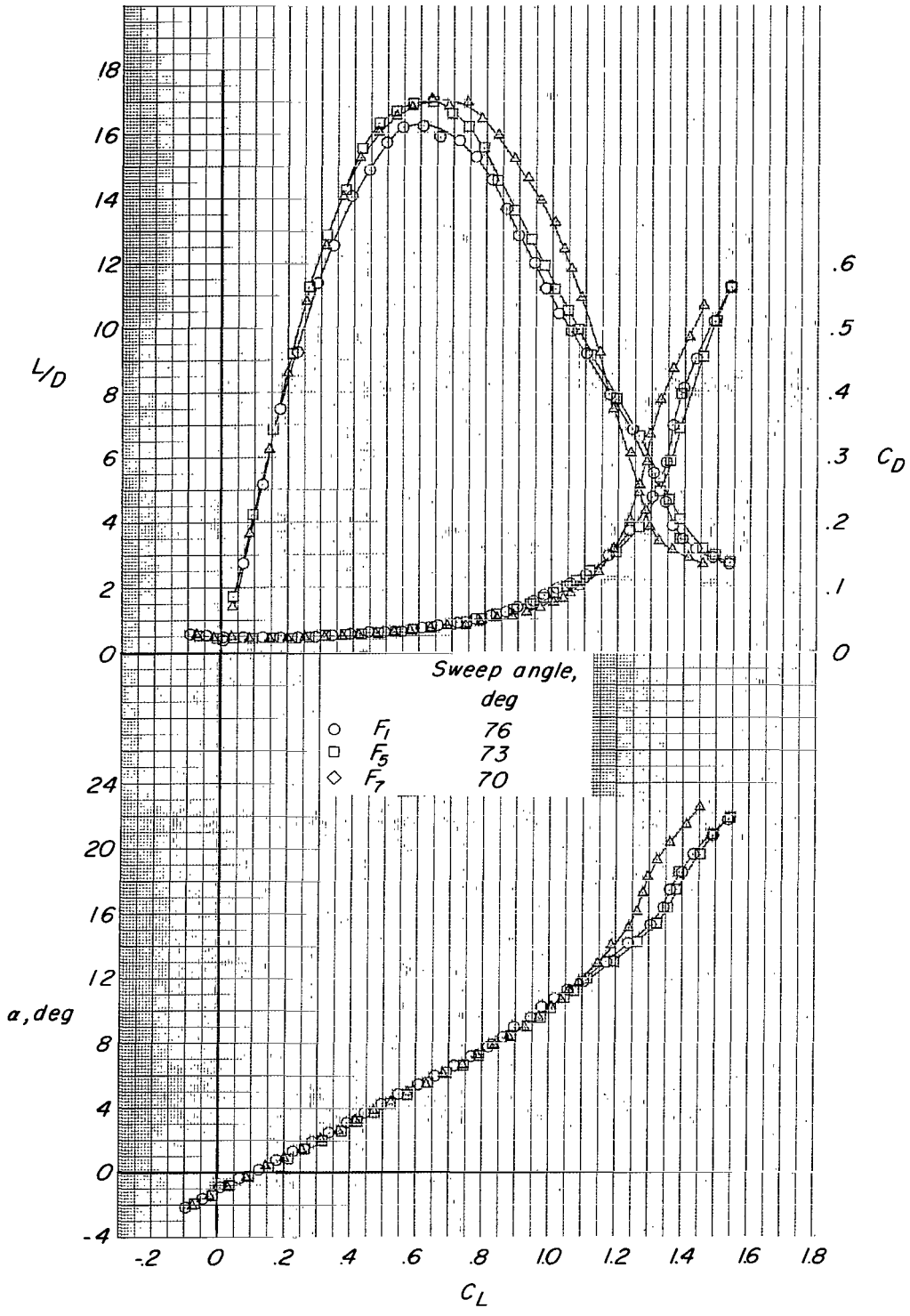

(b) Horizontal tail off.

Figure 12.- Continued.

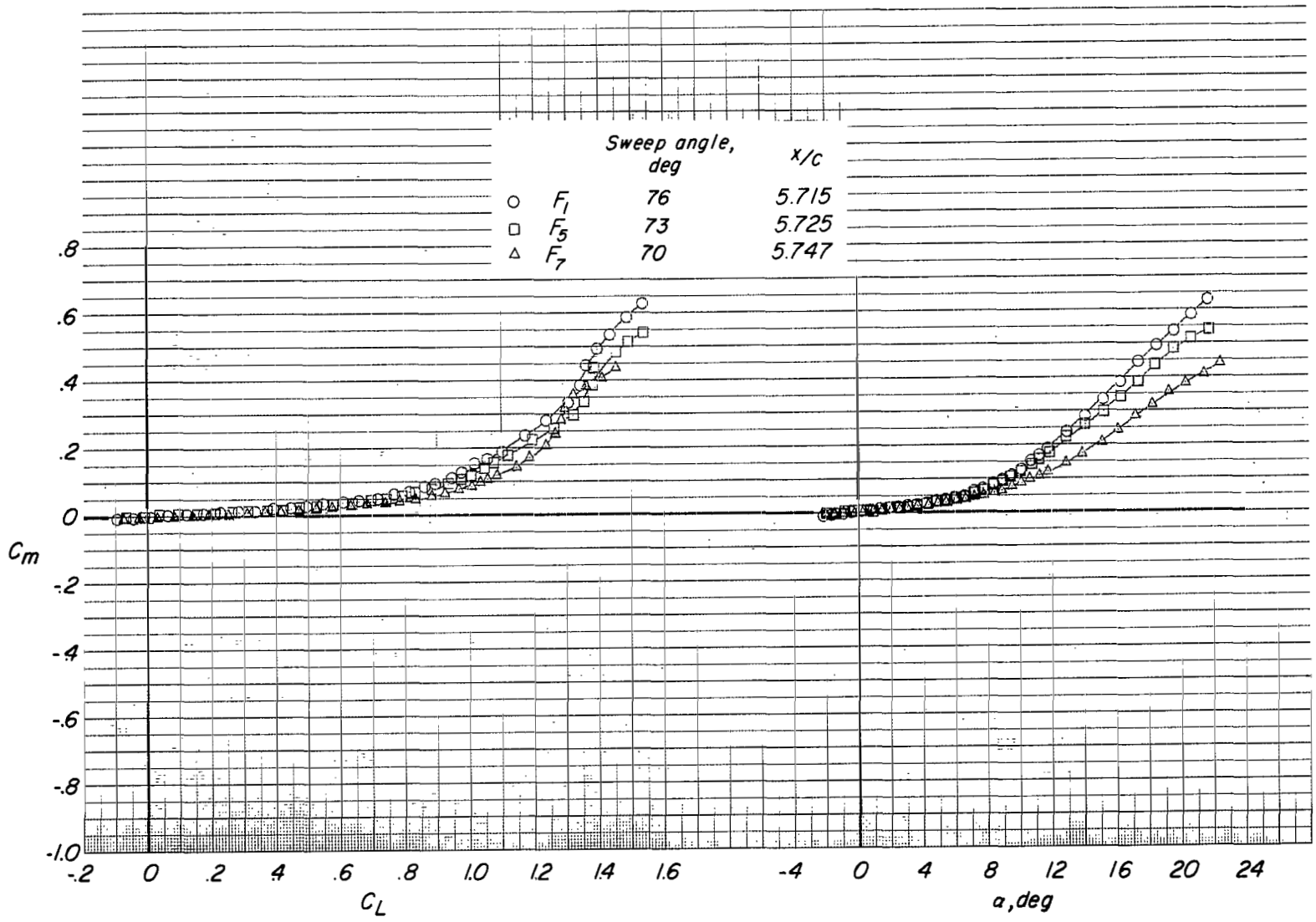

(b) Concluded.

Figure 12.- Concluded.

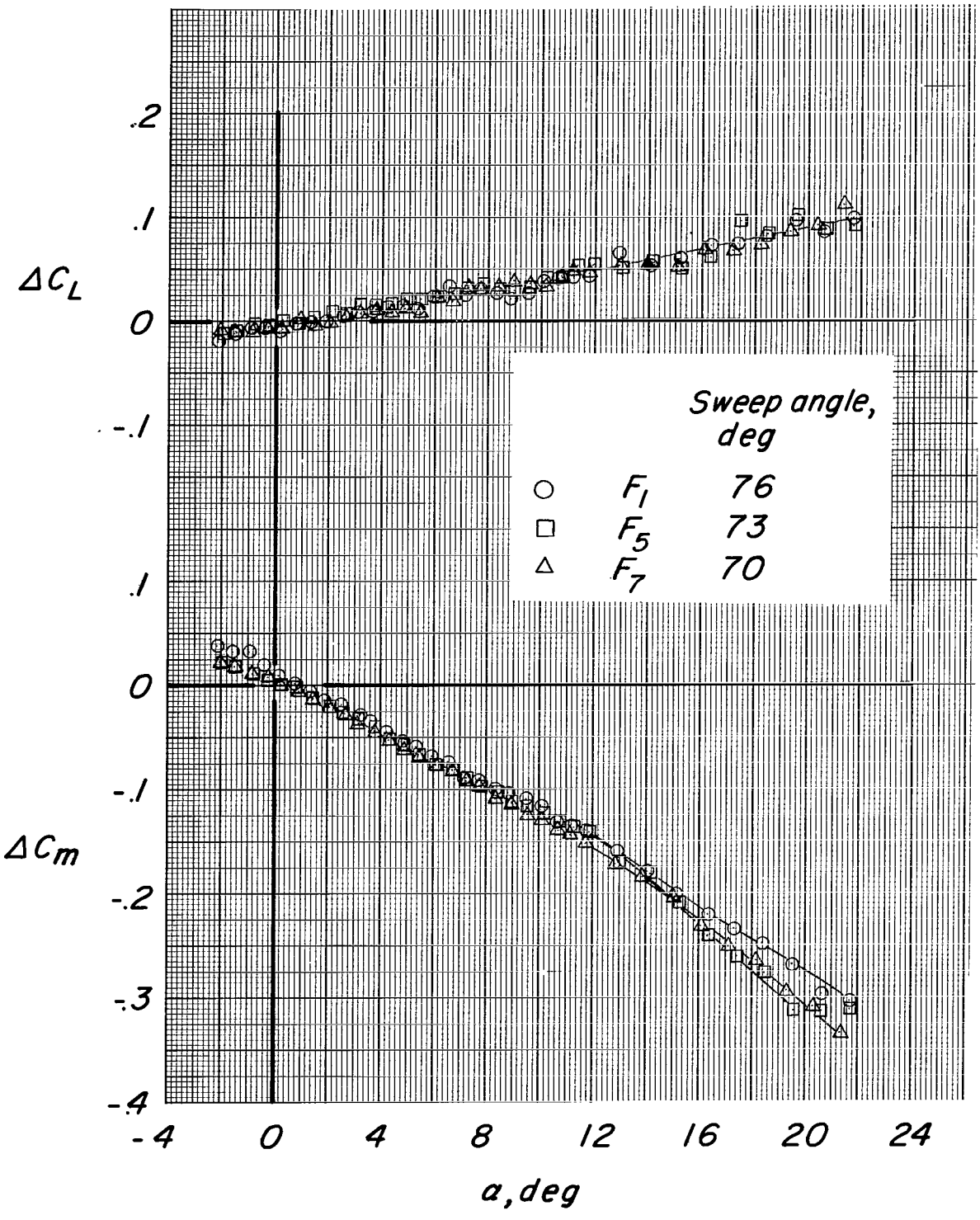

Figure 13.- Effect of forewing-flap sweep on the increment in pitching moment and lift coefficients due to the addition of the horizontal tail. $B_1WH_1V_NN$; $\Lambda = 16^0$; $\delta_h = 0^0$; $\delta_f = 0^0$; $i_w = 0^0$.

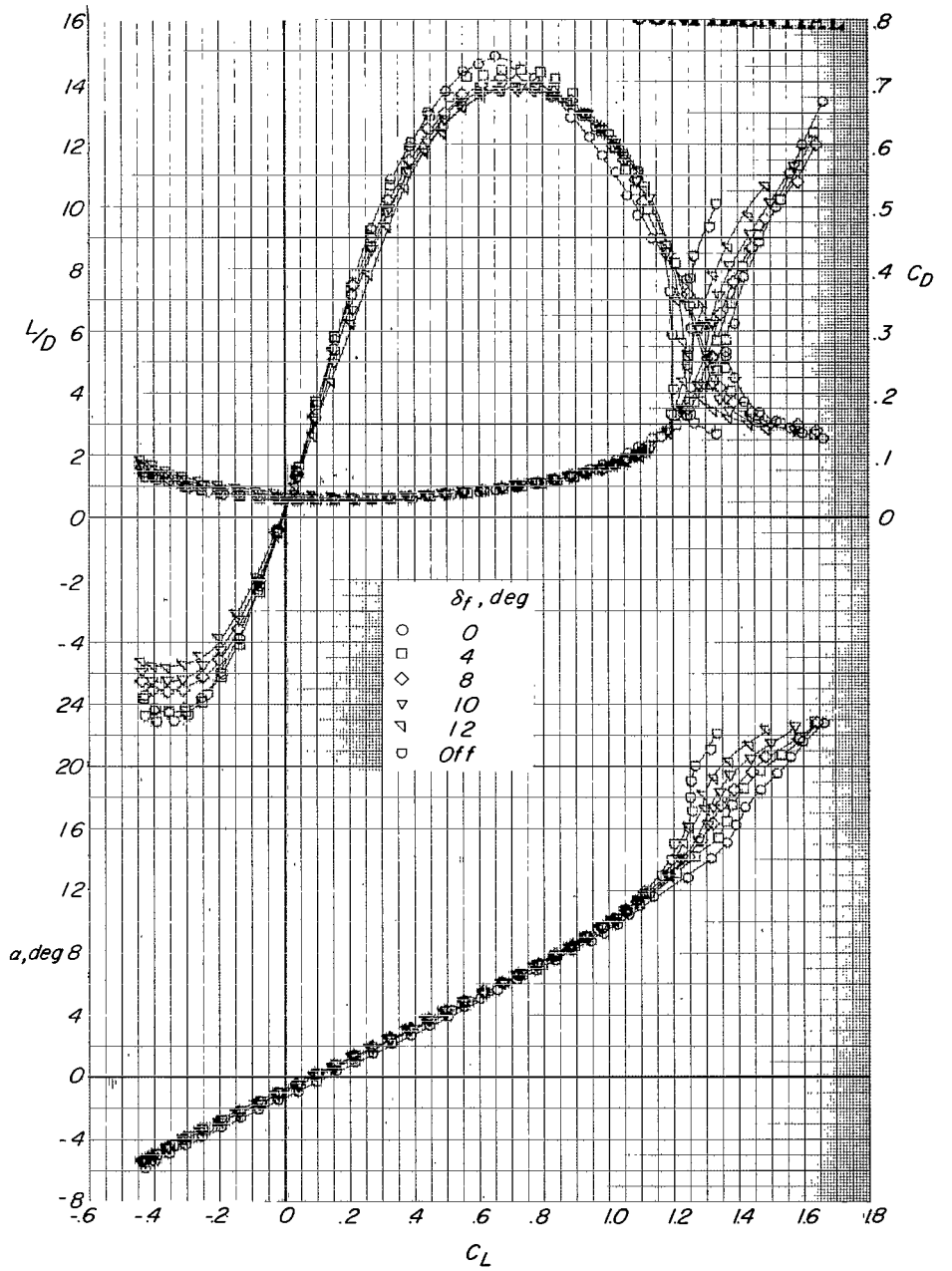

(a) F_1.

Figure 14.- Effect of forewing-flap deflection on the aerodynamic characteristics. $B_1WH_1V_NN$; $\Lambda = 16^0$; $\delta_h = 0^0$; $x/c = 5.715$; $i_w = 0^0$.

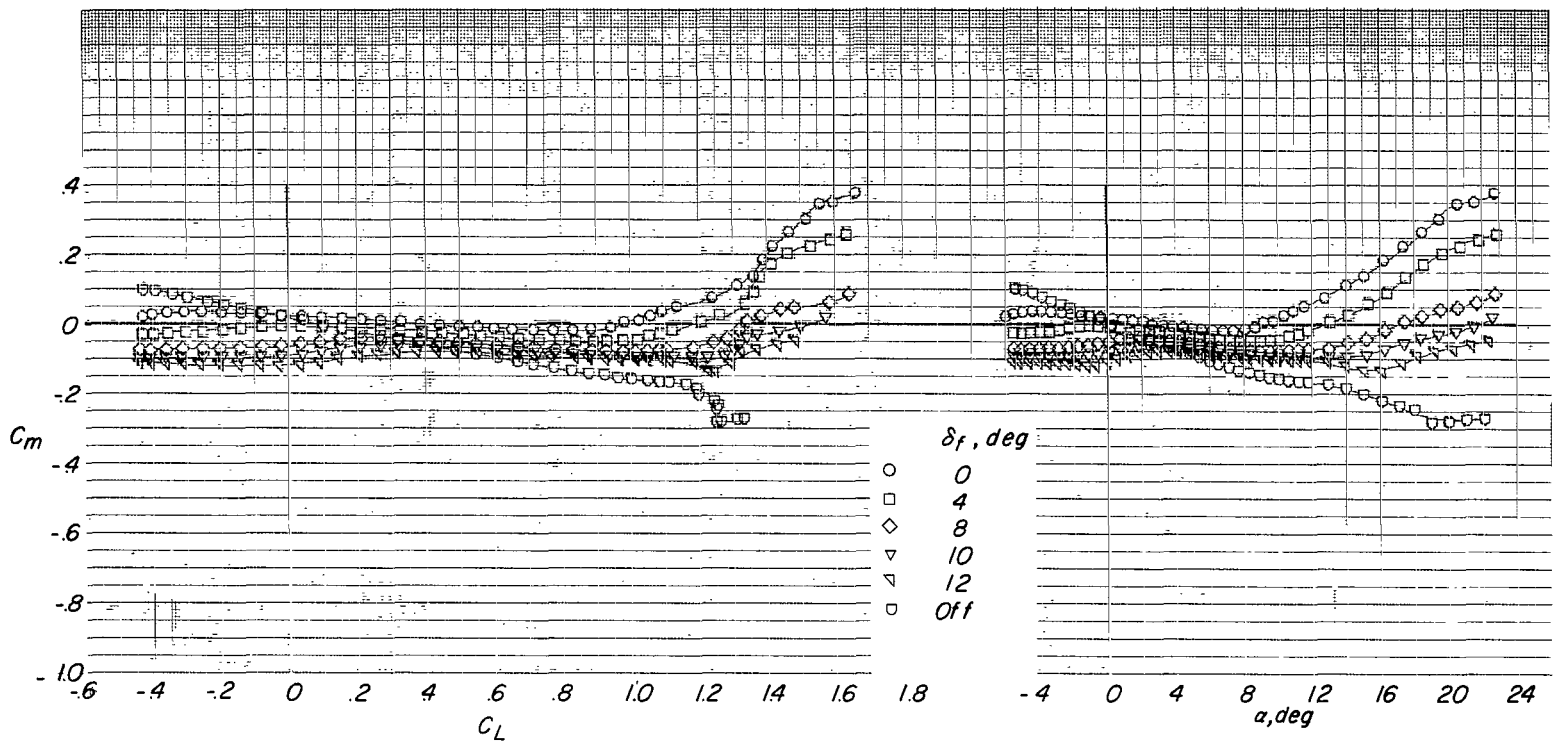

(a) Concluded.

Figure 14.- Continued.

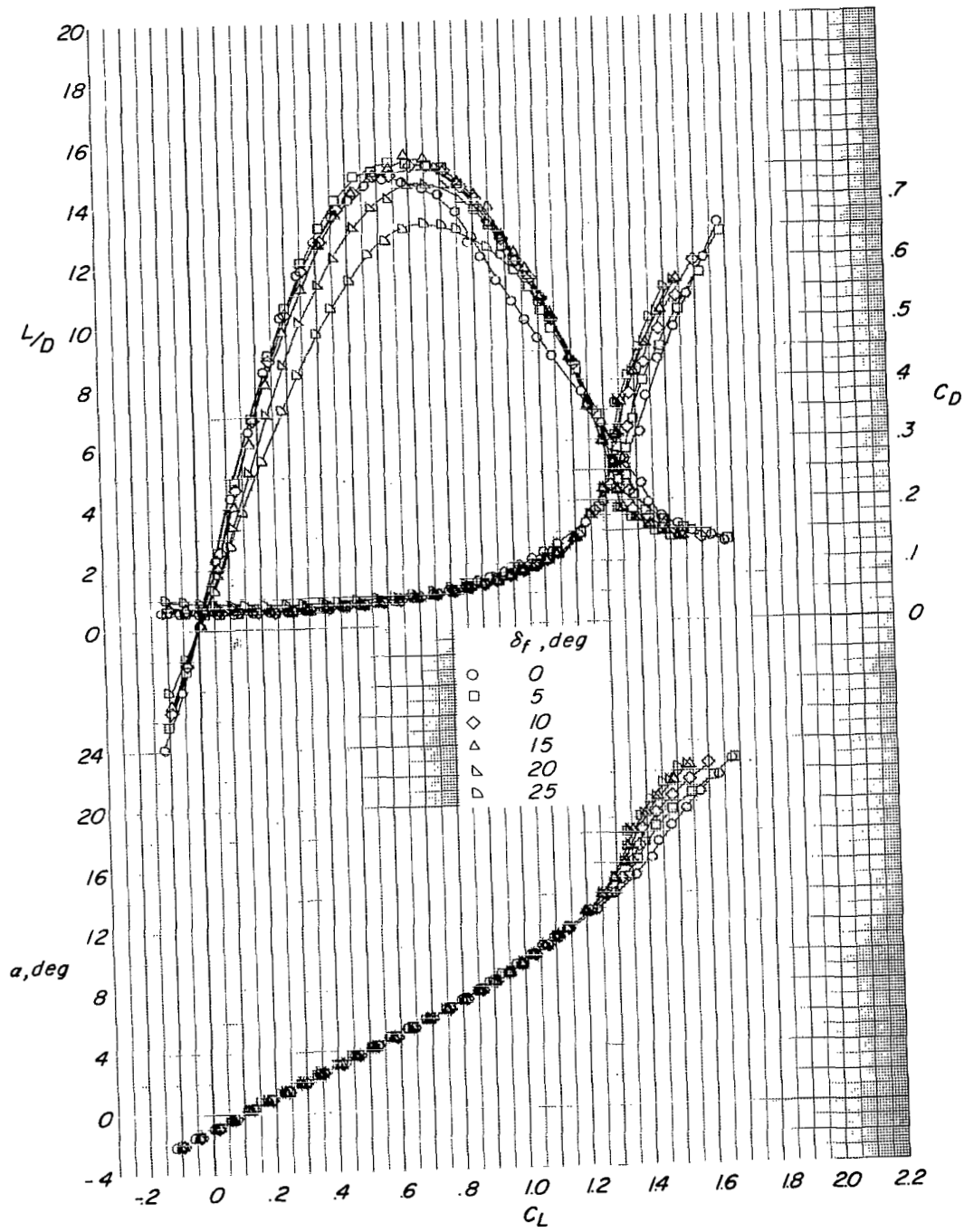

(b) F_2.

Figure 14.- Continued.

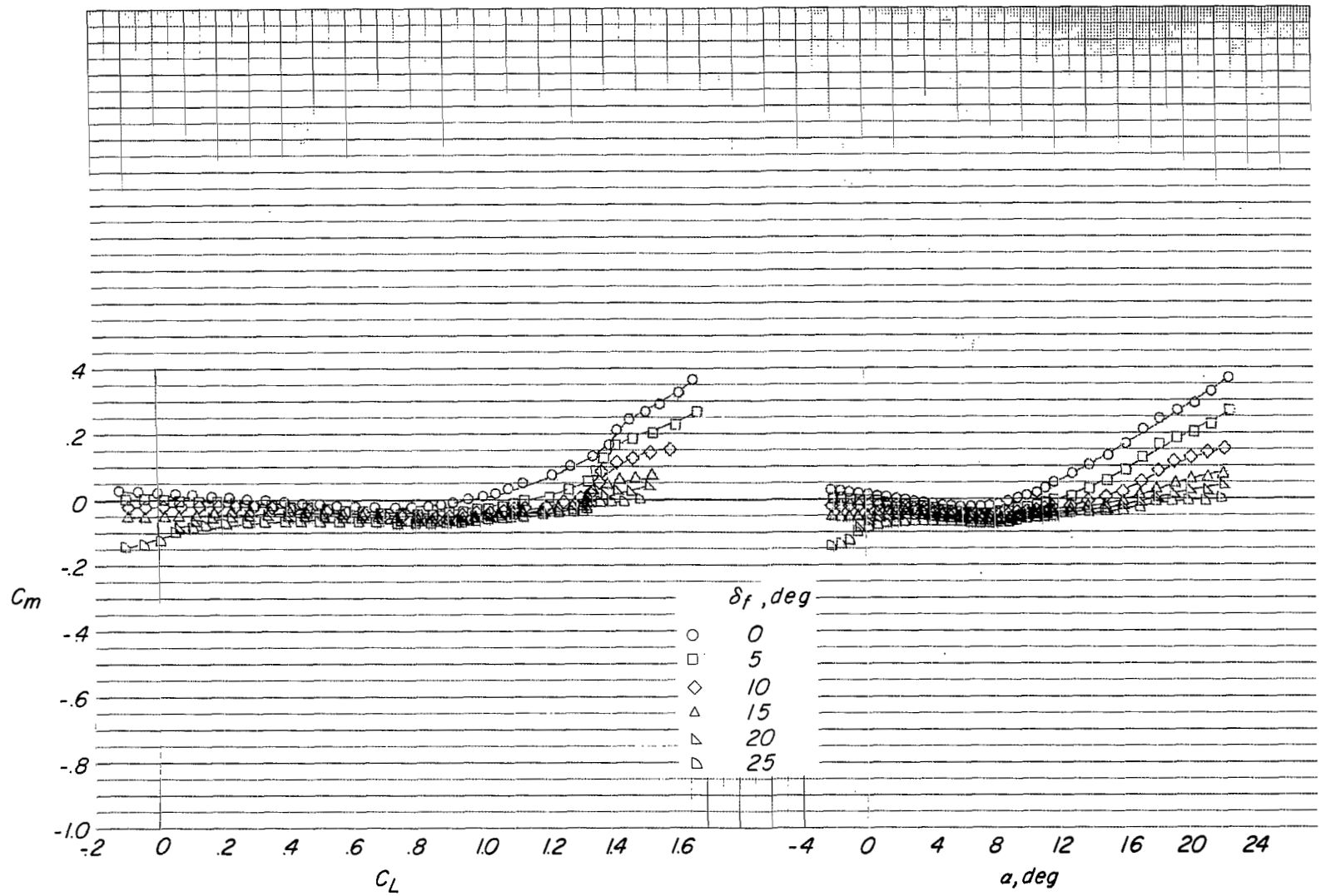

(b) Concluded.

Figure 14.- Continued.

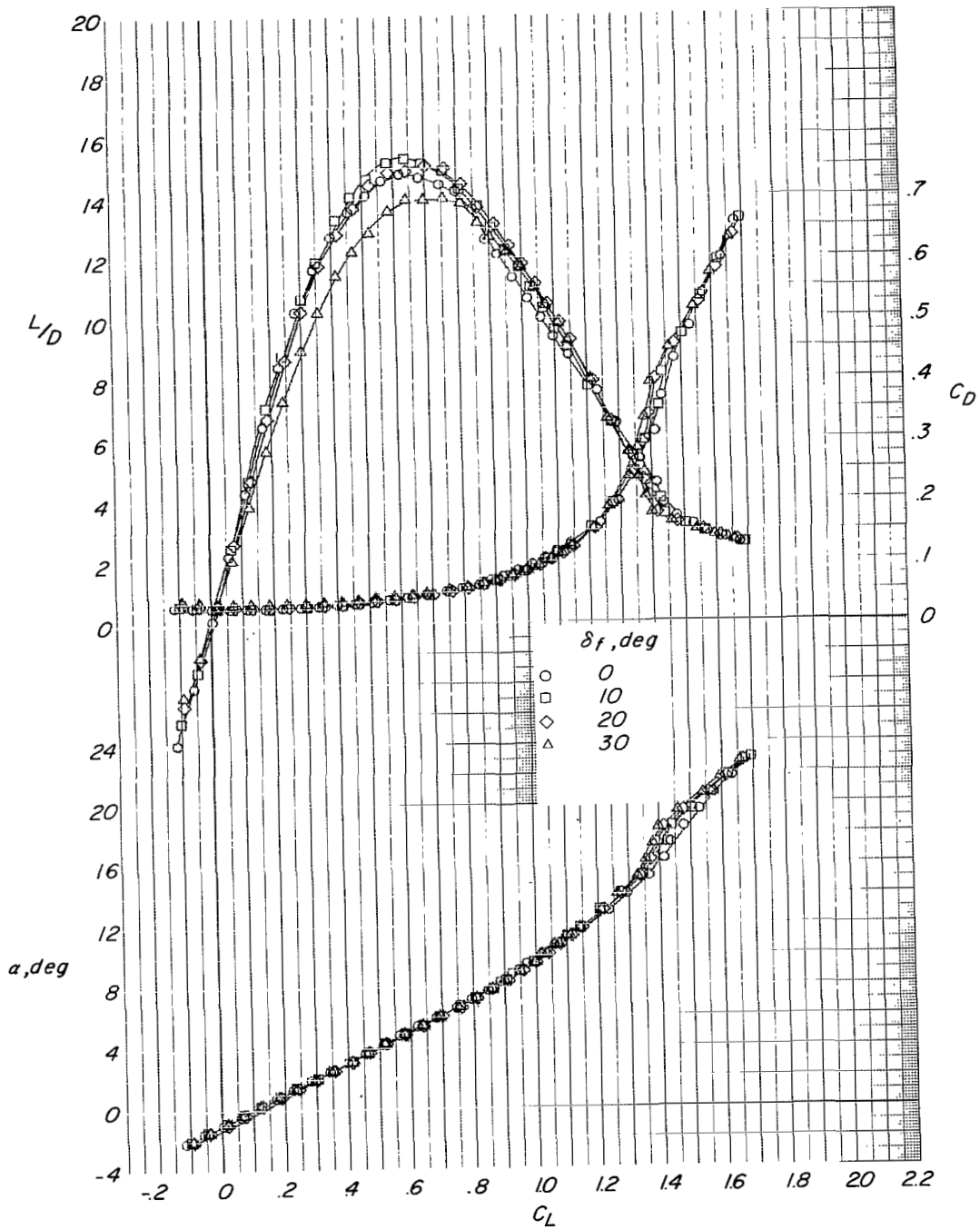

(c) F_3.

Figure 14.- Continued.

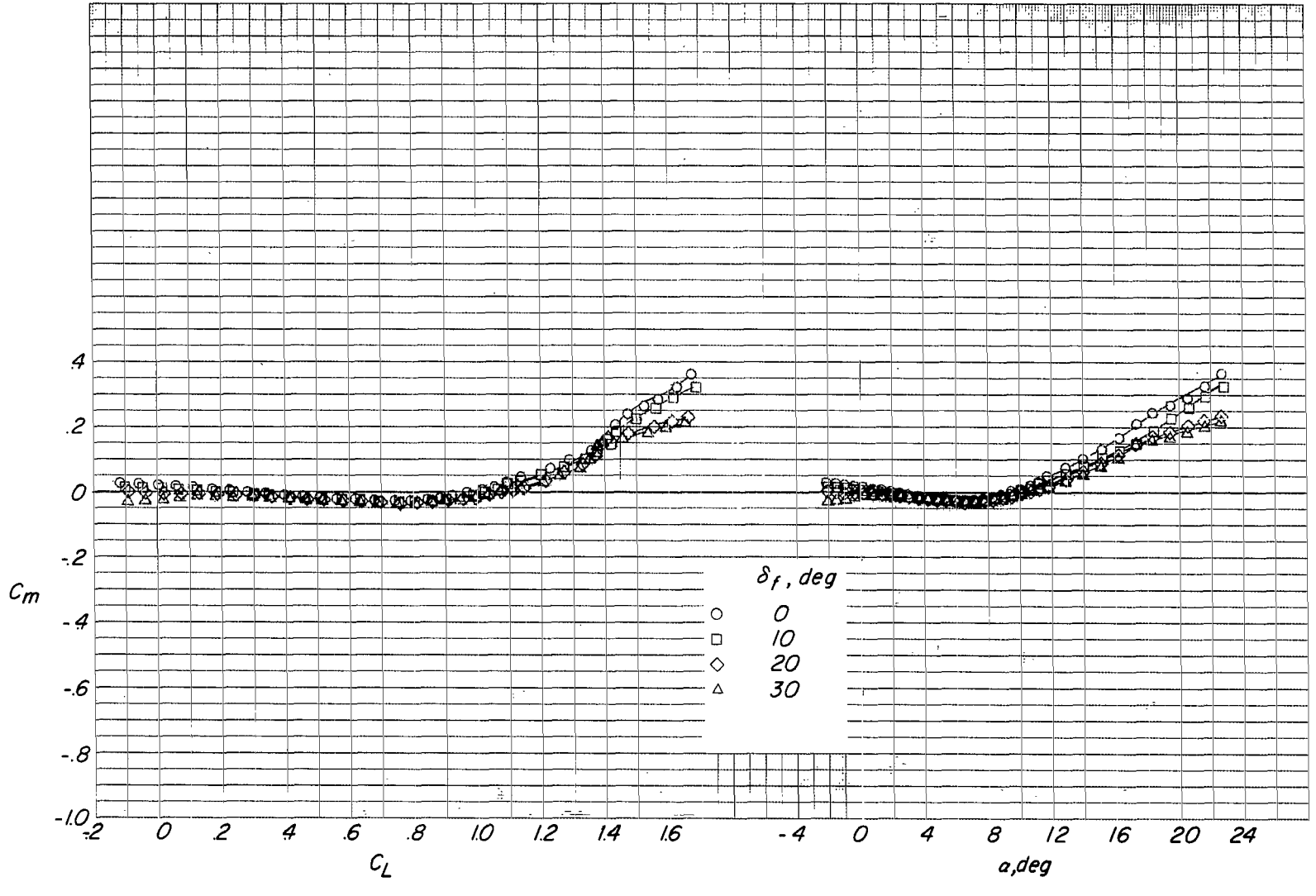

(c) Concluded.

Figure 14.- Concluded.

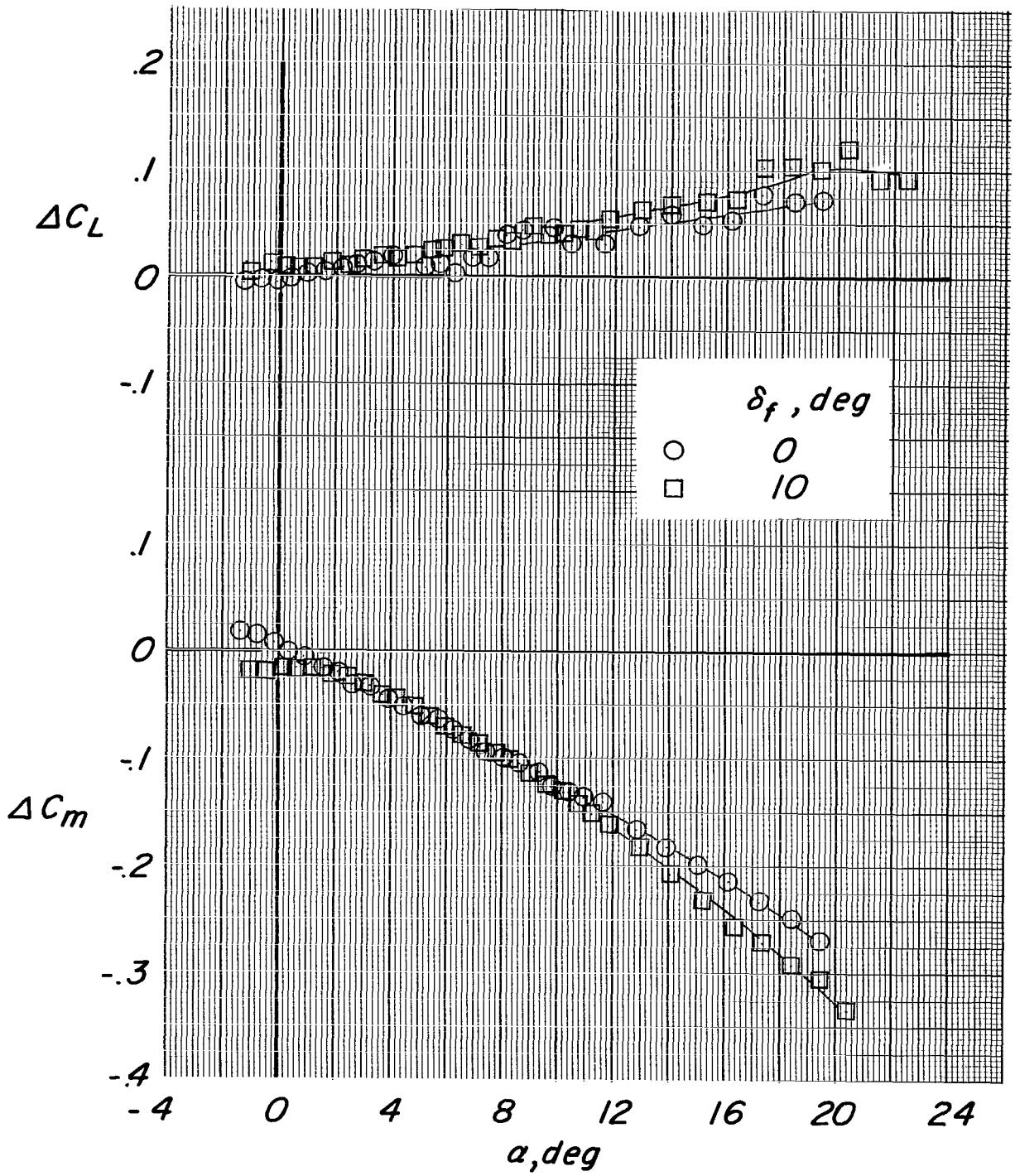

Figure 15.- Effect of forewing-flap deflection on the increment in pitching-moment and lift coefficients due to the addition of the horizontal tail. $B_1WHV_NNF_1$; $\Lambda = 16^0$; $i_w = 0^0$.

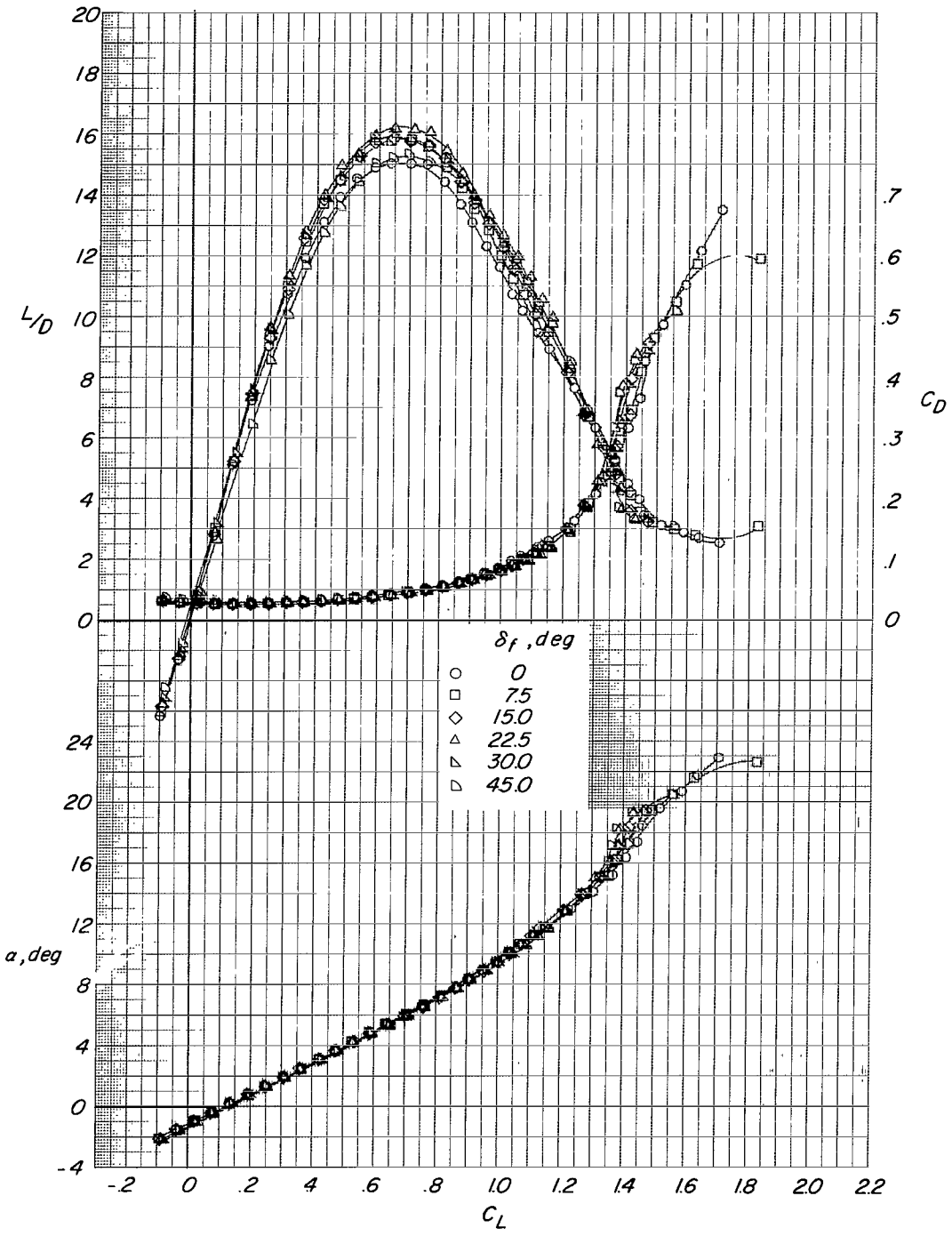

(a) F_4; x/c = 5.715.

Figure 16.- Effect of forewing-flap deflection on the aerodynamic characteristics. $B_1WH_1V_NN$; $\Lambda = 16^0$; $\delta_h = 0^0$; $i_w = 0^0$.

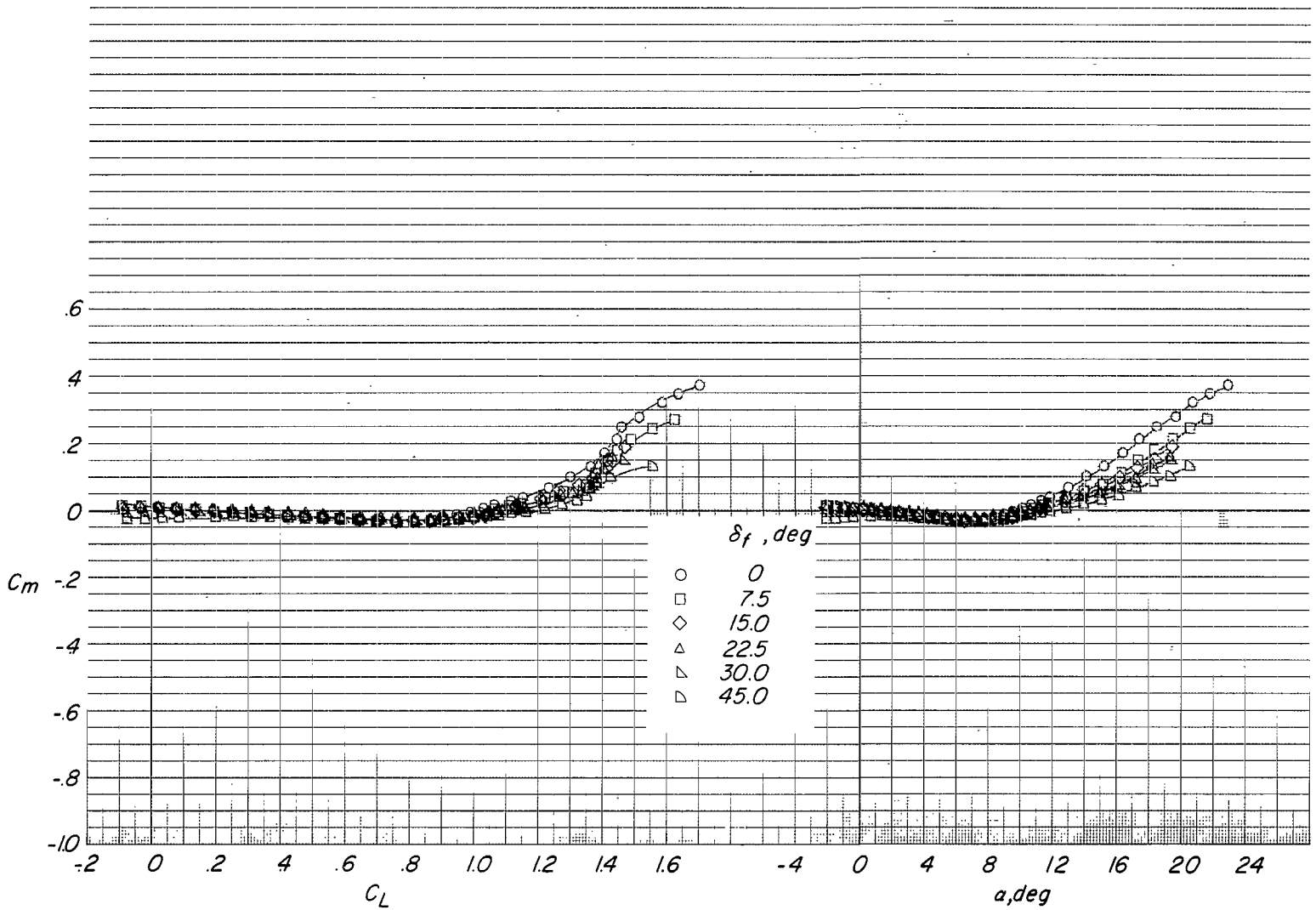

(a) Concluded.

Figure 16.- Continued.

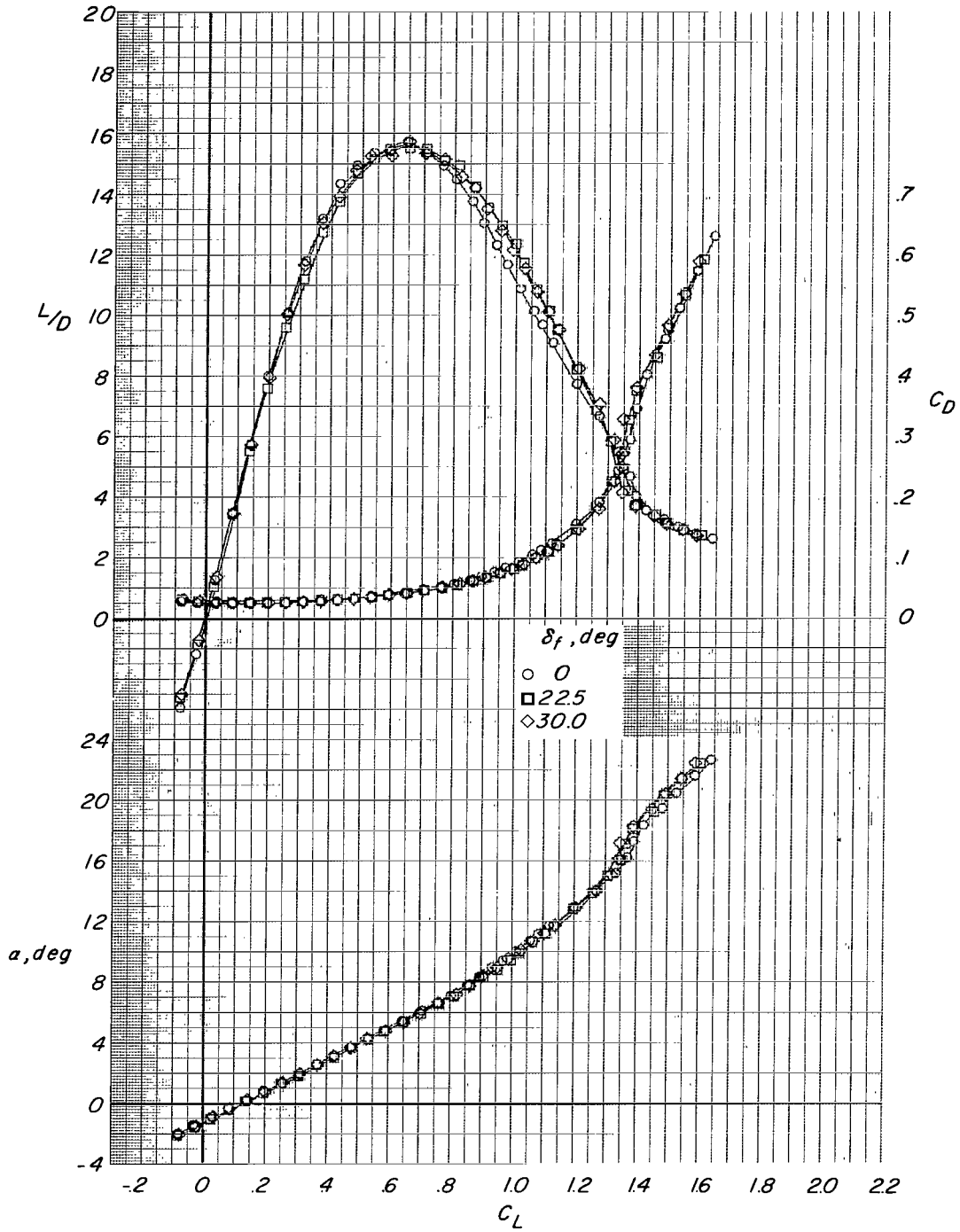

(b) F_6; x/c = 5.735.

Figure 16.- Continued.

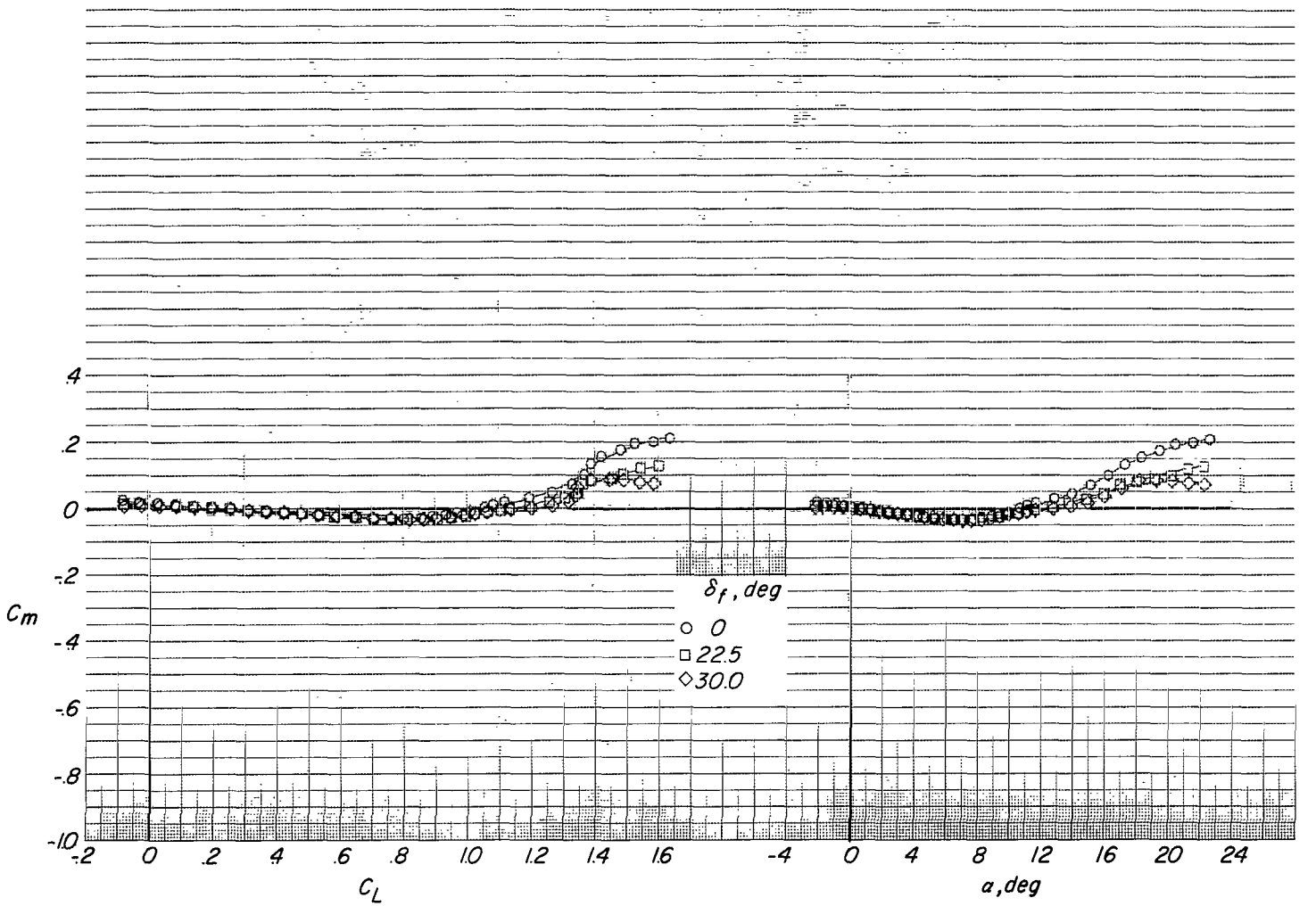

(b) Concluded.

Figure 16.- Concluded.

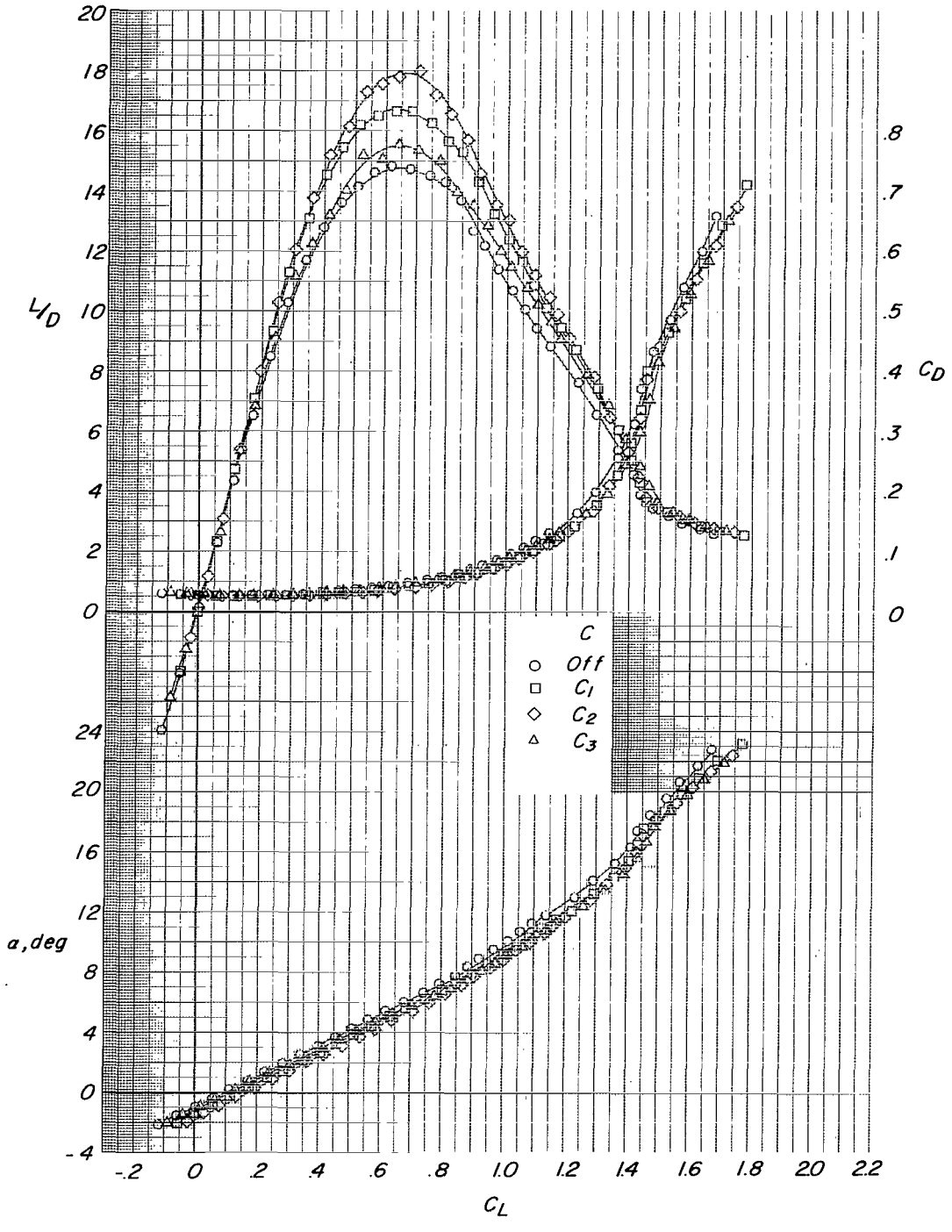

(a) H_1.

Figure 17.- Effect of canard size on the aerodynamic characteristics. $B_1WH_1V_VNF_1$; $\Lambda = 16^0$; $\delta_h = 0^0$; $\delta_c = 0^0$; $\delta_f = 0^0$; $i_w = 0^0$.

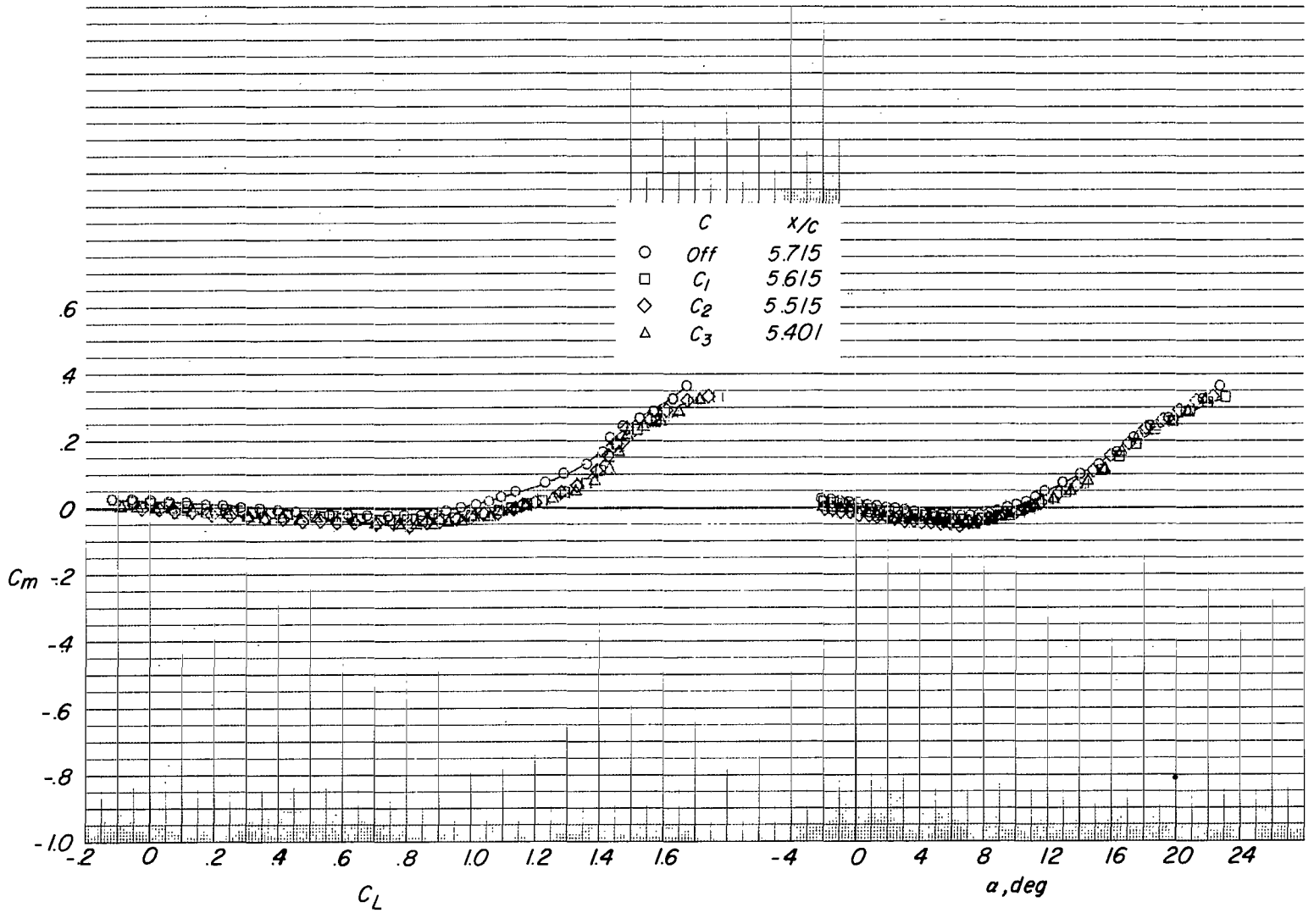

(a) Concluded.

Figure 17.- Continued.

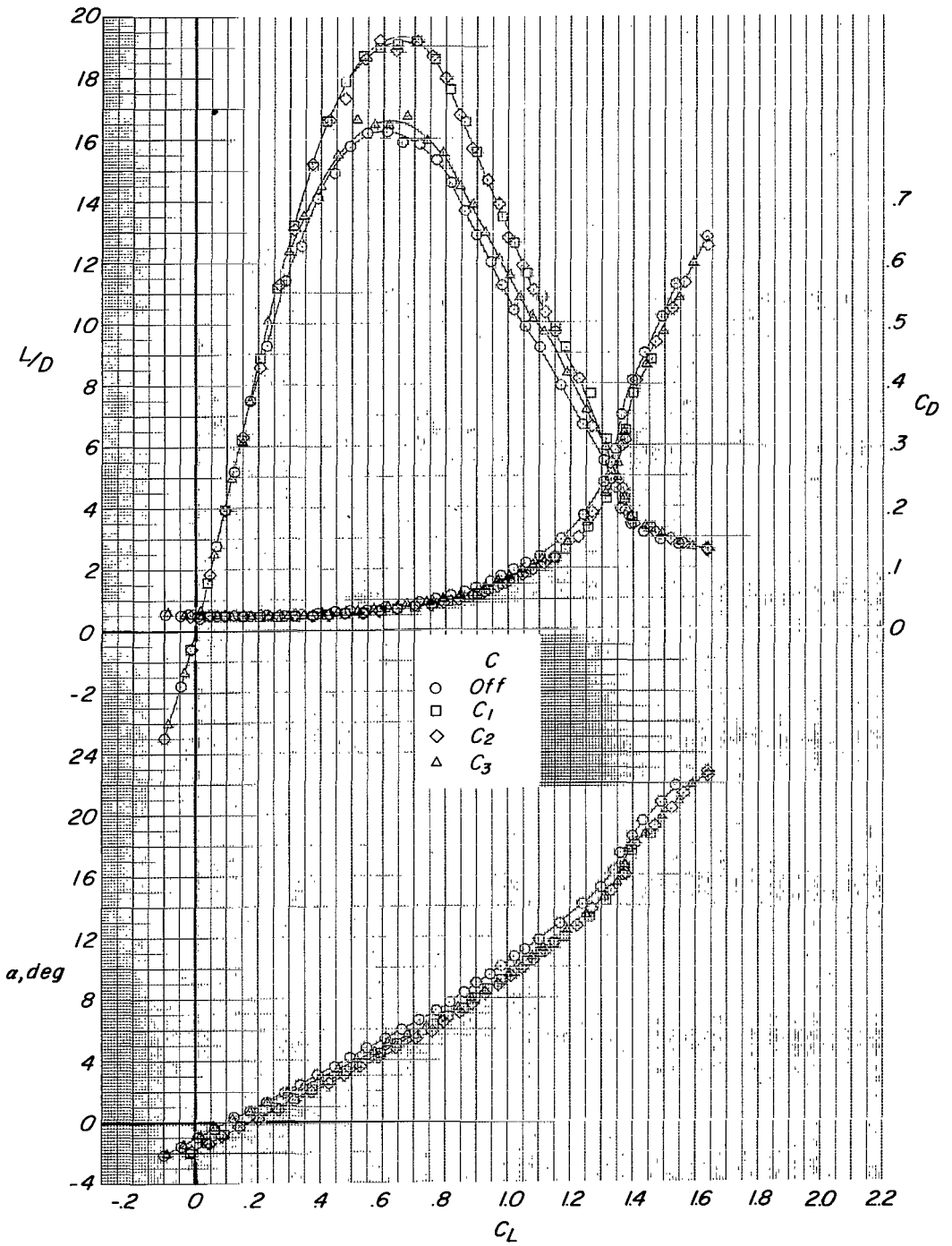

(b) Horizontal tail off.

Figure 17.- Continued.

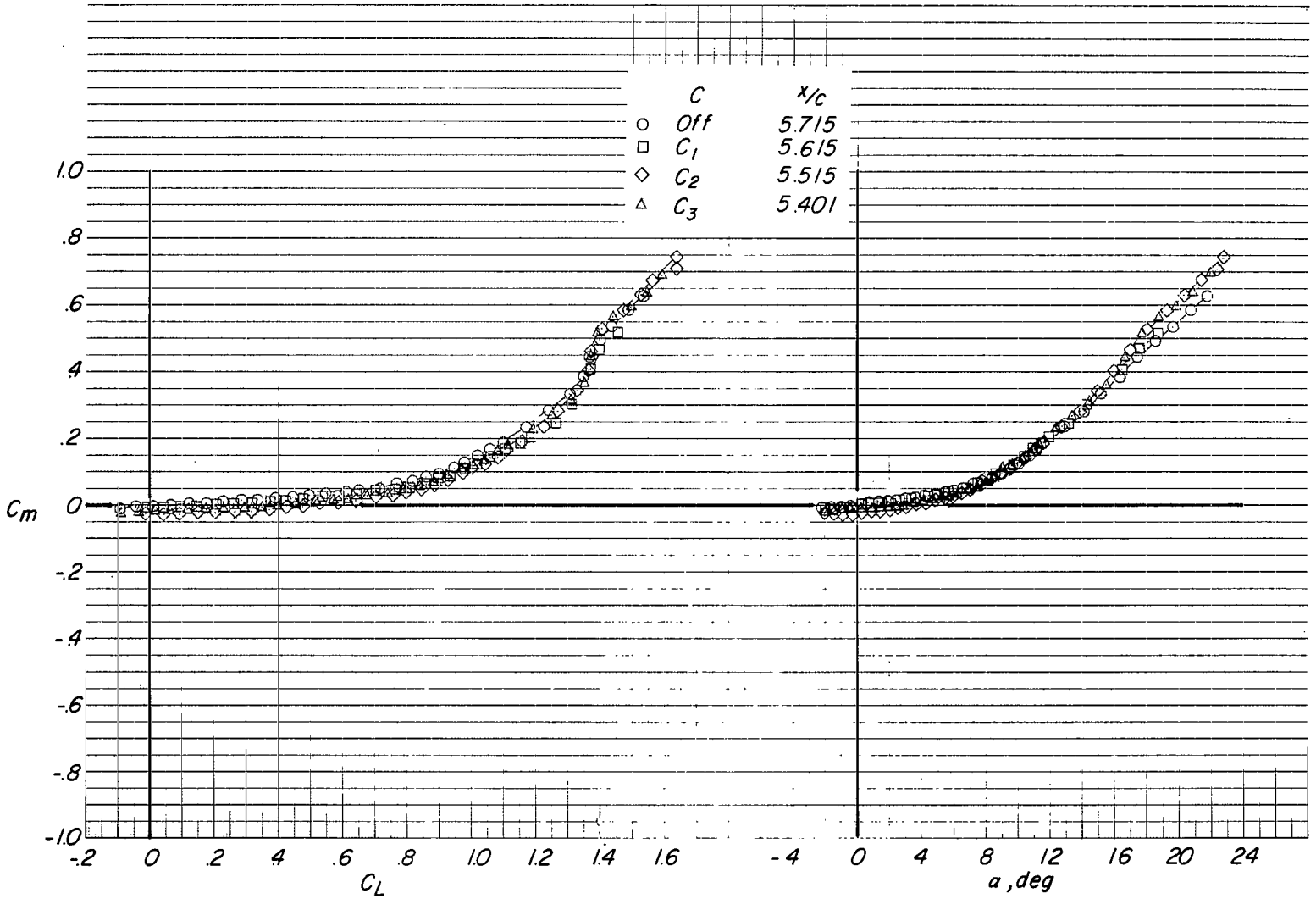

(b) Concluded.

Figure 17.- Concluded.

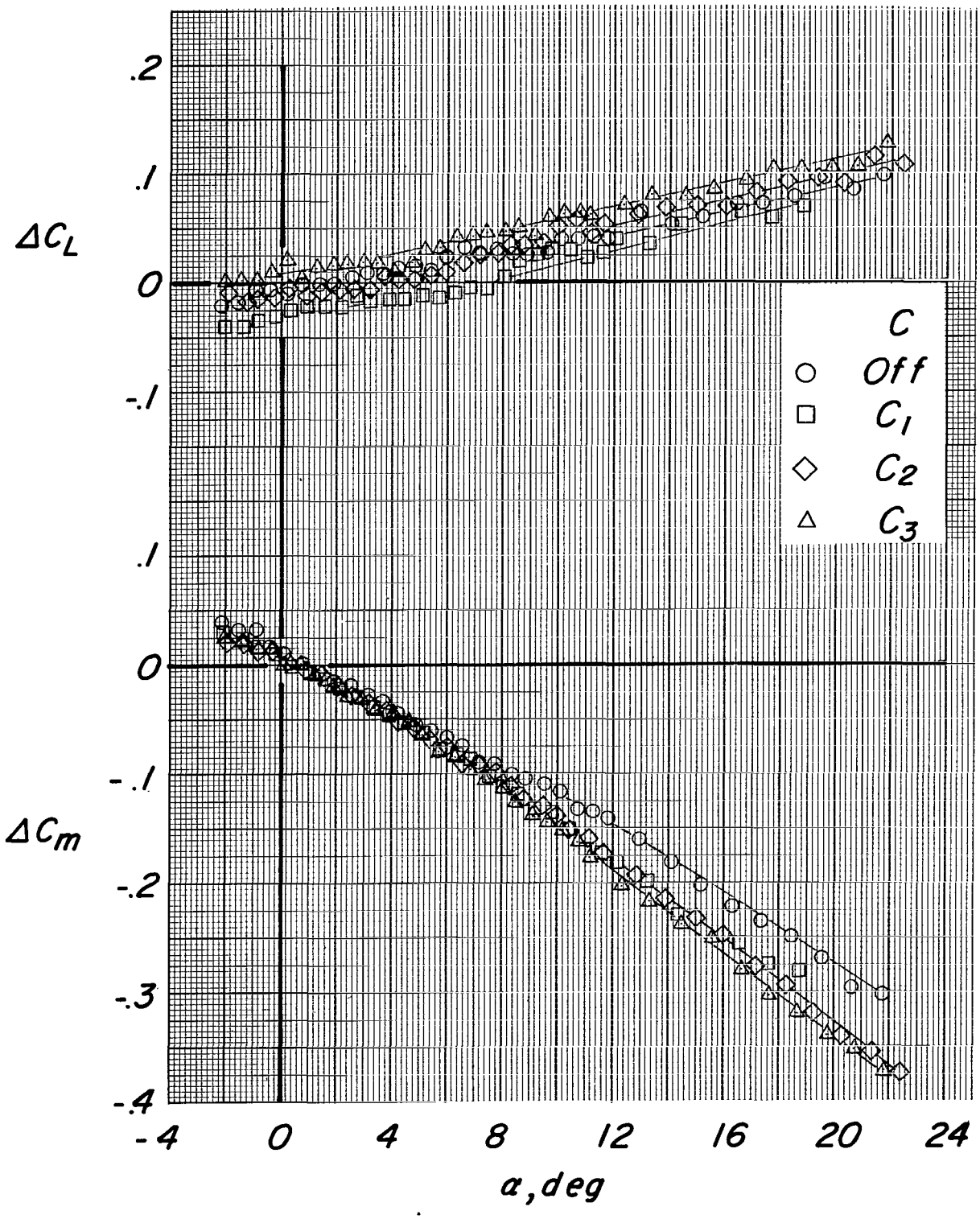

Figure 18.- Effect of canard size on the increment in pitching moment and lift coefficients due to the addition of the horizontal tail. $B_1WH_1V_NNF_1$; $\Lambda = 16^o$; $\delta_h = 0^o$; $\delta_c = 0^o$; $\delta_f = 0^o$; $i_w = 0^o$.

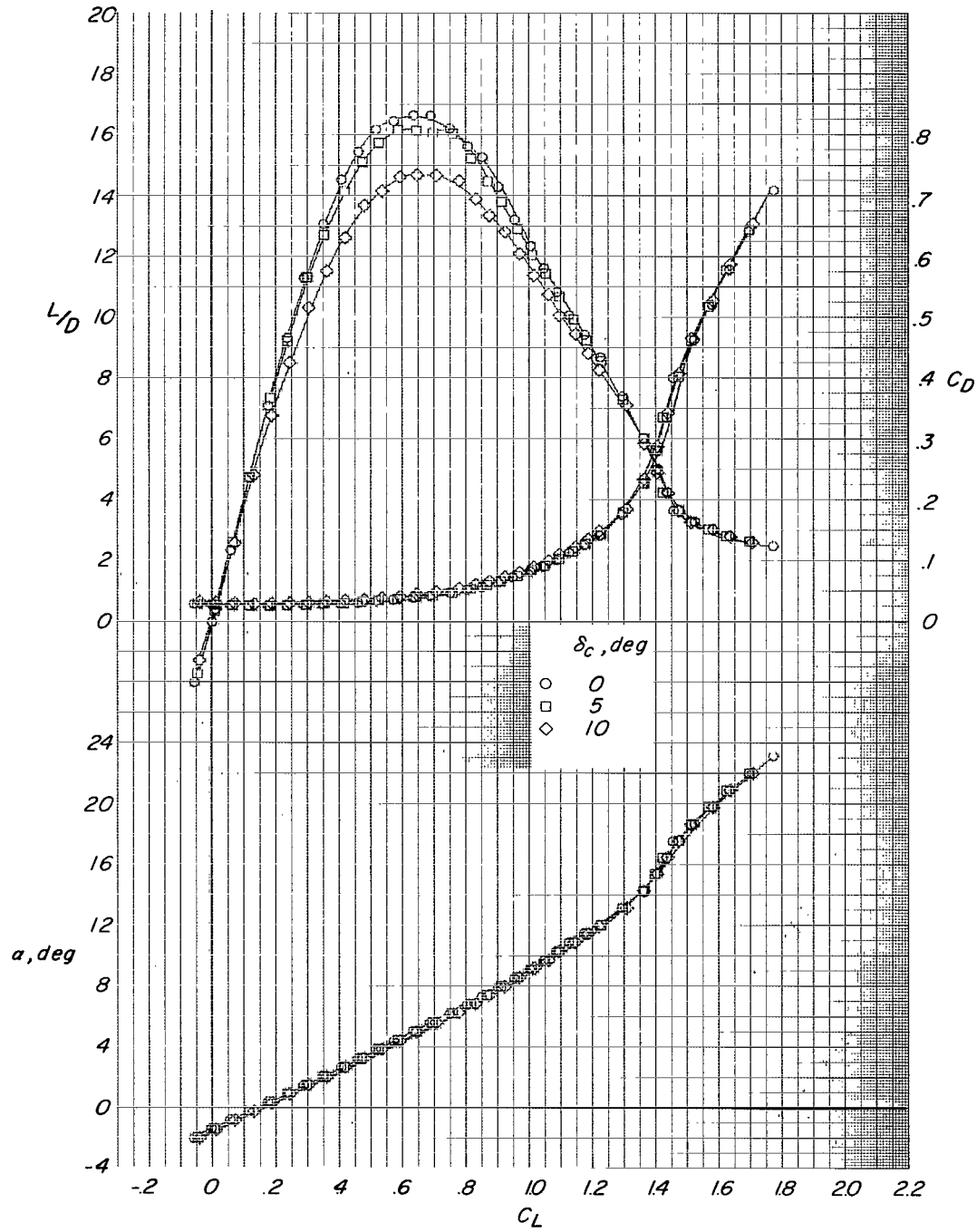

(a) C_1; x/c = 5.615.

Figure 19.- Effect of canard deflection on the aerodynamic characteristics. $B_1W_2H_1V_NNF_1$; $\Lambda = 16^0$; $\delta_h = 0^0$; $\delta_f = 0^0$; $i_w = 0^0$.

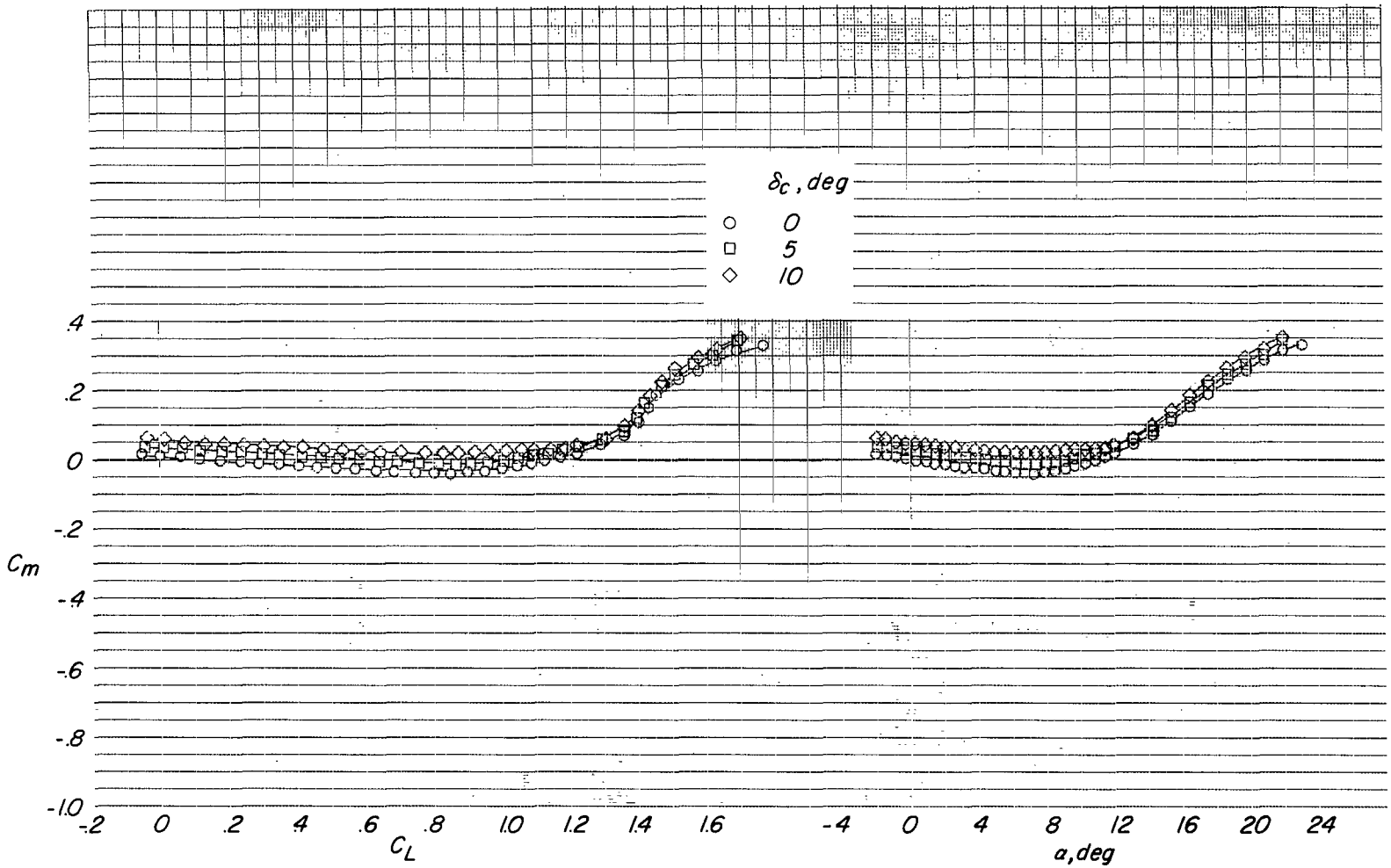

(a) Concluded.

Figure 19.- Continued.

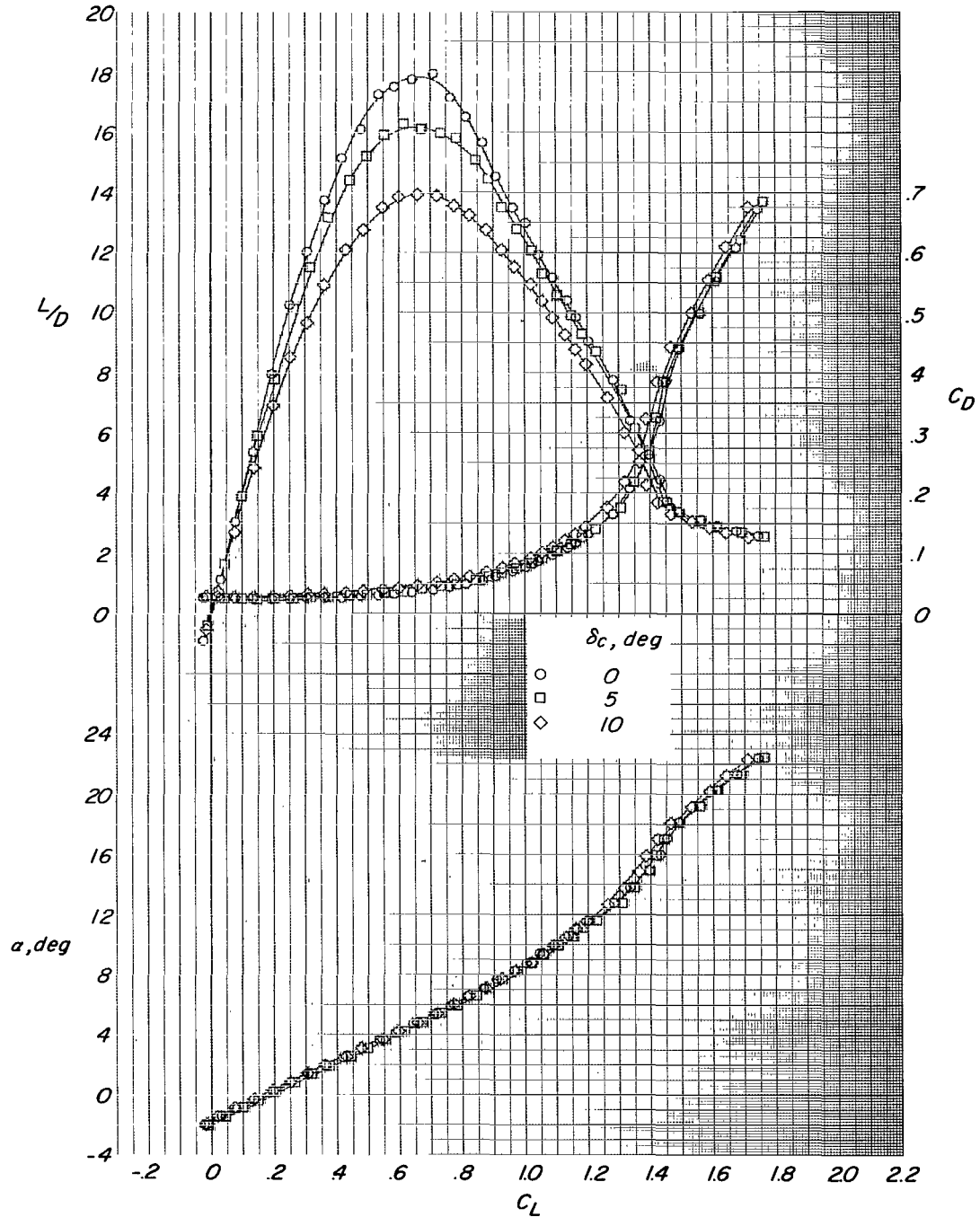

(b) C_2; x/c = 5.515.

Figure 19.- Continued.

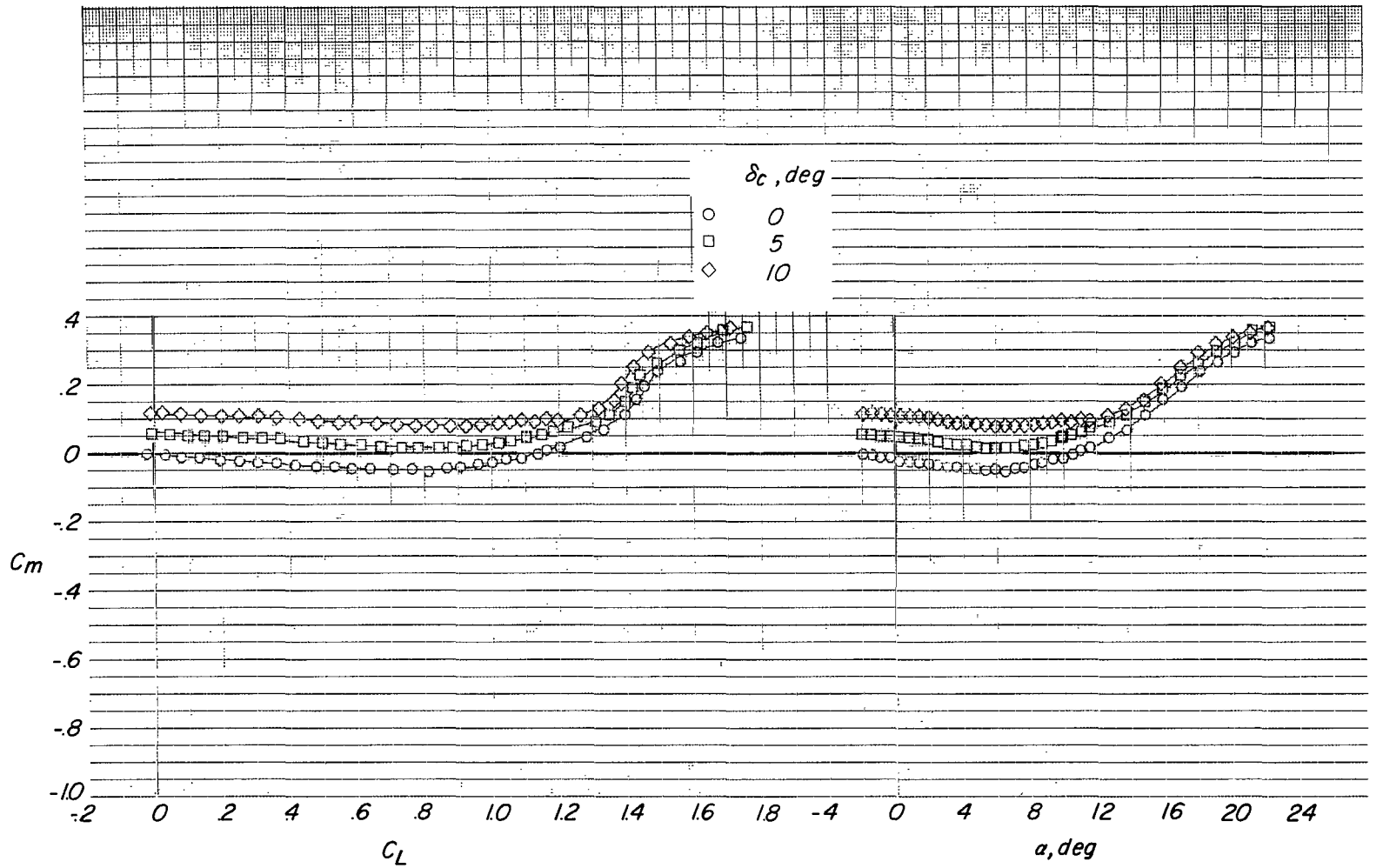

(b) Concluded.

Figure 19.- Continued.

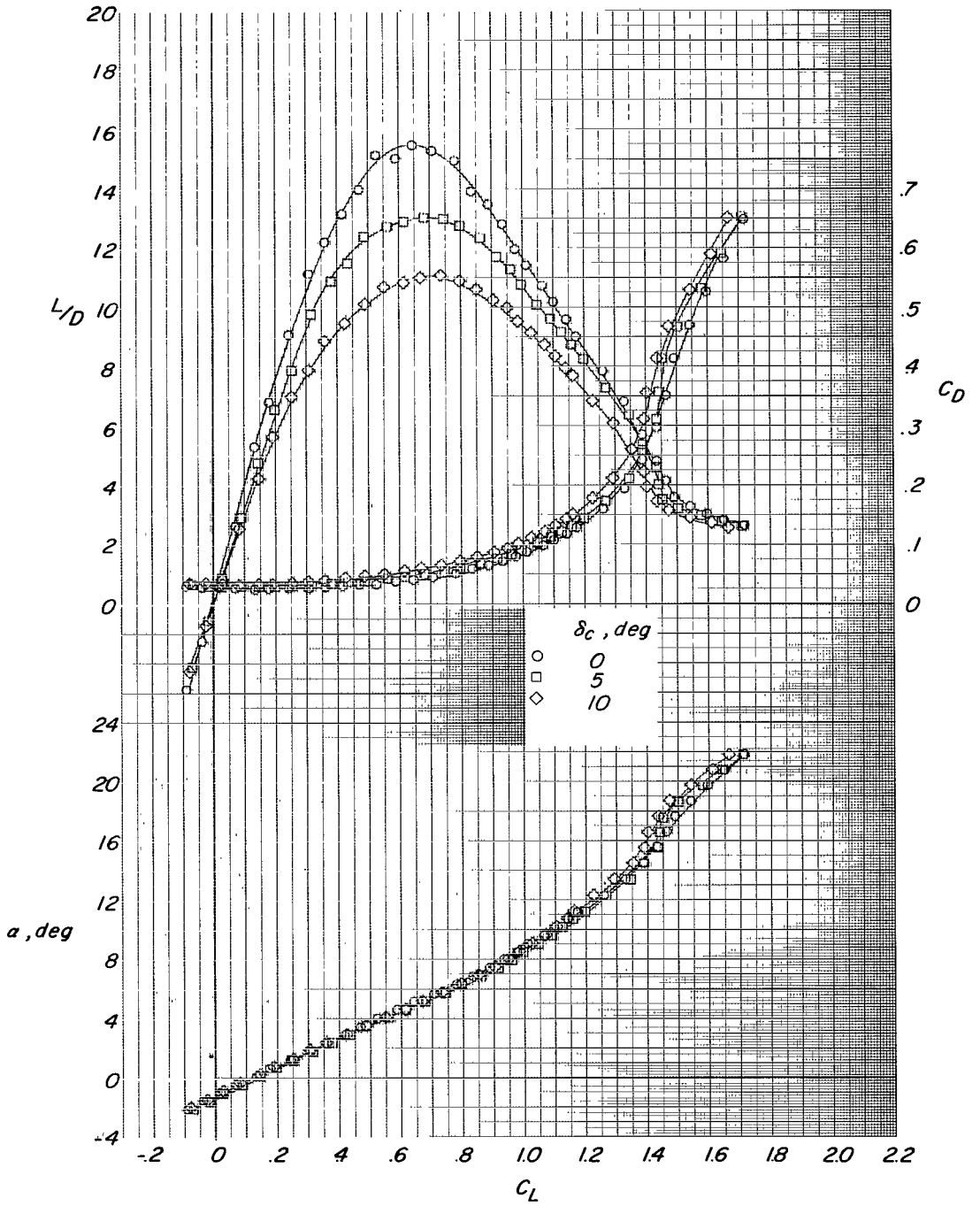

(c) C_3; x/c = 5.401.

Figure 19.- Continued.

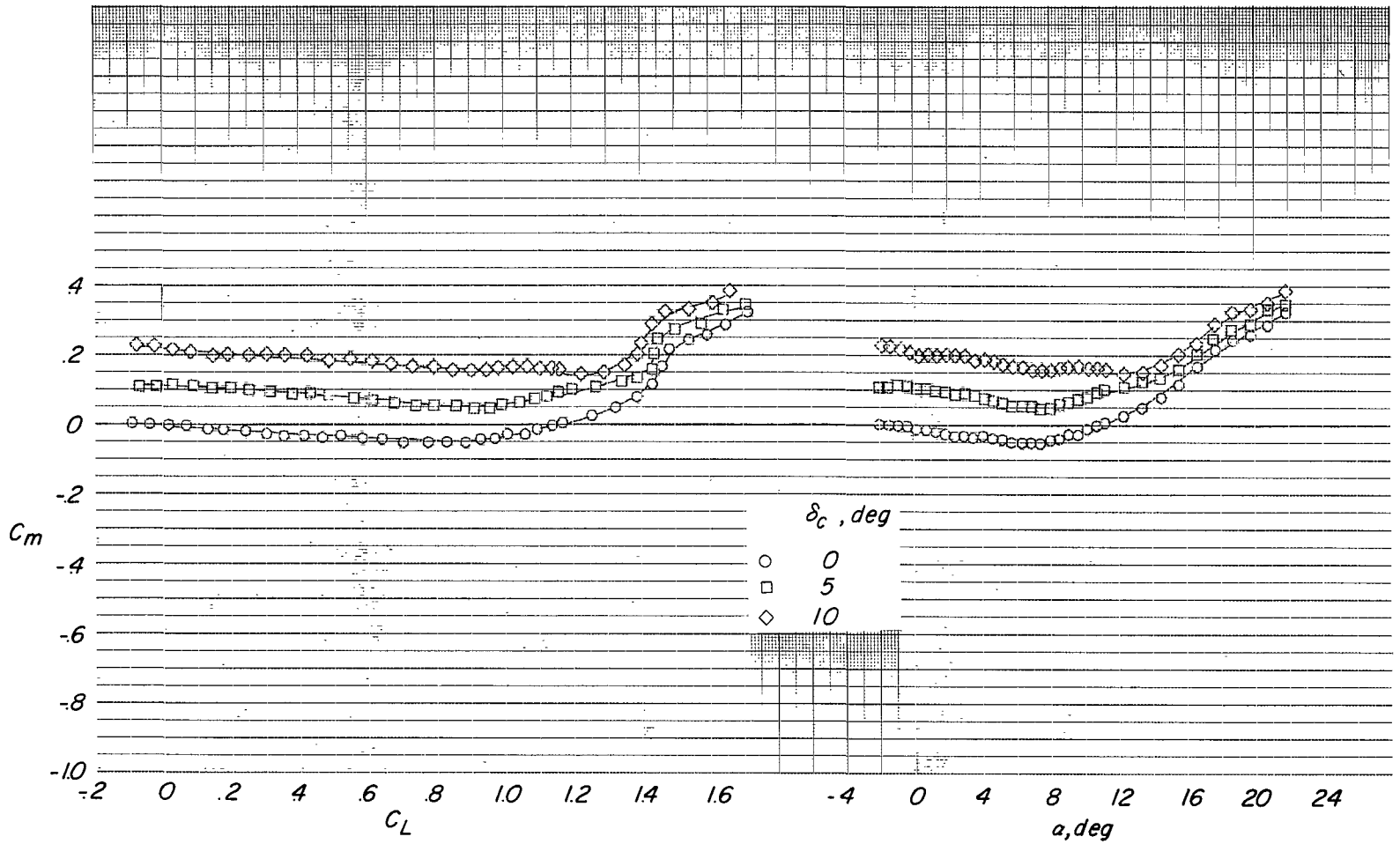

(c) Concluded.

Figure 19.- Concluded.

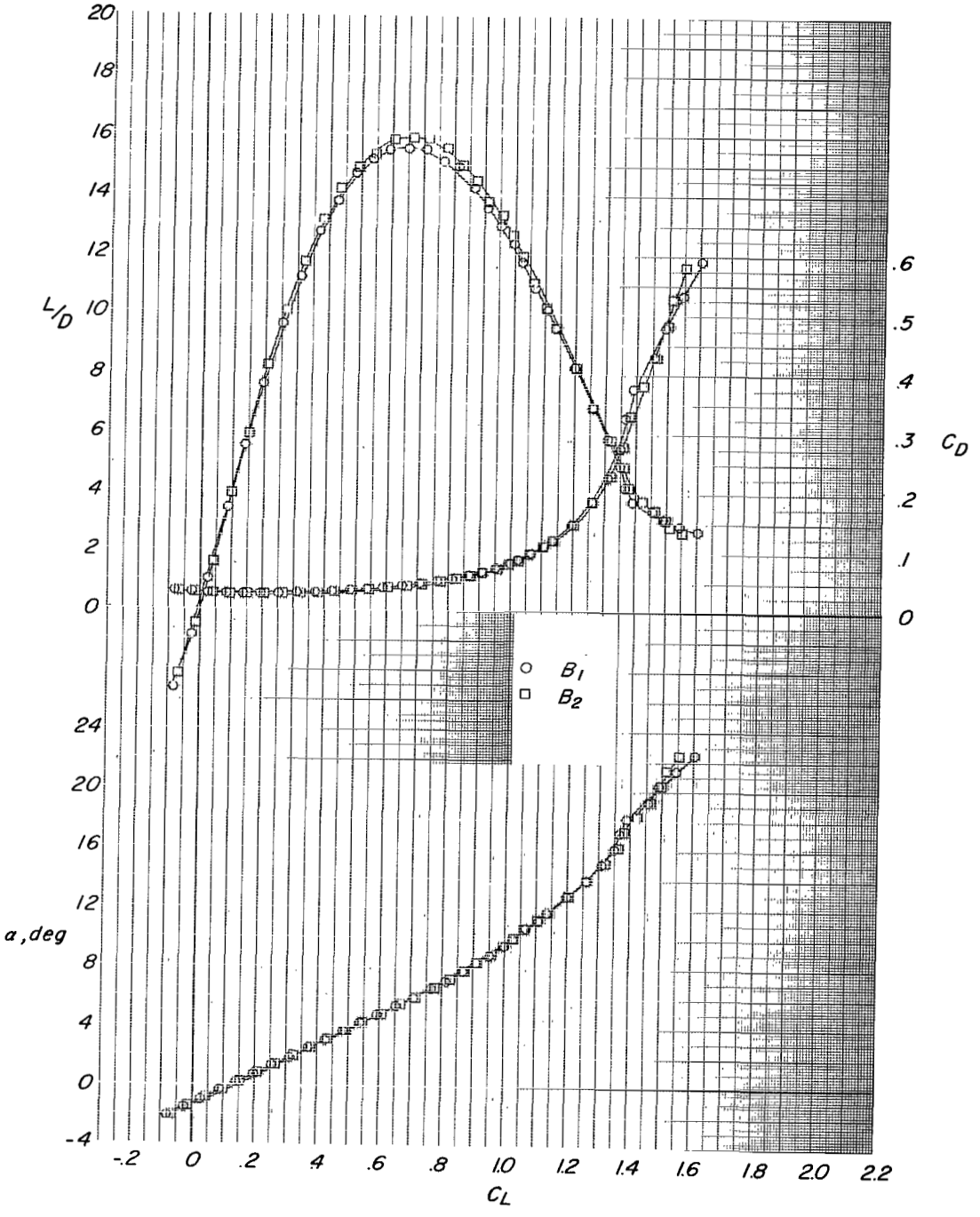

Figure 20.- Effect of fuselage cross section on the aerodynamic characteristics. $BWH_1V_NNF_6$; $\Lambda = 16^0$; $\delta_h = 0^0$; $\delta_f = 22.5^0$; $x/c = 5.735$; $i_w = 0^0$.

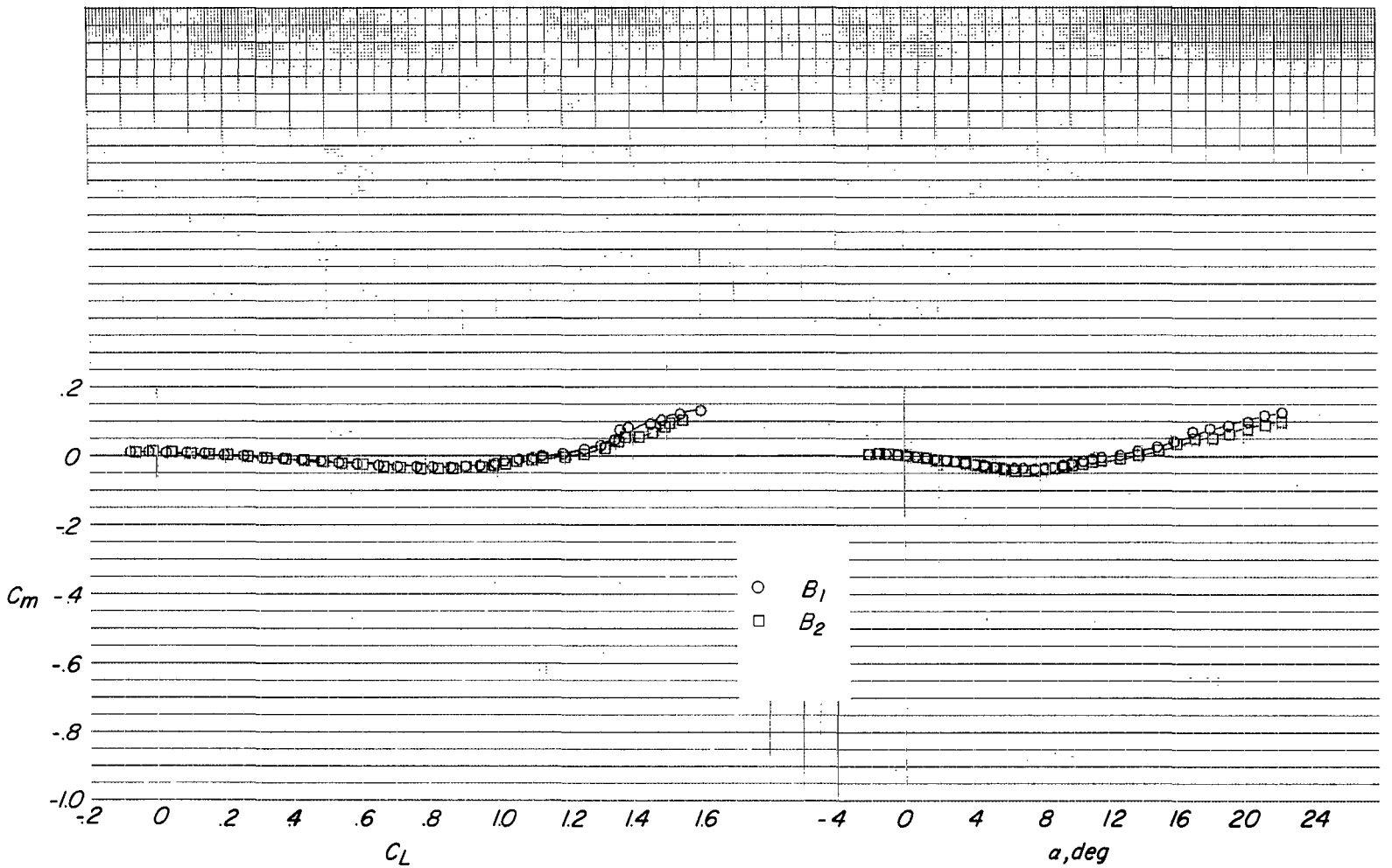

Figure 20.- Concluded.

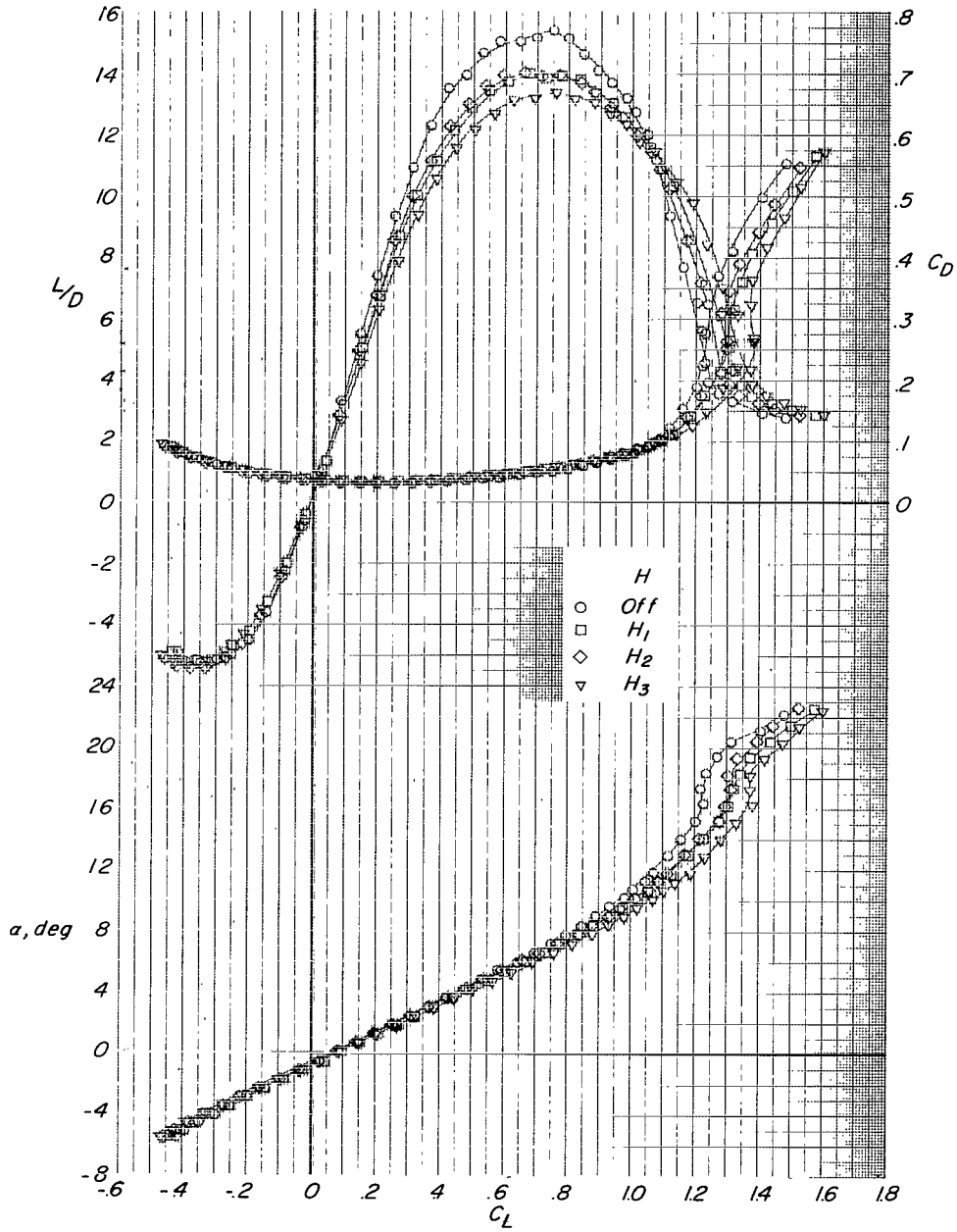

Figure 21.- Effect of horizontal-tail size on the aerodynamic characteristics. $B_1WHV_NNF_1$; $\Lambda = 16^0$; $\delta_f = 10^0$; $\delta_h = 0^0$; $x/c = 5.715$; $i_w = 0^0$.

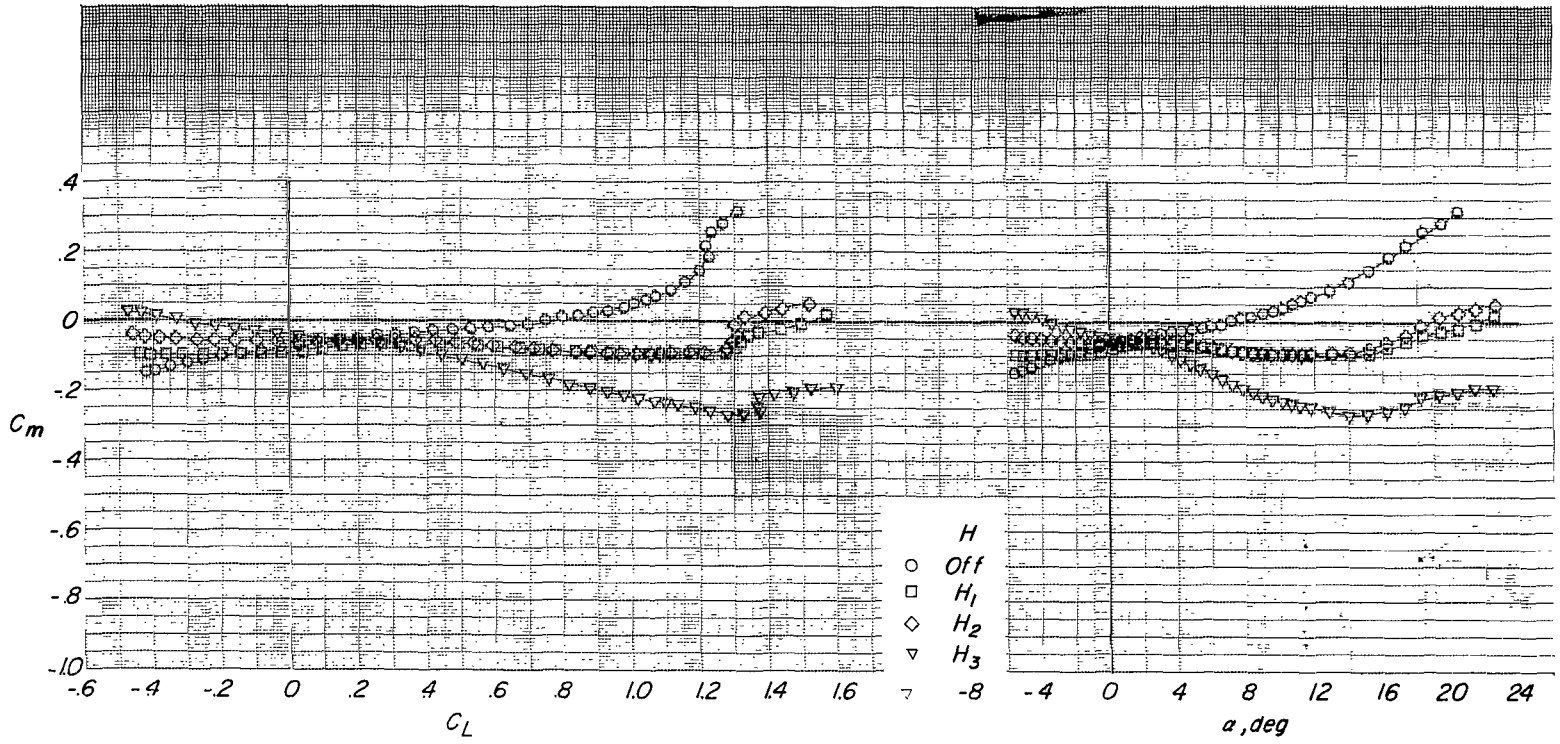

Figure 21.- Concluded.

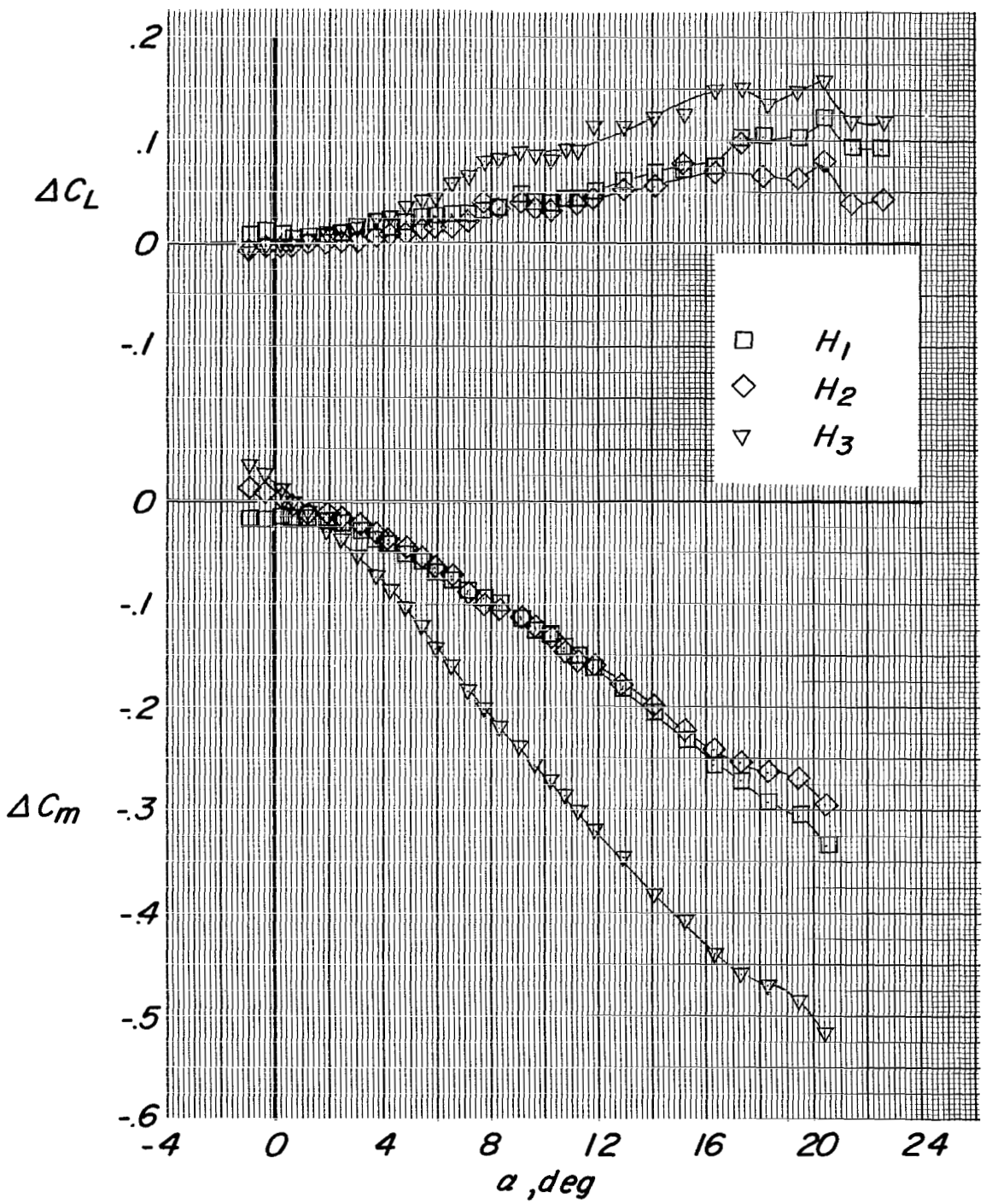

Figure 22.- Increment in pitching-moment and lift coefficients due to the addition of the horizontal tail. $B_1WHV_NNF_1$; $\Lambda = 16^0$; $\delta_f = 10^0$; $i_w = 0^0$.

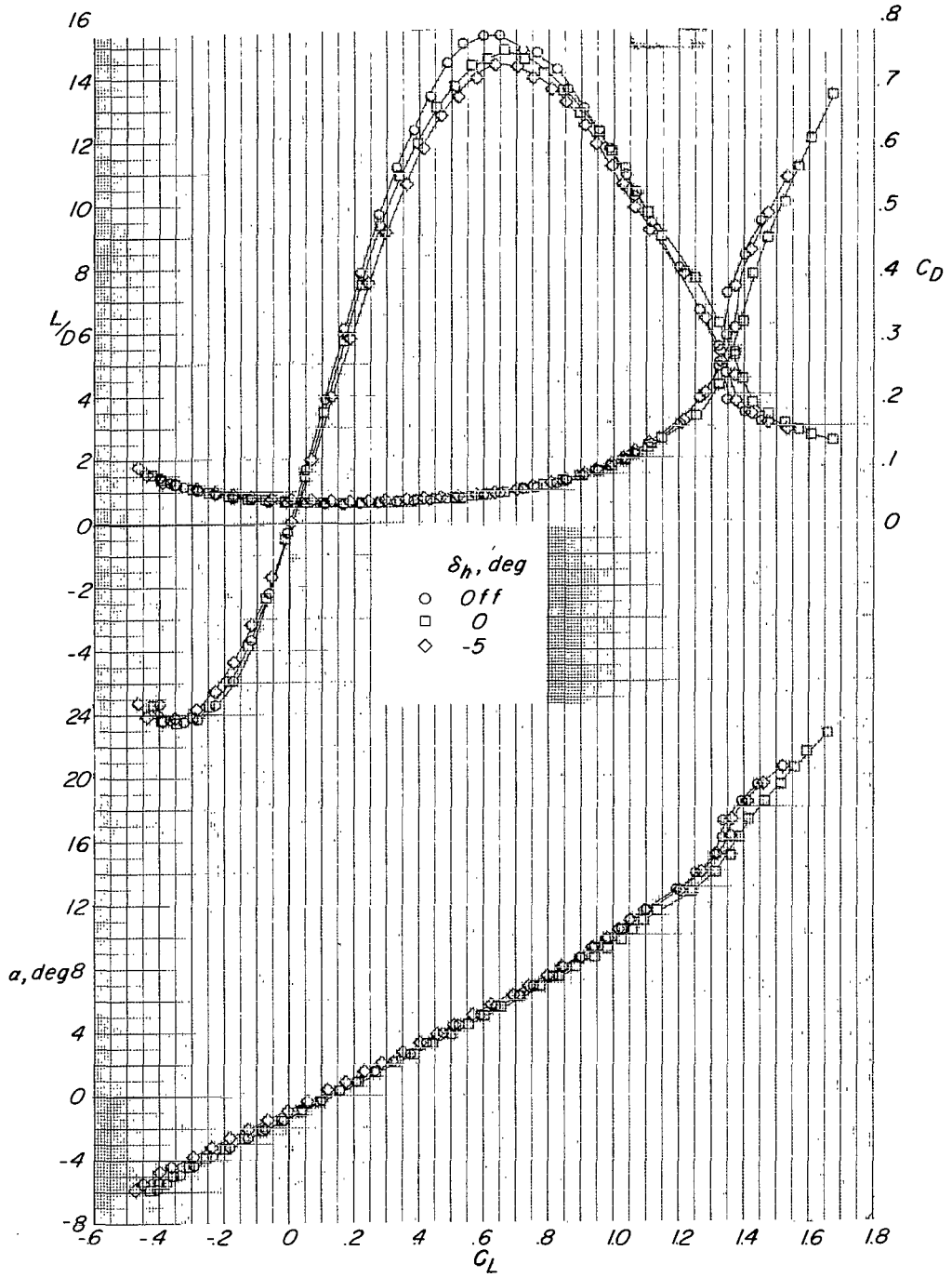

(a) H_1; $\delta_f = 0^0$.

Figure 23.- Effect of horizontal tail on the aerodynamic characteristics. $B_1WHV_NNF_1$; $\Lambda = 16^0$; x/c = 5.715; $i_w = 0^0$.

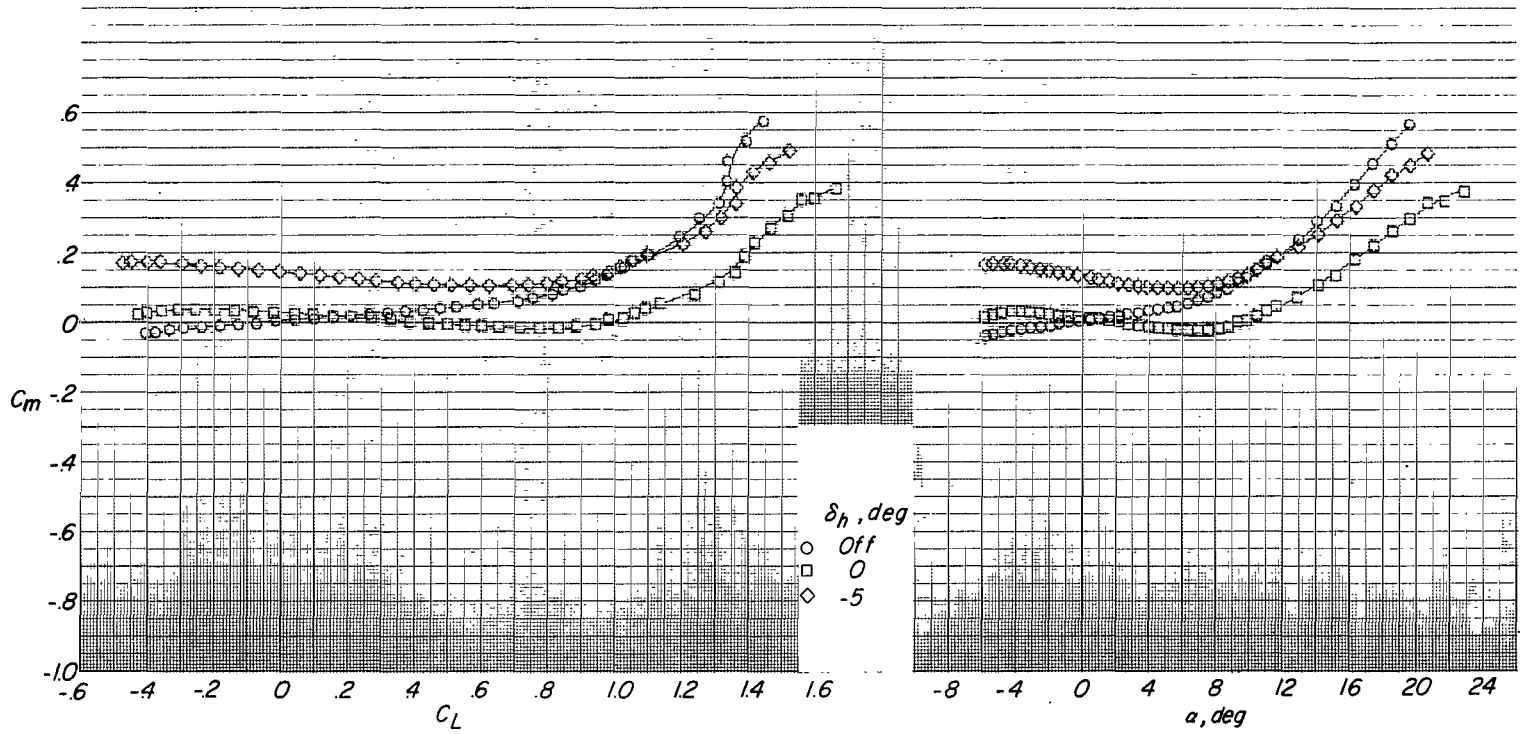

(a) Concluded.

Figure 23.- Continued.

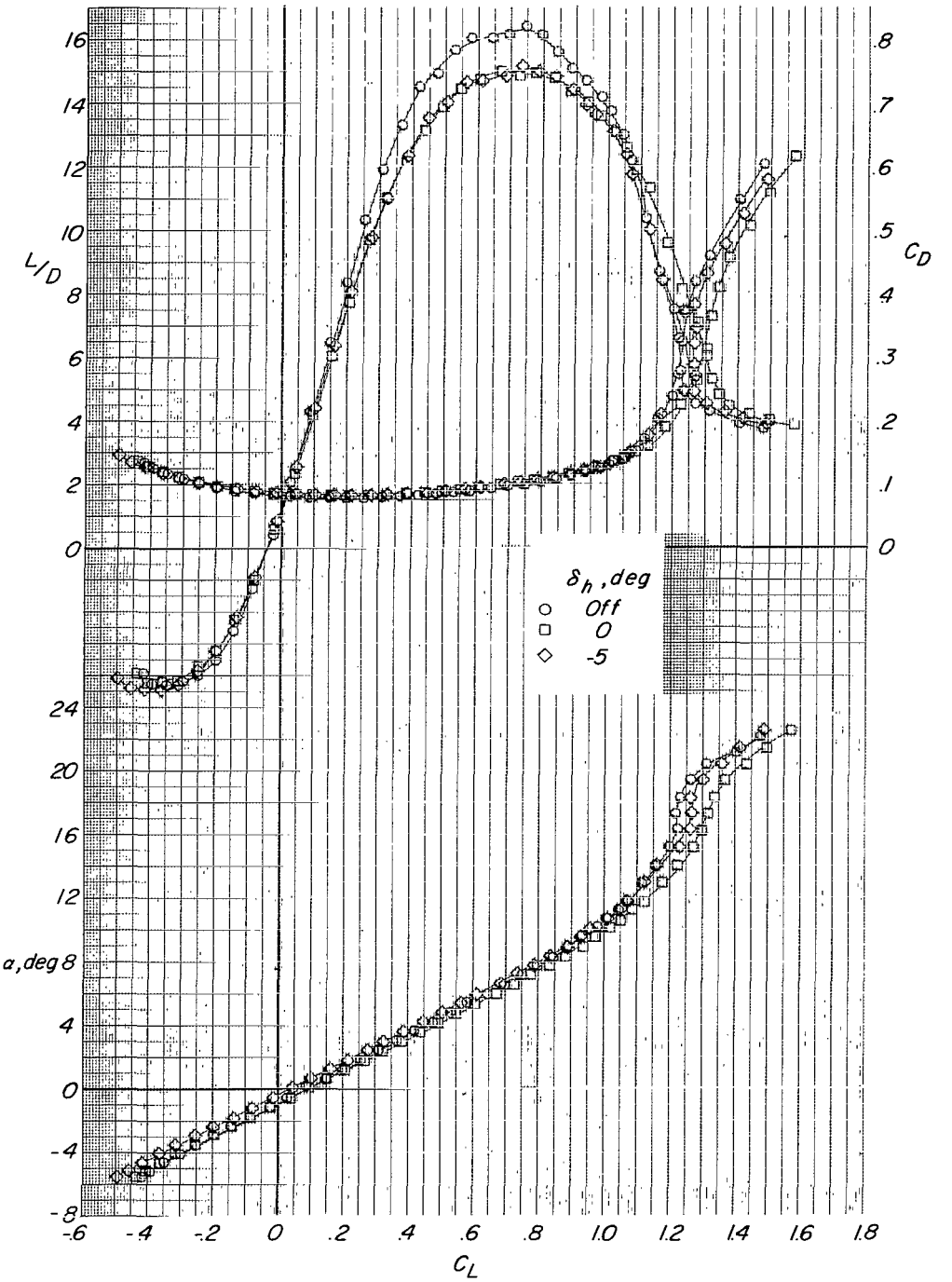

(b) H_1; $\delta_f = 10^0$.

Figure 23.- Continued.

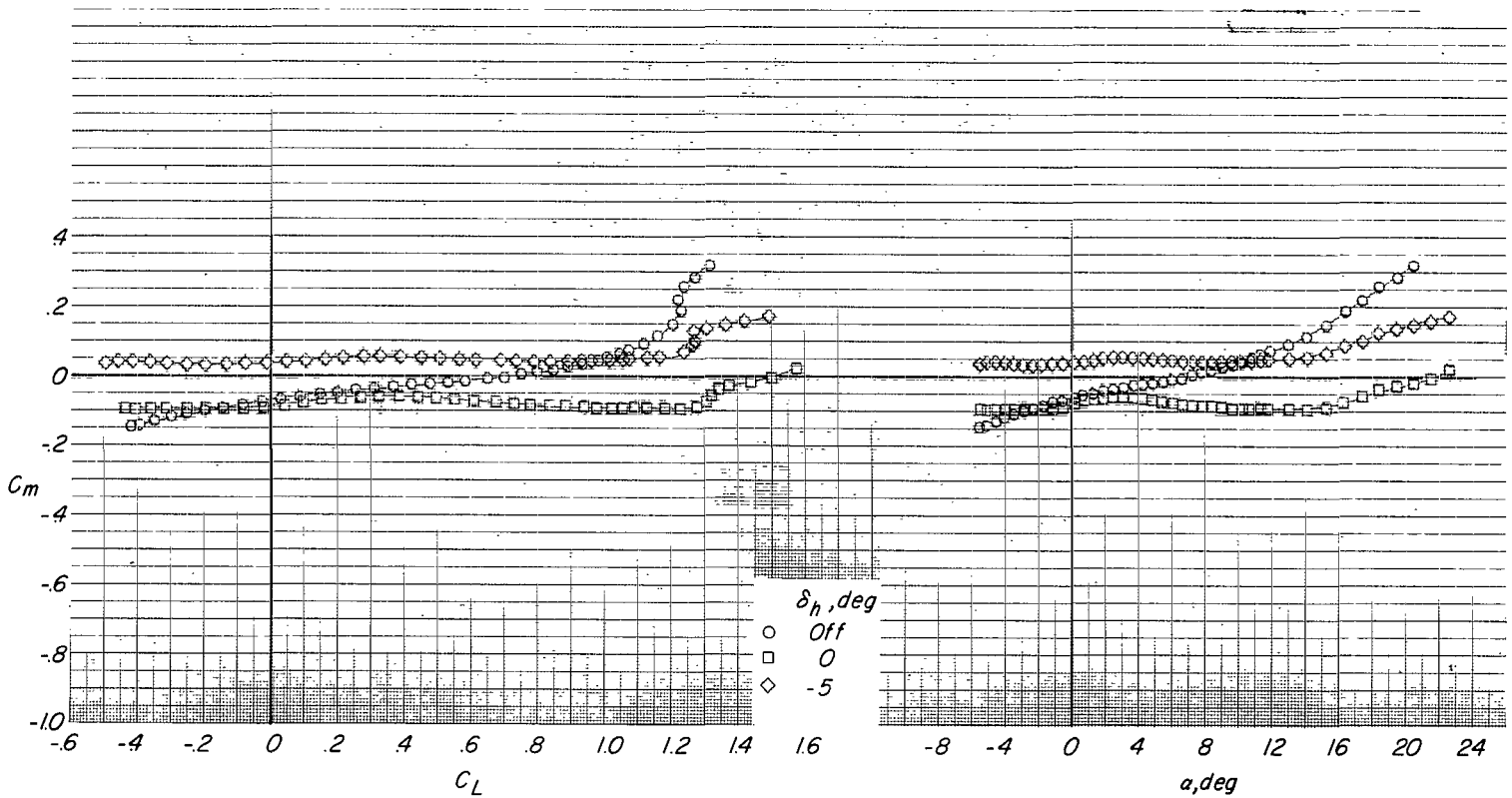

(b) Concluded.

Figure 23.- Continued.

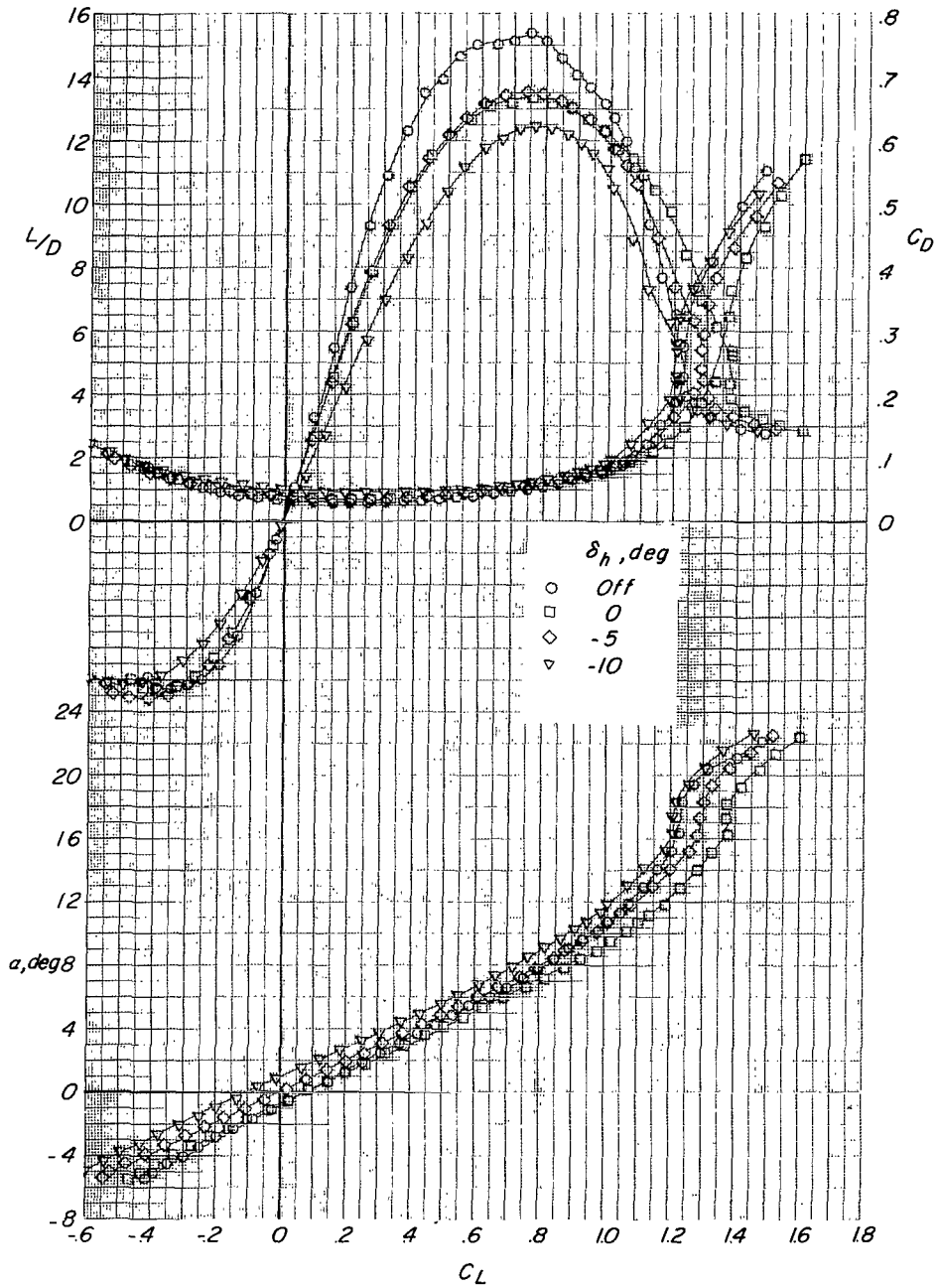

(c) H_3; $\delta_f = 10^0$.

Figure 23.- Continued.

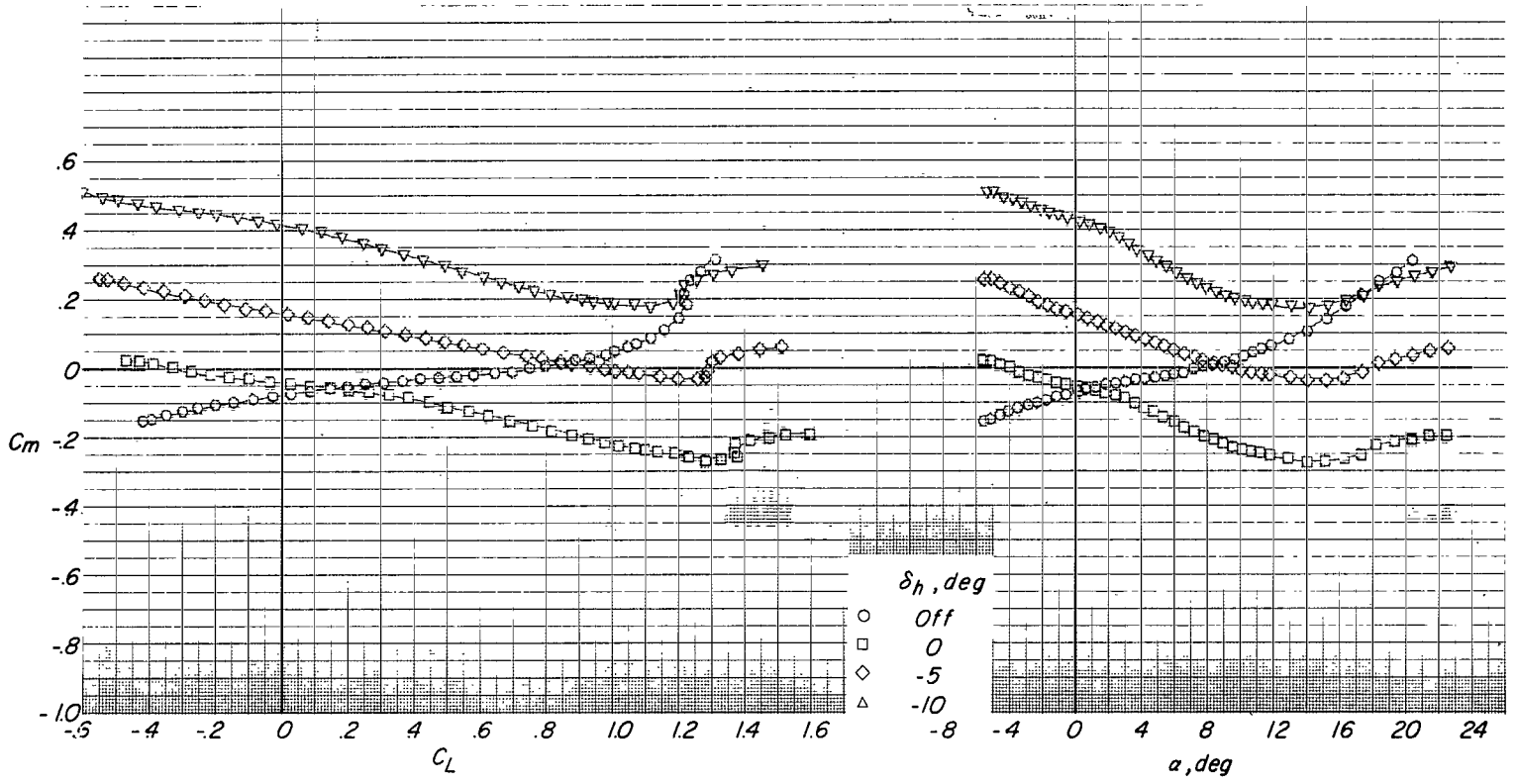

(c) Concluded.

Figure 23.- Concluded.

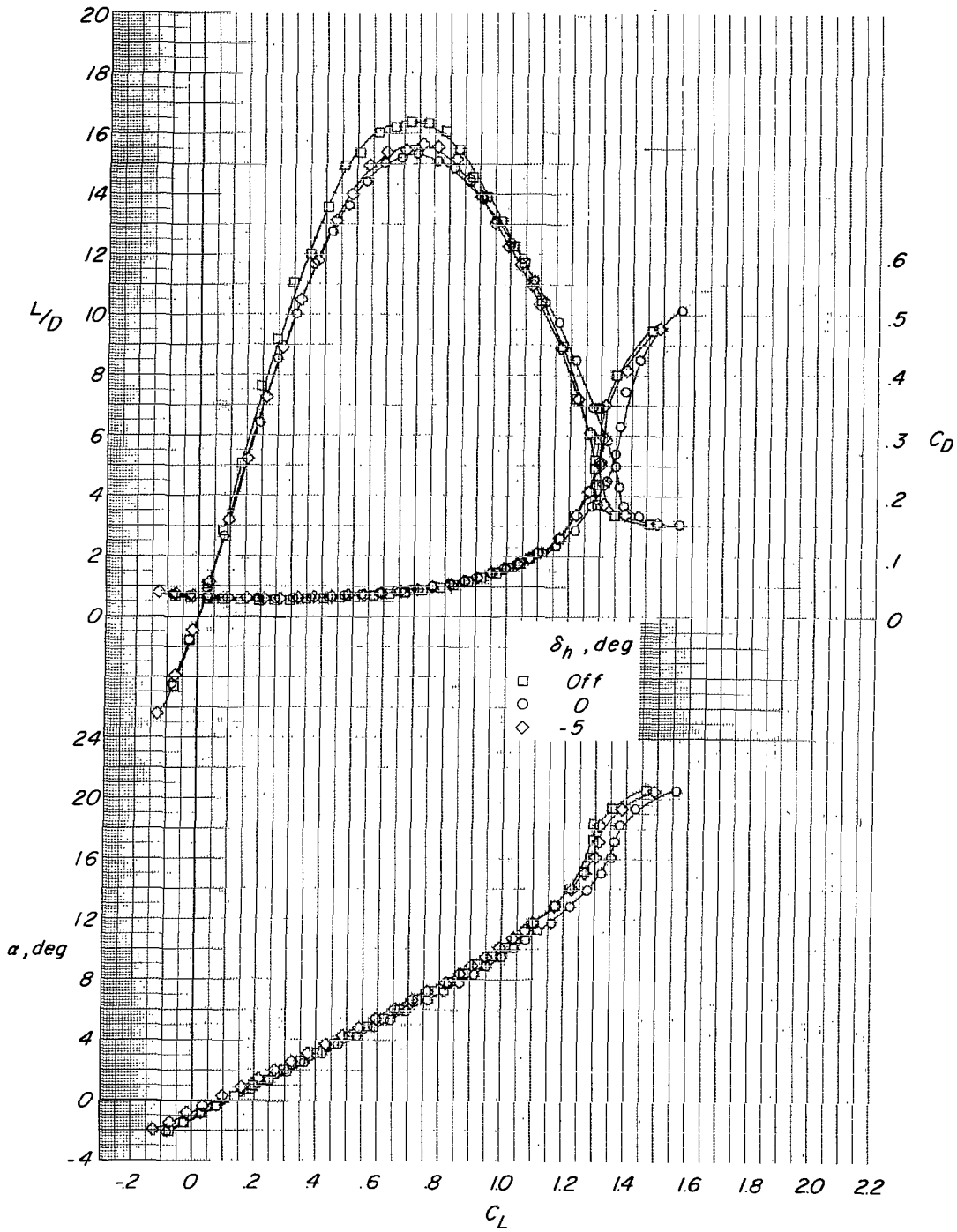

Figure 24.- Effect of horizontal tail on the aerodynamic characteristics. $B_1WH_1V_NNF_4$; $\Lambda = 16^0$; $\delta_f = 45^0$; $x/c = 5.715$; $i_w = 0^0$.

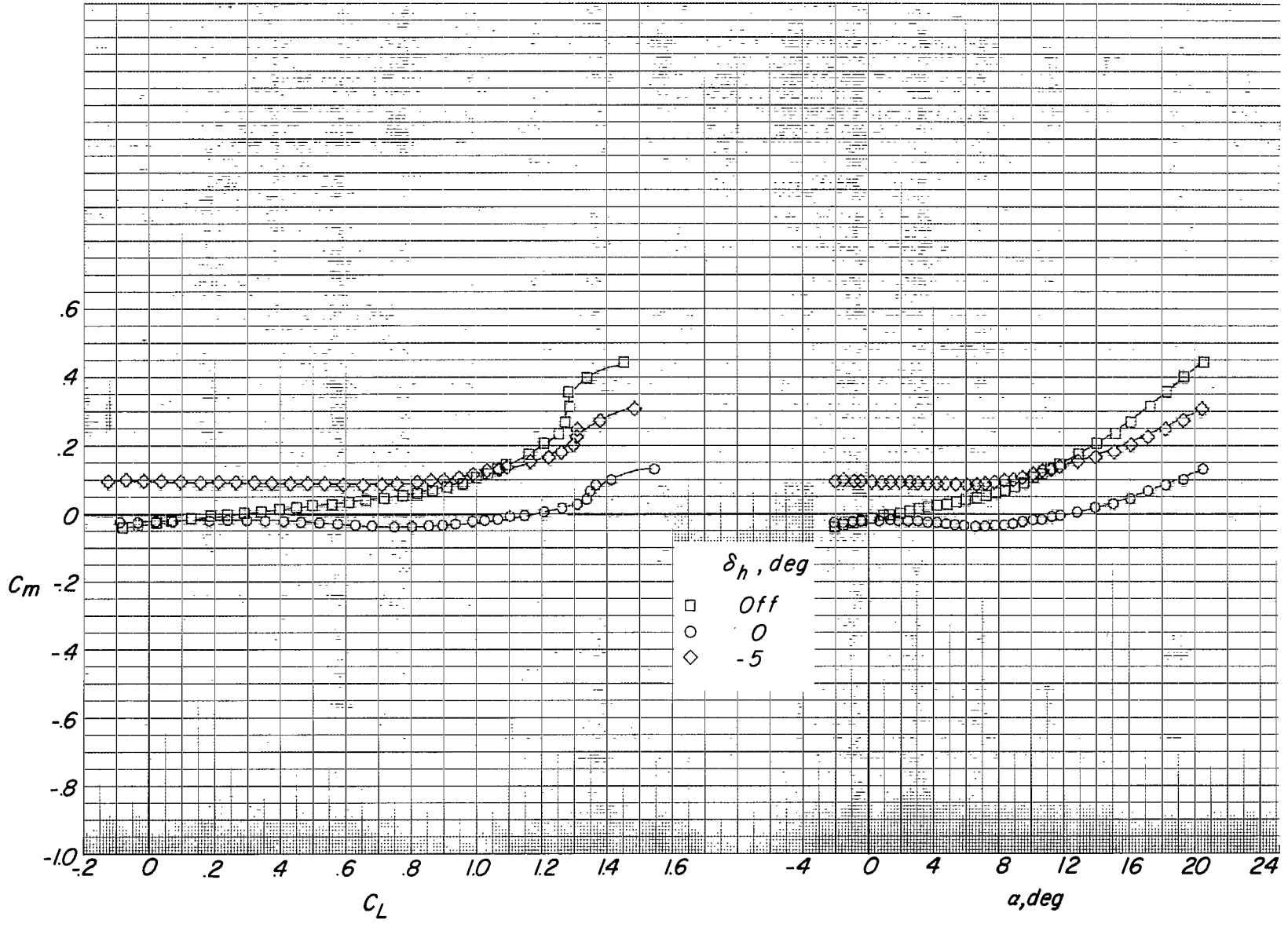

Figure 24.- Concluded.

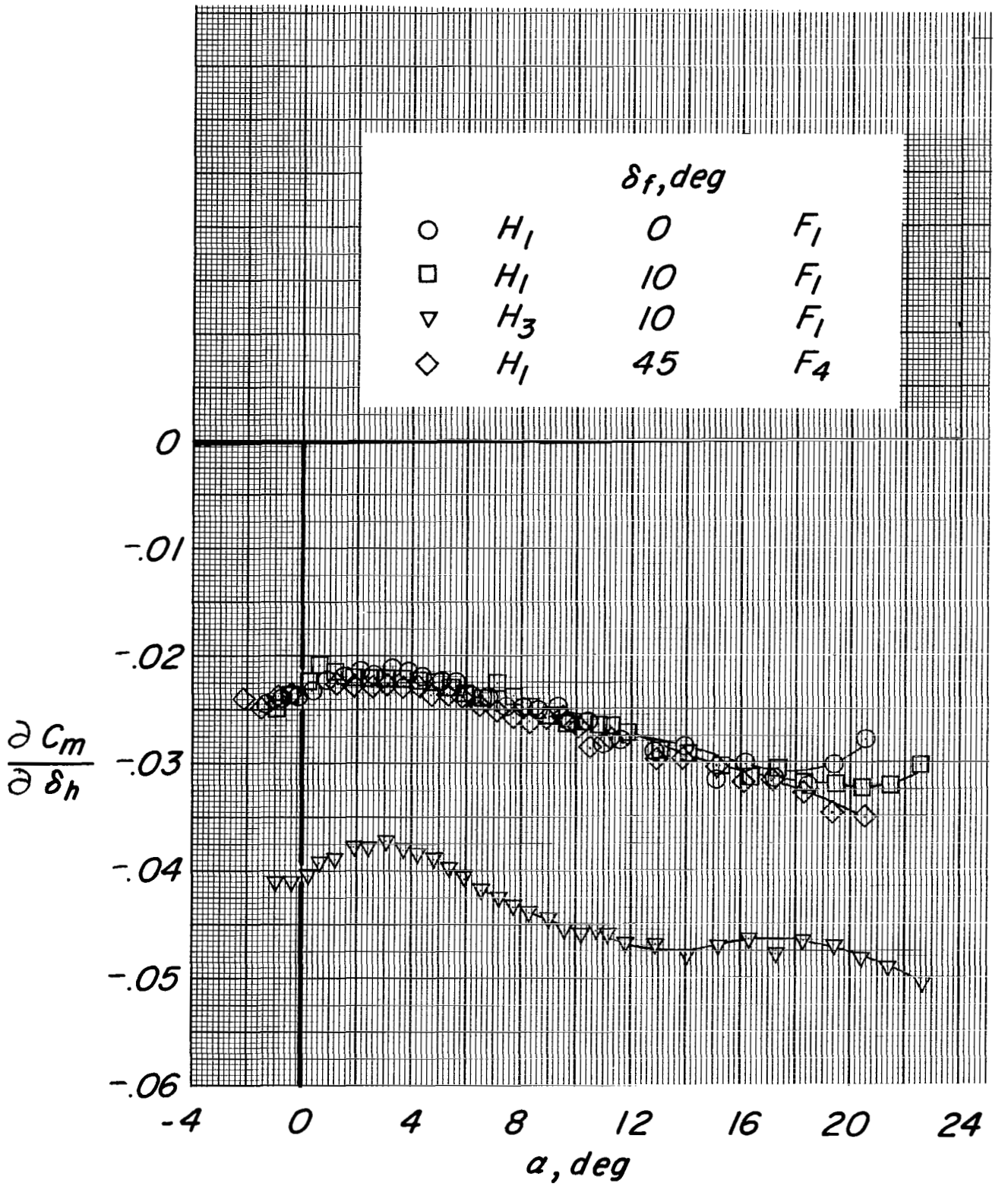

Figure 25.- Effect of horizontal-tail size and forewing-flap deflection on the horizontal-control parameter. $\partial C_m/\partial \delta_h$. B_1WHV_NNF. $\Lambda = 16^o$; $i_w = 0^o$.

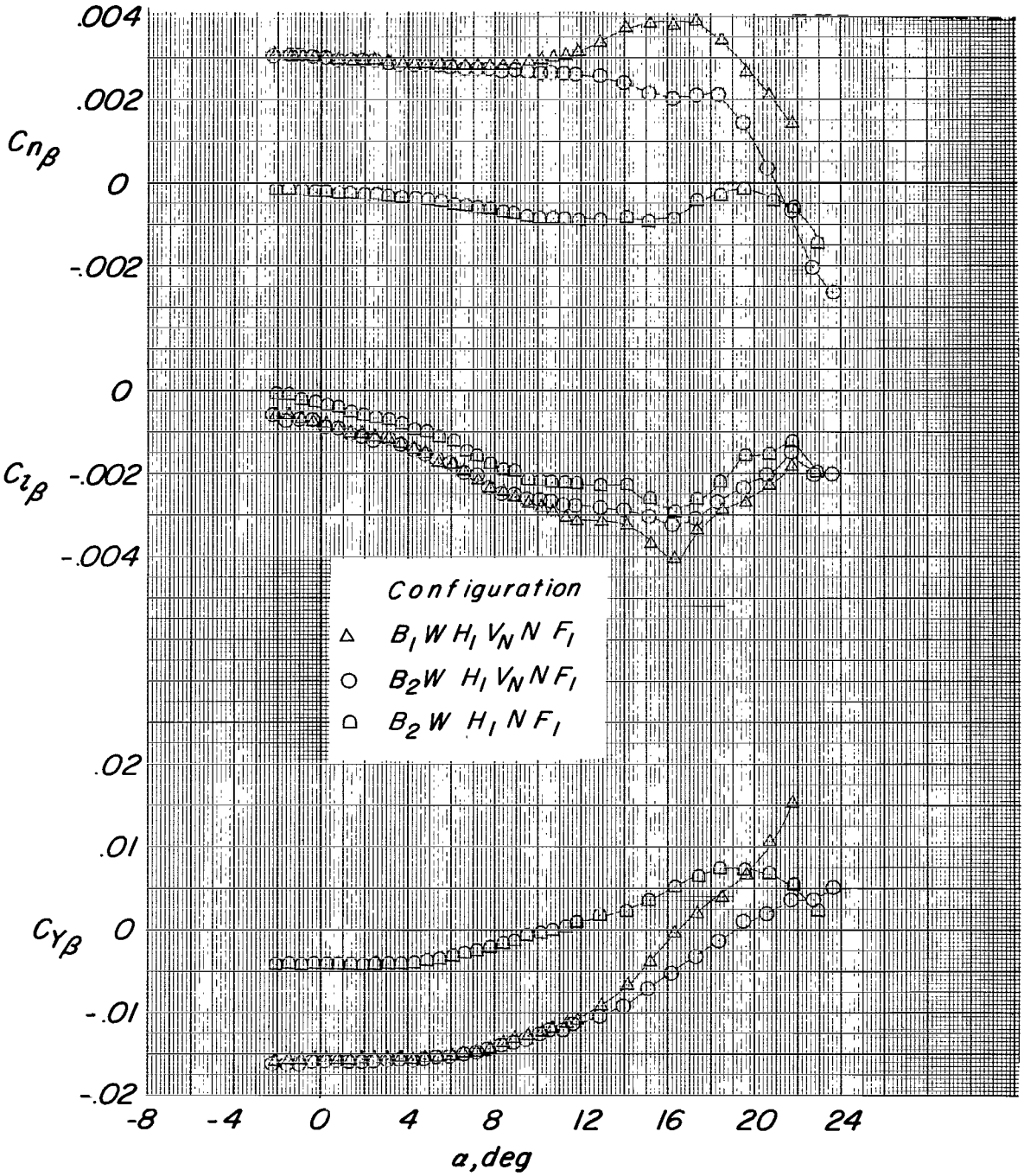

Figure 26.- Effect of fuselage nose cross-sectional shape and vertical tail on the lateral directional stability characteristics in pitch. $\Lambda = 16^0$; $\sigma_h = 0^0$; $\delta_f = 0^0$; $i_w = 0^0$.

"The aeronautical and space activities of the United States shall be conducted so as to contribute . . . to the expansion of human knowledge of phenomena in the atmosphere and space. The Administration shall provide for the widest practicable and appropriate dissemination of information concerning its activities and the results thereof."

—NATIONAL AERONAUTICS AND SPACE ACT OF 1958

NASA SCIENTIFIC AND TECHNICAL PUBLICATIONS

TECHNICAL REPORTS: Scientific and technical information considered important, complete, and a lasting contribution to existing knowledge.

TECHNICAL NOTES: Information less broad in scope but nevertheless of importance as a contribution to existing knowledge.

TECHNICAL MEMORANDUMS: Information receiving limited distribution because of preliminary data, security classification, or other reasons.

CONTRACTOR REPORTS: Technical information generated in connection with a NASA contract or grant and released under NASA auspices.

TECHNICAL TRANSLATIONS: Information published in a foreign language considered to merit NASA distribution in English.

TECHNICAL REPRINTS: Information derived from NASA activities and initially published in the form of journal articles.

SPECIAL PUBLICATIONS: Information derived from or of value to NASA activities but not necessarily reporting the results of individual NASA-programmed scientific efforts. Publications include conference proceedings, monographs, data compilations, handbooks, sourcebooks, and special bibliographies.

Details on the availability of these publications may be obtained from:

SCIENTIFIC AND TECHNICAL INFORMATION DIVISION

NATIONAL AERONAUTICS AND SPACE ADMINISTRATION

Washington, D.C. 20546